

Two-photon absorption: an overview of measurements and principles

Mariacristina Rumi^{1,3} and Joseph W. Perry^{1,2}

¹School of Chemistry and Biochemistry and Center for Organic Photonics and Electronics, Georgia Institute of Technology, Atlanta, Georgia 30332-0400, USA

²e-mail: joe.perry@gatech.edu

³e-mail: mrumi@gatech.edu

Received March 26, 2010; revised July 7, 2010; accepted July 8, 2010; published August 26, 2010 (Doc. ID 126053)

The range of organic compounds whose degenerate two-photon absorption (2PA) spectrum has been reported has increased rapidly in recent years, in parallel with the growing interest in applications based on the 2PA process. The comparison of results from different techniques is not always straightforward, and experimental conditions employed may vary significantly. We overview the concepts underlying 2PA measurements and the common assumptions and approximations used in the data analysis for various techniques. The importance of selecting appropriate excitation regimes under which measurements should be performed and of avoiding contributions from absorption mechanisms in addition to 2PA will be emphasized. © 2010 Optical Society of America

OCIS codes: 190.4180, 190.4710, 300.6410, 160.4890, 020.4180.

| | |
|--|-----|
| 1. Introduction. | 453 |
| 2. Experimental Techniques Used to Quantify 2PA. | 455 |
| 2.1. Direct Methods. | 459 |
| 2.2. Indirect Methods. | 460 |
| 2.3. Wave Mixing Techniques. | 461 |
| 3. 2PA Excitation Rates and Conditions to Avoid Beam Depletion and Saturation. | 463 |
| 3.1. Indirect Methods. | 463 |
| 3.1a. High-Repetition-Rate Femtosecond Laser, Collimated Beam. | 467 |
| 3.1b. Amplified Femtosecond Laser, f/15 Focusing. | 468 |
| 3.1c. Nanosecond Laser, Collimated Beam. | 470 |
| 3.2. Direct Methods. | 471 |
| 3.2a. Collimated Beam, Rectangular Profile in Space and Time. | 471 |
| 3.2b. Collimated Beam, Gaussian Profile in Space, Rectangular Profile in Time. | 472 |
| 3.2c. Focused Beam, Rectangular Profile in Space. | 473 |

| | |
|---|-----|
| 3.2d. Focused Beam, Gaussian Profile in Space and Time: | |
| Open-Aperture Z-Scan. | 475 |
| 4. Pulse Width Effects and Other Temporal Considerations. | 479 |
| 4.1. Significance of the $\langle \phi^2 \rangle$ Term. | 479 |
| 4.2. Pulse Width Effects. | 482 |
| 4.3. Excited State Absorption. | 484 |
| 4.3a. ESA and Indirect Measurements: 2PIF Methods. | 486 |
| 4.3b. ESA and Indirect Measurements: Thermal Methods. | 487 |
| 4.3c. ESA and Direct Measurements: NLT and Z-scan Methods.. | 488 |
| 4.3d. Conclusions Regarding ESA Effect on 2PA Measurements.. | 492 |
| 4.4. Absolute and Relative Measurements. | 493 |
| 5. Advantages and Disadvantages of Various Methods. | 500 |
| 5.1. Direct Methods. | 500 |
| 5.2. Indirect Methods. | 500 |
| 5.3. Wave Mixing Methods. | 501 |
| 6. Conclusions and Outlook. | 502 |
| 7. List of Symbols Used. | 502 |
| 8. List of Abbreviations Used. | 504 |
| Acknowledgments. | 504 |
| References and Notes. | 504 |

Two-photon absorption: an overview of measurements and principles

Mariacristina Rumi and Joseph W. Perry

1. Introduction

Two-photon absorption (2PA) is the process by which a molecule or material absorbs a pair of photons, the sum of whose energy equals the transition energy. The probability that a molecule undergoes 2PA when exposed to light of a given photon energy (or combination of photon energies) depends on certain intrinsic characteristics of the material and of the environment in which the molecule is immersed. Thus, 2PA spectroscopy can be used as a tool to probe molecular properties, for example, the energy of the two-photon active excited states and, to some extent through the strength of the 2PA transitions, the differences in electronic structure between the ground and excited states of the system. This information can be different from, and complementary to, what is obtainable from one-photon absorption (1PA) spectroscopy, because different selection rules apply in the 1PA and 2PA cases and because the behavior of a material under two-photon excitation conditions (but not one-photon excitation) depends on the polarization state of the excitation beam or beams even for an isotropic sample. Since the first experimental demonstration of 2PA, there has been a fundamental interest in 2PA spectroscopy for the study of basic properties of materials and of matter–light interactions. More recently, interest in materials that exhibit 2PA has also been spurred by the development of applications such as 3D microfabrication [1], optical data storage [2,3], two-photon fluorescence imaging [1,4], and optical limiting [5,6]. These applications exploit the fact that the transition probability for the 2PA process depends on the square of the intensity of the light beam used for the excitation, if the two photons have the same energy (in the case of photons with different energies, the transition probability depends on the product of the intensities of the two light beams). This intensity dependence can be used to spatially control the excitation of a material in three dimensions or to modify the propagation characteristics of light in a medium with the light itself. The interest in 2PA in general and the investigation of the 2PA properties of organic materials in particular, including the identification of so-called structure-property relationships (that is, the determination of how the wavelength and strength of the 2PA process depends on molecular structure and other material parameters), have grown significantly in the past fifteen years or so, in conjunction with the development of the applications mentioned above. This is because, for each application, materials need to be identified that satisfy a certain set of requirements, typically the combination of a sizable probability of 2PA at the wavelength of interest (quantified by the 2PA cross section, as discussed below) and high sensitivity for a process to take place after the absorption of the two photons, such as fluorescence emission, a photochemical reaction, or the sensi-

tization of another material. From both fundamental and application perspectives, it is thus necessary to monitor and quantify the strength of the 2PA process and to determine how material parameters and experimental conditions control it.

Over the years, a number of different experimental techniques have been used to determine the 2PA spectra of materials and to measure their 2PA cross sections. The techniques most often used to date can be classified as *direct* methods, in which the attenuation of the excitation beam is monitored, and *indirect* methods, in which a secondary effect of the 2PA process, such as induced fluorescence, phosphorescence, or a temperature change in the sample, is measured. With these techniques, researchers have obtained a wealth of spectroscopic information on existing and newly prepared compounds [7–13] and demonstrated the use of many materials in advanced technological applications [11,14–18].

Despite the fact that the scope of 2PA spectroscopy and the range of materials to which it is applied have been expanding at a fast rate in the past decade and that in 1973 Hochstrasser, Sung, and Wessel stated that the spectra of naphthalene and 1-chloronaphthalene that they were reporting “were obtained as reproducibly and easily as conventional one-photon absorption measurements,” [19] the measurement of 2PA spectra and cross sections still poses a number of experimental problems. As is the case in the measurement of other nonlinear optical parameters, experimental uncertainties in 2PA spectroscopy are still quite large (typically well above 10%). Reproducibility issues are encountered across laboratories and across techniques (for example, results obtained when a material is studied by using different techniques or setups are not always in agreement; for a selection of papers that discuss comparisons between different techniques, see [20–25]). The number of materials that can be used as reliable internal standards, though, has increased recently. An improved understanding and proper implementation of 2PA measurement techniques would be beneficial in furthering the development of this research area and for the effective use of improved nonlinear materials in technological applications.

In this contribution we provide an overview of the experimental methods most commonly used to measure 2PA spectra and cross sections. We do not aim at providing a comprehensive description of all the techniques and how to implement them in practice, as papers and reviews on a number of specific techniques have already been published (see [9,26–28] for overviews of the main methods used to date; [17,25,29] for in-depth discussion of fluorescence-based methods; [30–33] for transmission-based methods, specifically the Z-scan technique; and [34–38] for wave mixing methods). Additionally, many variations in the optical setups have been employed, and the techniques will continue to evolve with the commercialization of new generations of lasers and detectors. Our focus is on the *conceptual differences* between the various types of methods and how these are reflected in the choice of experimental conditions and analyses that can be employed. We will discuss the fundamental concepts behind the measurements and how the experimental observable of interest is related to the 2PA cross section. In particular, we will review the basic theory used to describe the process of two-photon absorption, and we will discuss the typical approximations underlying the measurement of 2PA spectra and cross sections for various techniques. In this context, we will elaborate on ways to judge the suitability of experimental conditions in various techniques, with particular emphasis on the identification of excitation regimes under which the method’s assumptions are satisfied. In particular, we will see that the *fractional change in molecular population in the ex-*

cited state during a laser pulse and the *fractional change in photon flux* are essential quantities for the selection of excitation regimes in the measurements and can prove useful for comparing results from the literature.

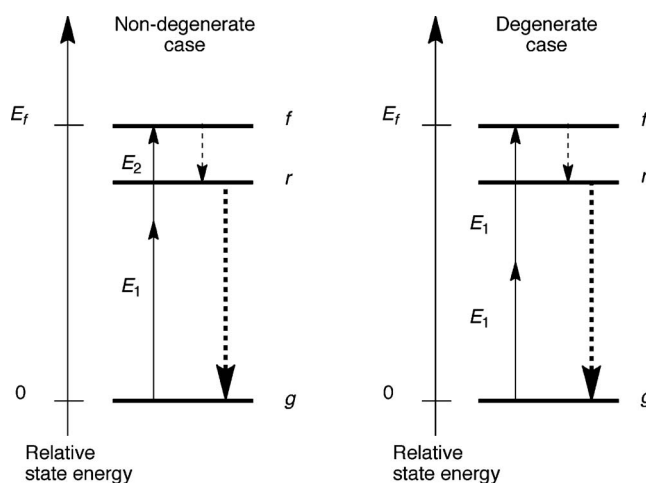
We will describe the possible influence of two-photon-induced excited state absorption (ESA) and other higher-order absorption processes in transmission-based 2PA measurements, and how such processes can lead to rather dramatic apparent pulse-width dependences of the 2PA cross section. Finally, we will compare the characteristics and merits of relative and absolute measurements.

Our aim is to provide a guide on basic issues in 2PA measurements that is accessible to researchers that are new to this area and a critical overview of the techniques and analytical tools for use in an assessment of results reported in the literature.

2. Experimental Techniques Used to Quantify 2PA

The process of two-photon absorption, first described theoretically in 1931 by Maria Göppert-Mayer [39], involves the simultaneous absorption of two photons (of energies E_1 and E_2) by a material system, for example a molecule, that occurs when the energy $E_1 + E_2$ is in resonance with one of the electronic states of the system. As a result of the absorption process, the two absorbed photons are lost from the excitation beams, correspondingly reducing their intensity, and the molecule is brought to an excited state (state f in Fig. 1), at $E_1 + E_2$ above the ground state (state g). This process can be thought of as an initial interaction of a

Figure 1



Schematic energy level diagram showing the excitation of a molecule from the ground state, g , to an excited state, f , located at energy E_f above the g state by the absorption of two photons (vertical solid arrows). The photons can have the same energy, E_1 (degenerate case, $E_f = 2E_1$), or different energies, E_1 and E_2 (nondegenerate case, $E_f = E_1 + E_2$). After excitation, the system relaxes quickly to state r , the lowest vibronic level of the lowest-energy excited state, by internal conversion or vibrational relaxation (dashed arrow). The system finally returns to the ground state by radiative or nonradiative pathways (bold dashed arrow).

photon of energy E_1 with the molecule, which is thus left in a temporary virtual state of energy E_1 above the ground state (similar to what occurs in Rayleigh scattering or nonresonant Raman scattering) [40,41]. This is not a real state (eigenstate) of the molecule and it exists only for a short time interval, τ_v . If during τ_v a photon of energy E_2 interacts with the molecule, it can be excited to state f . The order of magnitude for τ_v , which can be estimated from the uncertainty principle, is 10^{-15} – 10^{-16} s for photon energies in the visible and near-IR ranges [17,40,42]. The qualifier “simultaneous” for 2PA is used to indicate that the two photons interact with the molecule within the time τ_v and that no real states act as an intermediate state in this process. As in the case of 1PA, the existence of an electronic state of the appropriate energy, here $E_1 + E_2$, is not sufficient per se to lead to the absorption of the two photons. Symmetry selection rules also need to be satisfied for the 2PA process to be allowed. These selection rules have been derived and described within the dipole approximation in many contributions in the past [29,40,41,43]. The selection rules for 2PA are different from those for 1PA and, specifically in a system with an inversion center, transitions are two-photon allowed only if they connect states with the same symmetry with respect to the inversion operation. Thus, if the ground state is of *gerade* (even) symmetry, only other *gerade* states can be reached by a 2PA transition, whereas *ungerade* (odd) states are one-photon allowed. For molecules without an inversion center, this selection rule is not applicable; however, in all cases the symmetry species of the final electronic state and the polarization state of the excitation beam or beams determine which components of the two-photon tensor are active under given experimental conditions [44–47]. The two-photon tensor is, within the framework of the second-order perturbation theory for the interaction of a molecule with an electromagnetic field in the dipole approximation, a two-by-two matrix that can be expressed as a sum over all molecular electronic states, i , of terms of the form

$$\frac{(\mathbf{e}_1 \cdot \mathbf{M}_{gi})(\mathbf{M}_{if} \cdot \mathbf{e}_2)}{E_i - E_1}, \quad \frac{(\mathbf{e}_2 \cdot \mathbf{M}_{gi})(\mathbf{M}_{if} \cdot \mathbf{e}_1)}{E_i - E_2},$$

where \mathbf{e}_1 and \mathbf{e}_2 are the polarization vectors for the photons of energy E_1 and E_2 , and $\mathbf{M}_{\alpha\beta}$ is the transition dipole moment vector between states α and β [39,40,44,46–49]. In general, a transition from the ground state g to state f is symmetry allowed in 2PA if the two-photon tensor has components that transform as one of the ij symmetry operations (where $i, j = x, y, z$ are the Cartesian coordinates) [50].

The great majority of reports on measurement of 2PA cross sections in the literature refer to studies in which the following are true:

1. The two photons have the same energy: $E_1 = E_2$. This usually called the “degenerate” or “one-color” case (Fig. 1, right).
2. The two photons belong to the same excitation beam (or, equivalently, the two excitation beams are collinear).
3. The excitation beam is generated by a coherent source, such as a laser. Even though 2PA can occur when incoherent light is used, the 2PA transition probabilities are typically too small to give rise to detectable signals unless large excitation intensities, which can easily be achieved with lasers, are employed.
4. The excitation beam is linearly polarized.

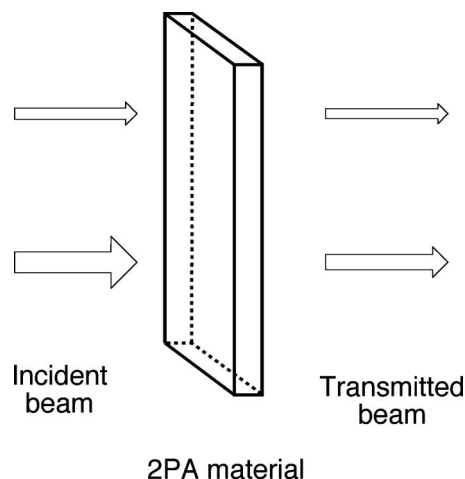
While these conditions may appear restrictive, they are the ones that can be more easily implemented for either the characterization of the 2PA process in a specific material or for use in a practical application. For example, two-photon-

induced fluorescence imaging [1,4,17,18,51] and two-photon-induced micro-fabrication (based on the activation of chemistry by 2PA) [14–16,52–55] have been developed making use of a single excitation beam. Similarly, optical limiting applications are implemented using one laser beam incident on a nonlinear absorbing material [6]. The mechanism of the suppression of the optical pulses derives from the fact that, because two photons are absorbed simultaneously, the transmittance of a 2PA material depends on the intensity of the incident beam, as illustrated schematically in Fig. 2. This will be discussed in detail in Subsections 2.1 and 3.2.

Some applications making use of nondegenerate or noncollinear beams have been described and may become more widespread once material properties under those conditions become better understood. For example, the writing schemes utilized for 3D optical data storage by Rentzepis and collaborators [2,56] involve two beams, one at 1064 nm and the other at 532 nm, intersecting spatially and temporally in the recordable medium. Another example is that of two-photon 4Pi confocal fluorescence microscopy, in which a sample is illuminated by two coherent beams (at the same wavelength) in counterpropagation directions and interfering constructively at the focal plane, and confocal illumination and detection are used, a configuration that results in an enhancement of resolution in the axial direction [57–59]. Interference of multiple beams originating from the same source has also been used for holographic recording in a photopatternable material in which the polymerization process is initiated by 2PA [60–62].

In this review we will focus on the case of degenerate 2PA (condition 1 above). Most of the techniques that have been employed also satisfy conditions 2–4. As the degenerate case has been more widely studied, a large number of characterization techniques have been developed using it. As discussed in detail in later sections, these techniques differ in how the effect of two-photon absorption on the material is monitored and in the range of excitation conditions necessary to

Figure 2



Schematic representation of the attenuation of a beam incident on a slab of material that exhibits two-photon absorption. Because of the nonlinear nature of the phenomenon, the transmittance of the material depends on the intensity of the incident beam (here represented by the width of the arrows): a weak beam (top) is absorbed to a smaller degree than an intense beam (bottom).

observe an effect. Because of these differences and the possible influence of other nonlinear effects or sources of noise, it is sometimes difficult to assess whether results obtained from the various techniques can be compared. Indeed, many examples can be found in the literature in which spectral features or cross section magnitudes for a given material vary significantly from laboratory to laboratory or from method to method (a few cases will be presented in Subsections 4.3c and 4.4). Fewer methods have been developed so far for the study of nondegenerate 2PA [63,64], and rarely have the different methods been applied to the same material, but uncertainty and repeatability issues are likely to surface in this area also.

One possible solution to the problems mentioned above would be the establishment of a protocol for measurements of 2PA spectra and cross sections, by selecting a measurement technique, conditions to be used for the excitation of the molecular system and the collection of the target signal, and standard procedures for the analysis of the data. Unfortunately, this possibility is not practical for various reasons, foremost of which is that a single technique and set of conditions is not flexible enough to be applicable to all sample types, and probably even all molecules, of interest. (For example, is it unlikely that the same conditions can be used for liquid samples and solid samples, for solutions over a wide range of concentrations, or for materials with fluorescence or phosphorescence yields differing by many orders of magnitude.) In the absence of a standard or preferred method, some guidelines need to be developed for how and when comparisons of measurements across methods (or implementations of methods) can be performed. The goal of this tutorial review is to provide an overview of the most commonly used methods and a critical discussion of the working principles, approximations, and applicability of those methods (Section 3).

Before discussing the main techniques used to measure 2PA cross sections, we begin with a brief review of the basic principles of the 2PA process. We use a phenomenological description of the 2PA process, mainly from a microscopic (or molecular) point of view: given an incident beam at the appropriate wavelength and a material, the 2PA process involves the loss of two photons from the beam and the promotion of one molecule to an excited state. The effect of 2PA can be quantified by introducing the parameter typically called the *2PA cross section*, δ [65,66]. The 2PA cross section can be defined by using the following form of the propagation equation for a beam of wavelength λ and angular frequency ω incident on a 2PA material:

$$\frac{d\phi}{dz} = -\delta N_g \phi^2, \quad (1)$$

where ϕ is the photon flux (number of photons per unit area and time), N_g is the number density of molecules in the ground state (number of molecules per unit volume) and z is the propagation direction [6,26]. If the material also exhibits 1PA at the same excitation wavelength, the propagation equation is written as

$$\frac{d\phi}{dz} = -\sigma N_g \phi - \delta N_g \phi^2 \quad (2)$$

where σ is the 1PA cross section. The dimensions of δ are $\text{length}^4 \times \text{time} / (\text{molecule} \times \text{photon})$ (or simply $\text{length}^4 \times \text{time}$) in both the SI and the cgs systems [67], and the dimensions for σ are $\text{length}^2 / \text{molecule}$. The photon flux is related to the beam intensity, I (power per unit area) by the photon energy,

$E_{\text{ph}} = hc/\lambda = \hbar\omega$ (h is Planck's constant and c the speed of light):

$$\phi = I/E_{\text{ph}}. \quad (3)$$

Substituting Eq. (3) into Eq. (2), the propagation equation can be expressed in terms of the beam intensity:

$$\frac{dI}{dz} = -\sigma N_g I - \frac{\delta}{E_{\text{ph}}} N_g I^2. \quad (4)$$

The quantity $\delta^* = \delta/E_{\text{ph}}$ is also often called 2PA cross section. Clearly the dimensions for δ^* , $\text{length}^4/(\text{molecule} \times \text{power})$, are different from those for δ [68]. Thus, a dimensional analysis or the observation of units used in the source unequivocally distinguishes between δ and δ^* . It should be kept in mind that, while both parameters depend on excitation wavelength because they reflect the spectral dependence of the probability of a two-photon transition in a material, δ^* also depends on λ through the term E_{ph} . As such, magnitudes of δ^* should not be compared directly from system to system if they refer to different excitation wavelengths.

Experimental methods in 2PA spectroscopy may be categorized as *direct*, *indirect*, and *wave mixing* techniques. Direct methods are based on the measurement of the beam attenuation after it traverses the absorbing medium (Subsection 2.1). In indirect methods, the quantity to be measured is one of the effects caused by the generation of population in the excited state r , reached after 2PA, such as fluorescence emission or heat produced (Subsection 2.2). Wave mixing techniques do not satisfy condition 2 described above, as they involve more than one beam, usually incident on the sample from different directions (Subsection 2.3).

2.1. Direct Methods

In direct methods, the effect of 2PA is observed as a decrease in the intensity of the excitation beam itself [Eq. (1)]. These methods can be thought of as extensions of techniques used to characterize 1PA by measuring the (linear) transmittance or absorbance of a sample. 2PA cross sections can be obtained by monitoring how the transmittance of a sample changes when the incident intensity changes (this can be performed, for example, by varying the pulse energy for a given spot size or the spot size for a given pulse energy). Nonlinear transmission and Z-scan measurements are examples of techniques in this category [26].

In a nonlinear transmission (NLT) experiment, a sample is placed in the path of the excitation beam and the pulse energy is measured before and after the sample. The measurement is repeated over a range of incident pulse energies. Because of the nonlinear absorption process, the transmittance depends on the incident energy. Knowing the optical configuration and pulse characteristics, it is possible to determine the 2PA cross section of the material [5,6,26].

In a Z-scan experiment, the pulse energy is kept constant, but changes in intensity are achieved by moving the sample along the propagation direction, z (hence the term “Z-scan”), of a focused beam and thus varying the beam cross sectional area [26,30,31]. The transmittance is measured at each position of the sample. For typical configurations (where the sample is thin, there is no 1PA, and all the transmitted light is collected), the transmittance is 1 when the sample is far from the focus of the beam, decreases as the sample is moved closer to the focus, and

reaches a minimum at the focus (where the intensity is maximum). The trend is reversed as the sample is moved away from the focus in the opposite direction.

A loss modulation scheme has also been used to measure 2PA cross sections by quantifying the change in transmittance in a sample due to 2PA [69]. In this case, the beam focused on the sample is also modulated at a given frequency (different from the repetition frequency of the laser), and the transmitted light is monitored and analyzed with a lock-in amplifier. The main difference with respect to the nonlinear transmission experiment mentioned earlier is that, in the modulation case, 2PA leads to the presence of a component of the signal at the second harmonic of the modulation frequency, which can be easily separated from the components at the modulation frequency or other frequencies, even if the overall change in transmittance is small.

2.2. Indirect Methods

A molecule that undergoes 2PA is promoted to an excited electronic state (Fig. 1). After an initial nonradiative relaxation from state f to state r , the remaining excitation energy is eventually released to the environment surrounding the molecule through one or more physical processes. Indirect methods monitor one of the possible outcomes of this de-excitation process as molecules return to the ground state g (bold dashed arrow in Fig. 1) or directly probe the excited state r or f .

The most commonly used indirect technique is the *two-photon-induced fluorescence* (2PIF) method, in which the intensity of the fluorescence emission induced by 2PA is measured [17,26,29]. In most cases, irrespective of the final state reached by 2PA (state f), a molecule relaxes quickly (typically within ~ 1 ps) [70,71] to the lowest vibronic level of the first excited state by internal conversion (state r), and from this state radiative or nonradiative relaxation to the ground state can take place (with a characteristic lifetime). By monitoring the intensity of this fluorescence signal, it is possible to obtain relative or absolute 2PA spectra (depending on what information is available on the emission properties of the material, the spatial and temporal characteristics of the excitation beam, and calibration of the detection system). This method is effectively the two-photon version of a fluorescence excitation experiment; thus spectra collected by using this technique are often called 2PIF excitation spectra.

It is possible, however, to follow the de-excitation of the molecules in other ways. For example, in materials with large intersystem crossing rates, the intensity of the *two-photon-induced phosphorescence* [72,73] emitted by the chromophore can be measured, as well as the phosphorescence from singlet oxygen, produced by oxygen quenching of the triplet state of the compound [74]. Because phosphorescence emission typically occurs on a time scale much longer than the fluorescence lifetime and the pulse duration, it may be possible to separate the desired signal from contributions due to fluorescence emission and scattering and thus reduce the background signal in the measurement [72]. Singlet oxygen phosphorescence can also be separated spectrally from other possible signals reaching the detector, further improving the sensitivity of the technique [74].

The *thermal lensing* (or *thermal blooming*) technique, instead, tracks nonradiative decay pathways from r to g by measuring the optical effects generated by the energy that is dissipated as heat in the host medium [75–78]. The released en-

ergy leads to a local increase in the temperature of the material and a consequent change in its refractive index. The details of the change in index and its evolution in time depend on the characteristic of the beam, the 2PA cross section of the material, the cross section for any other competitive absorption processes, and the thermal properties of the medium (such as thermal diffusivity and conductivity). The change in refractive index can be detected by monitoring the on-axis intensity of a weak probe beam collinear with the intense excitation beam. Alternatively, the change in temperature induced by 2PA absorption can be detected calorimetrically by using a thermocouple [79]. It is also possible to measure the pressure change or acoustic waves generated by the thermal gradient [80–83]. These methods are extensions of those developed for the measurement of weak 1PA effects in materials [84,85], for absolute measurements of fluorescence quantum yields [86–88], or for monitoring other photoinduced physical processes [89].

In *multiphoton ionization (MPI) spectroscopy*, 2PA is characterized by measuring the ion current generated after molecules are first excited by 2PA and then ionized by absorption of one or more additional photons, before they can relax to the ground state [90].

An alternative indirect method based on a *pump–probe approach* has also been proposed and utilized [91]. In this method, a first beam is used to pump the sample by 2PA. Photons from the second beam (probe), also focused in the sample, can be absorbed by molecules that are in the lowest excited state after 2PA. The absorbance for this ESA process is proportional to the population of molecules in the excited state and thus to the 2PA cross section and the square of the pump pulse energy.

2.3. Wave Mixing Techniques

The 2PA cross section is a component of the third-order polarizability γ or susceptibility $\chi^{(3)}$, which is an overall measure of nonlinear optical effects in a material that depend on the third power of the electric field of the incident monochromatic beam (or the product of three electric field intensities in a nondegenerate case) [26]. In-depth descriptions of the parameters γ or $\chi^{(3)}$, as well as the various conventions used to define them, can be found in various texts on nonlinear optics [92] and will not be covered here. For our purposes it is sufficient to mention that δ is proportional to the imaginary part of γ or $\chi^{(3)}$, as it describes a dissipative process; that the frequency arguments of γ and $\chi^{(3)}$ are usually expressed in a parenthesis after the parameter, for example $\gamma(-\omega_s; \omega_1, \omega_2, \omega_3)$ (where ω_i is the angular frequency of one of the interacting fields and $\omega_s = \omega_1 + \omega_2 + \omega_3$ is the angular frequency of the polarization component of interest); and that γ or $\chi^{(3)}$ are tensorial quantities (the component of the tensor is usually identified by four subscripts, representing the polarization directions of the induced polarization vector and of the three interacting electric fields) [92]. For a derivation of the relationship between δ and $\chi^{(3)}$ the reader is referred, for example, to Dick *et al.* [93] (it should be pointed out, though, that the proportionality constant between δ and $\chi^{(3)}$ depends on the conventions and definitions used for the nonlinear optics parameters and the electric field vector, and these should be explicitly stated when discussing experimental results).

When two or more laser beams overlap in space and time inside a material, its nonlinear properties can lead to induced polarization at certain frequencies, with

the generation of new beams (at the same or other frequencies) or the transfer of intensity from one beam to another. Some of these effects depend on the 2PA properties of the material (the frequency arguments for degenerate 2PA are $(-\omega; \omega, \omega, -\omega)$). Examples of these techniques, which by definition involve the use of more than one excitation beam, are the following:

- *Coherent anti-Stokes Raman scattering (CARS)*: two beams at frequencies ω and $\omega - \Delta\omega$ are overlapped in the nonlinear material and generate a third beam at frequency $\omega + \Delta\omega$. The intensity of this beam depends on those of the incident beams and on the susceptibility component $\chi^{(3)}(-\omega - \Delta\omega; \omega, \omega, -\omega + \Delta\omega)$, which in turn is related to the degenerate 2PA cross section δ of the material if $\Delta\omega \ll \omega$. $\Delta\omega$ is scanned in the range of one of the characteristic vibrational frequencies of the sample. The experiment can be performed under phase-matching conditions. The 2PA cross section can be determined relative to the absolute Raman scattering cross section of one of the solvent vibrational modes [94–96].
- *Degenerate four-wave mixing (DFWM)*: three beams at frequency ω overlap in space and time in a nonlinear material; a fourth beam at the same frequency is generated in the material in a direction determined by the phase-matching condition. This can be viewed as the diffraction of one of the incident beams from a grating formed by the interference of the other two beams in the material. The intensity of the diffracted beam is proportional to $|\chi^{(3)}(-\omega; \omega, \omega, -\omega)|^2$ and to the intensity of the three incident beams [26,37,97,98]. Various geometrical configurations can be chosen for the incident beams. By measurement of the generated beam intensity as a function of concentration of the nonlinear material, it is possible to determine both the real and imaginary components of $\chi^{(3)}(-\omega; \omega, \omega, -\omega)$. Measurements are typically performed using a solvent or other materials with known and real values of $\chi^{(3)}$ as reference. The effect of thermal gratings or population gratings may have to be included in the analysis if long pulses are used or the fraction of molecules in the excited state is significant [97,98].
- *Optical Kerr effect*: a strong pump beam at frequency ω_1 and a weak probe beam at frequency ω_2 , with polarization directions at 45° with respect to each other, cross at a small angle in the material, and the intensity of the transmitted beam depends on the difference of two susceptibility components: $\chi^{(3)}_{XXXX}(-\omega_2; \omega_2, \omega_1, -\omega_1) - \chi^{(3)}_{XXYY}(\omega_2; \omega_2, \omega_1, -\omega_1)$. This technique can utilize degenerate or nondegenerate excitation conditions. Various experimental and detection schemes have been described that allow the independent measurement of the real and imaginary parts of the hyperpolarizability difference [99,100].

In many cases, these techniques were originally developed to measure nonlinear optical parameters other than 2PA cross sections, and general details on experimental designs and measurement principles can be found in various textbooks and reviews on nonlinear optics. These techniques will not be discussed further in this contribution (except for some final remarks in Subsection 5.3), in light of the fact that they are not yet widely used in the field of 2PA spectroscopy.

3. 2PA Excitation Rates and Conditions to Avoid Beam Depletion and Saturation

3.1. Indirect Methods

The attenuation of a beam due to 2PA can be described by Eq. (1) of Section 2 (we assume here and in the rest of Section 3 that there is no 1PA from the material at this wavelength). As $d\phi/dz$ represents the rate of attenuation of the number of photons by 2PA along the propagation direction, the number of photons absorbed by the material per unit time and volume, $n_{\text{ph}}^{(2)}$, is [17,29,43]

$$n_{\text{ph}}^{(2)} = -\frac{d\phi}{dz} = \delta N_g \phi^2. \quad (5)$$

Similarly, the number of molecules excited per unit time and volume, $n_m^{(2)}$, is

$$n_m^{(2)} = \frac{1}{2} n_{\text{ph}}^{(2)} = \frac{1}{2} \delta N_g \phi^2. \quad (6)$$

Equation (6) can also be viewed as a definition of the 2PA cross section. The factor of 1/2 in Eq. (6) accounts for the fact that two absorbed photons produce one excited molecule. It should be mentioned that alternative definitions can be found in the literature [101–104]. Differences in parameter definitions, choice of units, and other conventions should be taken into account when results from different sources are compared.

In general, in Eq. (1) both ϕ and N_g depend on the spatial coordinate in the sample and on time. N_g is not constant because, as photons are absorbed, molecules are promoted to an excited state, and they cannot be excited further by 2PA until they return to the ground state [105], reducing the effective density of molecules with respect to the initial value, N_0 (total number of molecules per unit volume). Except for cases of very fast relaxation (that is, when the fluorescence lifetime of the excited state τ_{fl} , or more generally the ground state recovery time, is much shorter than the pulse duration, $\tau_{\text{fl}} \ll \tau$), N_g at time t , $N_g(t)$, depends not only on the photon flux at that time, but also on the total number of photons absorbed since the beginning of the pulse and can be written as

$$N_g(t) = N_0 - \int_0^t n_m^{(2)}(t') dt', \quad (7)$$

where the quantity $n_m^{(2)}$, which can also be time dependent, is integrated from the beginning of the pulse (time 0) to the desired time t . After substituting Eq. (7) into Eq. (1), the latter needs to be solved simultaneously with the rate equations for the population of all the states involved in the transition and by taking into account explicitly the spatial and temporal characteristic of the excitation beam. In many instances, this system of coupled differential equations can only be solved numerically.

Here we consider mainly simple cases in which analytical solutions can be obtained and discuss how these solutions are applied in practice for the measurement of 2PA cross sections. We will discuss some of the implications of the approximations made to obtain these solutions.

Let us consider the case of a beam that is collimated over the length of the sample (L), has constant intensity over the beam cross section a ($a = \pi w_0^2$), has pulse duration τ , and a rectangular profile in time (that is, the intensity is constant from time 0 to time τ , then it drops to zero until the next pulse arrives at time $1/f$, f being the repetition rate). It is also assumed that the excitation is instantaneous on the time scale of the excited state lifetime ($\tau \ll \tau_{\text{fl}}$) and that after excitation by one pulse the molecules and host medium relax completely before the arrival of the following pulse ($1/f \gg \tau_{\text{fl}}$). In this situation, the material is in the same condition every time a new pulse arrives, and the total number of photons absorbed or emitted is additive in the number of pulses.

If the number of photons absorbed per pulse is small [approximation (i); we will quantify this below], the total number of molecules excited (per unit volume) during each pulse, $N_m^{(2)}(\tau)$, can be obtained as follows. At each time t , $n_m^{(2)}$ has to be the opposite of the change in the population density for state g between time t and $t+dt$, because the total number of molecules is conserved:

$$n_m^{(2)} = - \frac{dN_g}{dt}. \quad (8)$$

Thus, Eq. (6) becomes

$$\frac{dN_g}{dt} = - \frac{1}{2} \delta N_g \phi^2, \quad (9)$$

which, after integration between $t=0$ and $t=\tau$ and using $N_g(0)=N_0$, gives

$$N_g(\tau) = N_0 e^{-(1/2)\delta\phi^2\tau}. \quad (10)$$

The total number of molecules excited (per unit volume) during each pulse is thus

$$N_m^{(2)}(\tau) = N_0 - N_g(\tau) = N_0(1 - e^{-(1/2)\delta\phi^2\tau}). \quad (11)$$

Further, if the argument of the exponential function in Eq. (11) is small $[(1/2)\delta\phi^2\tau \ll 1]$, the expression can be approximated by

$$N_m^{(2)}(\tau) \approx \frac{1}{2} \delta\phi^2 \tau N_0. \quad (12)$$

In all indirect methods, the measured signal is proportional to $N_m^{(2)}(\tau)$, whether it is represented by induced fluorescence in 2PIF experiments, heat deposited in the solvent by nonradiative relaxation in thermal lensing experiments [75,78], number of molecules ionized through the absorption of an additional photon or photons in multiphoton ionization experiments [90], or the population of an excited state probed by a second beam [91,106]. For example, the intensity of the 2PA induced fluorescence signal per unit volume, S , reaching a detector after each pulse is

$$S \propto \eta G N_m^{(2)}(\tau) \approx \frac{1}{2} \eta G \delta\phi^2 \tau N_0, \quad (13)$$

where η is the fluorescence quantum yield of the molecule [107] and G is a collection efficiency factor that depends on the optical geometry of the excitation

and detection components of the experiments, the excitation volume, the wavelength dispersion of optics and detectors, and the refractive index of the solvent (see also Subsection 4.4). For other indirect measurements, equations similar to relation (13) can be written by including appropriate yields and efficiencies for each case. An example of the dependence of the thermal lensing signal on the power of laser excitation beam is shown in Fig. 3, where the solid curve represents the best quadratic fit to the experimental data points.

The fraction of molecules excited per pulse can be derived from Eq. (11) as

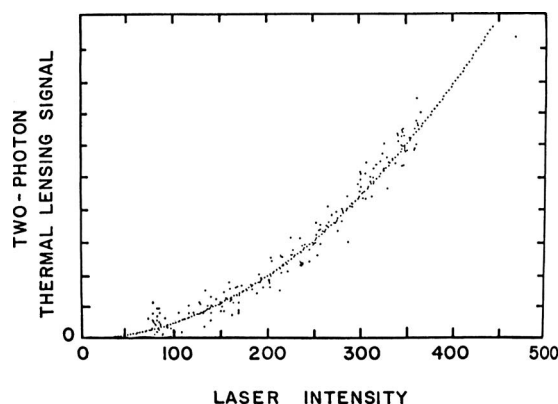
$$\Delta_m^{(2)} = \frac{N_m^{(2)}(\tau)}{N_0} = (1 - e^{-(1/2)\delta\phi^2\tau}), \quad (14)$$

which, if the exponent of e is small, becomes

$$\Delta_m^{(2)} \approx \frac{1}{2}\delta\phi^2\tau. \quad (15)$$

Thus, the approximation used to go from Eq. (11) to Eq. (12) corresponds to a situation in which only a small fraction of molecules is excited per pulse; that is, the ground state of the system is far from being depleted during the pulse [108]. [We will call this situation approximation (ii).] The error in using the approximate [Eq. (15)] or “exact” [Eq. (14)] [109] forms of $\Delta_m^{(2)}$ is about $(1/2)\Delta_m^{(2)}$. It has been recommended that $\Delta_m^{(2)}$ be kept below 1% [29]. It should be pointed out that if approximations (i) and (ii) are valid under a given set of experimental conditions, Eq. (15) can be derived simply from Eq. (6) after multiplying the right-hand side by τ and dividing by N_0 . If approximation (ii) is not valid for a given set of experimental conditions, then the right-hand side of Eq. (13), that is, the dependence of a measured signal on the square of the incident photon flux, is also not applicable.

Figure 3



Magnitude of thermal lensing signal induced by 2PA as a function of the laser intensity of the excitation beam. The dotted line is the best fit of the data points to $\text{signal} = AI^2$, where A is a constant and I is the laser intensity. Sample, toluene; excitation wavelength $\lambda = 497.5$ nm. Reproduced with permission from Rice and Anderson [78]. Copyright 1986 American Chemical Society.

We shift now from the perspective of the 2PA material to that of the beam propagating through it and calculate the number of photons absorbed by the material during each pulse. The total number of photons, N_{ph} , in a pulse of energy E and the photon flux for the beam configuration described above (cylindrically symmetric beam, with uniform profile in time and space) can be expressed, respectively, as

$$N_{\text{ph}} = \frac{E}{E_{\text{ph}}} = E \frac{\lambda}{hc}, \quad (16)$$

$$\phi = \frac{N_{\text{ph}}}{a\tau} = \frac{1}{\pi w_0^2 \tau} \frac{E}{E_{\text{ph}}} = \frac{\lambda E}{\pi w_0^2 \tau hc}. \quad (17)$$

The number of photons absorbed per pulse can be obtained from Eq. (12) and the excitation volume, $V=aL$ (as before, based on our definition of δ , the factor of 2 indicates that two photons are absorbed per molecule excited) [110]:

$$N_{\text{ph}}^{(2)}(\tau) = 2N_m^{(2)}(\tau)V \approx \delta\phi^2\tau N_0\pi w_0^2L. \quad (18)$$

Then, the fraction of photons absorbed can be obtained from the ratio of Eqs. (18) and (16):

$$\Delta_{\text{ph}}^{(2)} = \frac{N_{\text{ph}}^{(2)}(\tau)}{N_{\text{ph}}} \approx \delta\phi N_0L. \quad (19)$$

In summary, Eqs. (15) and (19) define the *fraction of molecules excited* and the *fraction of photons absorbed* per pulse by 2PA, respectively. $\Delta_m^{(2)}$ and $\Delta_{\text{ph}}^{(2)}$ are directly proportional to δ , but their dependence on ϕ is different. $\Delta_{\text{ph}}^{(2)}$ is proportional to N_0 , and the sample concentration can be used to control this parameter independently of $\Delta_m^{(2)}$. (However, the overall indirect signal will also be proportional to N_0 .) In some cases it may be more convenient to express these equations as a function of the number of photons per pulse, instead of the photon flux:

$$\Delta_m^{(2)} \approx \frac{\delta N_{\text{ph}}^2}{2\tau(\pi w_0^2)^2}, \quad (20)$$

$$\Delta_{\text{ph}}^{(2)} \approx \frac{\delta N_{\text{ph}} N_0 L}{\pi w_0^2 \tau}. \quad (21)$$

At the same time, these equations define their own limits of applicability, because they were derived assuming small beam depletion [approximation (i)] and negligible ground state depletion [approximation (ii)], that is

$$\textbf{approximation (i): } \Delta_{\text{ph}}^{(2)} \ll 1 \text{ or } \delta\phi N_0L \ll 1, \quad (22)$$

$$\textbf{approximation (ii): } \Delta_m^{(2)} \ll 1 \text{ or } \frac{1}{2}\delta\phi^2\tau \ll 1. \quad (23)$$

As mentioned above, the dependence on photon flux is different for $\Delta_m^{(2)}$ and $\Delta_{\text{ph}}^{(2)}$, and thus the threshold photon flux under which approximation (i) is valid is generally not the same as the one for approximation (ii). All the equations written up to now are valid only if *both* conditions are met. The experimental conditions for

Approximation (i): $\Delta_{\text{ph}}^{(2)} \ll 1$ or $\delta\phi N_0 L \ll 1$,

Approximation (ii): $\Delta_m^{(2)} \ll 1$ or $\frac{1}{2}\delta\phi^2\tau \ll 1$.

2PIF measurements or the other indirect techniques introduced in Subsection 2.2 should be chosen to fall in this excitation regime. However, it is quite easy to achieve high excitation rates, especially for molecules with large 2PA cross sections and long laser pulses. When the conditions of Eqs. (22) and (23) are not met, the linearity of the induced fluorescence signal or of the thermal lensing signal with concentration of the 2PA absorber is lost, as well as the dependence of those signals on the square of the pulse energy. This is true even in the ideal case where the material does not exhibit any ESA or photodegradation, and if the probability of stimulated emission is negligible. Approximation (i) is basically an extension of the requirement behind the optically dilute solutions method for the measurements of fluorescence quantum yields [113], because when the optical density of the sample is low, the one-photon excitation rate is constant along the path length and the fluorescence intensity is directly proportional to the concentration of molecules and the intensity of the light source [114]. We will see in Subsection 3.2 that this requirement can be relaxed in the case of direct measurements of 2PA cross sections. In addition to restricting the range of photon fluxes that can reliably be used in indirect 2PA measurements, Eqs. (22) and (23) also impose some limits on the concentration of the sample. In fact, even if $\Delta_m^{(2)}$ does not depend on N_0 [Eq. (22)], the detected signal S does [Eq. (13)]. However, $\Delta_{\text{ph}}^{(2)}$ is also directly proportional to N_0 [Eq. (23)], and thus S cannot be increased indefinitely by simply using higher concentrations [115].

Only a fraction of the papers reporting 2PA spectra or cross sections provide all the optical configuration details necessary to estimate $\Delta_m^{(2)}$ and $\Delta_{\text{ph}}^{(2)}$. However, a wide range of excitation regimes has been used over time and across laboratories [20,74,101,116–120]. Some numerical examples are considered in detail below.

3.1a. High-Repetition-Rate Femtosecond Laser, Collimated Beam

If $\tau=100$ fs, $f=80$ MHz, $E=1.25$ nJ (this corresponds to an average power of 100 mW), $\lambda=800$ nm ($E_{\text{ph}}=2.48 \times 10^{-19}$ J/photon), $w_0=50$ μm , $L=1$ cm, $N_0=6.0 \times 10^{16}$ molecules/cm³ (molar concentration 1.0×10^{-4} M), and $\delta=1000$ GM, from Eqs. (16), (17), (15), and (19), we obtain

$$N_{\text{ph}} = 5.0 \times 10^9 \text{ photons/pulse,}$$

$$\phi = 6.4 \times 10^{26} \text{ photons cm}^{-2} \text{ s}^{-1},$$

$$\Delta_m^{(2)} = 2.1 \times 10^{-7},$$

$$\Delta_{\text{ph}}^{(2)} = 3.9 \times 10^{-4}.$$

These conditions are similar to those employed in the experiments described by Strehmel *et al.* [118] (the authors do not report the beam size, but they mention

that it is collimated over 1 cm, so the beam cannot be much smaller than what was used in this example). It is clear that approximations (i) and (ii) are valid in this case.

As the number of photons absorbed per pulse is quite low under these experimental conditions, the intensity of the induced fluorescence signal (or of the signal corresponding to any other 2PA-induced change) is also small. Detection of this signal may thus require integrating the response over a large number of pulses. When this type of detection scheme is chosen, care must be taken to ensure the maximum stability of the laser system and the minimum level of electronic and background noise [121], because the results could be biased in a way that is hard to track in both relative and absolute measurements if the laser exhibits significant intensity instability over the integration time.

3.1b. Amplified Femtosecond Laser, $f/15$ Focusing

If $\tau=160$ fs, $f=1$ kHz, $E=50$ nJ (average power $50 \mu\text{W}$), $\lambda=800$ nm ($E_{\text{ph}}=2.48 \times 10^{-19}$ J/photon), $w_0=15 \mu\text{m}$ (approximately an $f/15$ configuration), $L=0.1$ cm (of the order of the Rayleigh range for this optical configuration), $N_0=3.0 \times 10^{15}$ molecules/cm³ (molar concentration 5.0×10^{-6} M), and $\delta=1000$ GM, this time we obtain

$$N_{\text{ph}} = 2.0 \times 10^{11} \text{ photons/pulse,}$$

$$\phi = 1.8 \times 10^{29} \text{ photons cm}^{-2} \text{ s}^{-1},$$

$$\Delta_m^{(2)} = 2.5 \times 10^{-2},$$

$$\Delta_{\text{ph}}^{(2)} = 5.4 \times 10^{-4}.$$

It can be seen that these experimental conditions are at the limit where approximation (ii) holds. Conditions similar to the ones in the example were used in the experiments described by Lee *et al.* [120]. Higher photon fluxes or 2PA cross sections would lead to a situation where a significant fraction of molecules are in the excited state and thus to deviations from the expected behavior of the signal on pulse energy even for femtosecond (fs) excitation. For example, using the same pulse energy but focusing the beam tighter to a spot size of $w_0=10 \mu\text{m}$ would lead to $\Delta_m^{(2)}=0.13$, a value too large to be recommended, unless ground state depletion is explicitly considered in the data analysis.

It can also be noted that, even if the numerical case considered in this section leads to a significantly larger value of $\Delta_m^{(2)}$ and a slightly larger $\Delta_{\text{ph}}^{(2)}$ than the case of Subsection 3.1a, which considered a high-repetition rate fs laser and a gentler focusing, the total signal collected per unit time (a quantity proportional to $N_m^{(2)}(\tau) \times V \times f$) is three orders of magnitude larger in case 3.1a than in the current one. This difference can only be compensated in part by an increase in concentration, which is a factor of 20 smaller in the current situation. Thus adequate signal levels can be achieved even without amplified ultrafast laser systems.

This example also shows that it is not always advantageous to conduct the experiment with a very high photon flux or peak power, as pointed out early on by Birge [29]. Apart from the breakdown of the approximations (which can be overcome by solving the coupled equations numerically), a high flux can be reached today only by using lasers with modest repetition rate and high peak power (at

least for systems that are commercially available) and by focusing the beam to a relatively small spot size. This necessarily limits the available excitation volume and thus the number of photons absorbed per pulse [122]. This is illustrated in Fig. 4: the number of molecules excited over the whole excitation volume, $N_m^{(2)}(\tau) \times V$ [Eq. (12)], which is proportional to the total signal collected after each pulse, increases linearly with the path length for thin samples:

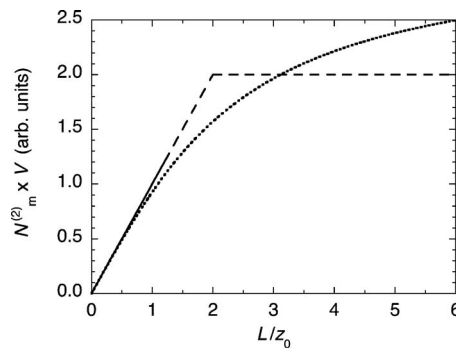
$$N_m^{(2)}(\tau)V = \frac{1}{2} \delta\phi^2 \tau N_0 (\pi w_0^2 L) = \frac{\delta N_0 N_{ph}^2}{2\tau} \frac{L}{\pi w_0^2} = \frac{\delta N_0 N_{ph}^2}{2\tau} \frac{nL}{\lambda z_0} \quad (\text{for } L < 2z_0). \quad (24)$$

However, when the path length exceeds a certain limit (here chosen to be twice the Rayleigh range, $L = 2z_0$; see also note [110]), $N_m^{(2)}(\tau) \times V$ levels off to the following value:

$$N_m^{(2)}(\tau)V \approx \frac{1}{2} \delta\phi^2 \tau N_0 \left(\pi w_0^2 \left(\frac{2\pi w_0^2 n}{\lambda} \right) \right) = \frac{\delta N_0 N_{ph}^2}{2\tau} \frac{2n}{\lambda} \quad (\text{for } L > 2z_0). \quad (25)$$

Any additional increase in path length does not lead to any gain in signal strength, because of the decrease in intensity away from the focal plane. The situation portrayed by Eq. (25) (and dashed straight lines in Fig. 4) is oversimplified, as we assumed for simplicity that no excitation occurs outside the cylinder of length $2z_0$. In more realistic situations the transition between the two regimes occurs gradually, but an asymptotic behavior is still reached for long path lengths. One such case is included in Fig. 4 for a Gaussian beam [123]. The results in Fig. 4 also indicate that, for a given pulse energy (fixed value of N_{ph}),

Figure 4



Number of molecules excited over the whole excitation volume, $N_m^{(2)}(\tau) \times V$, as a function of path length in the sample. For $L < 2z_0$, V is assumed to be $\pi w_0^2 L$, and the system response is given by Eq. (24) (straight line through the origin). For $L > 2z_0$, $V = 2\pi w_0^2 z_0$, and the system response is governed by Eq. (25) (horizontal line). The dashed portion of these lines represents the regions where Eqs. (24) and (25) are to be considered approximate estimates. For comparison, the total number of molecules excited by a beam with a Gaussian spatial profile (obtained by integrating the appropriate value of $N_m^{(2)}(\tau)$ over the excitation volume, $\int_V N_m^{(2)}(\tau) dV$) is shown for comparison (dotted curve). N_{ph} is the same in all cases.

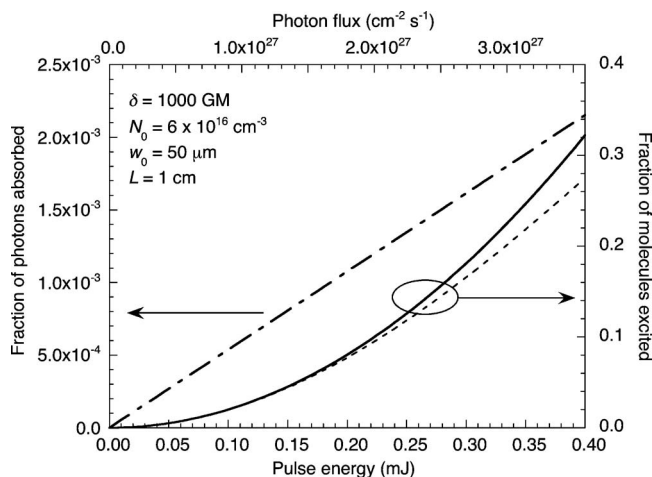
there is no advantage in decreasing the spot size below a value for which $z_0 \ll L/2$, because any local increase in photon flux (and thus excitation rate) is compensated by a decrease in the excitation volume [122].

3.1c. Nanosecond Laser, Collimated Beam

Let us consider now the following situation: $\tau=5$ ns, $f=10$ Hz, $\lambda=700$ nm ($E_{\text{ph}}=2.84 \times 10^{-19}$ J/photon), $w_0=50$ μm , $L=1.0$ cm, $N_0=6.0 \times 10^{16}$ molecules/ cm^3 (molar concentration 1.0×10^{-4} M), $\delta=1000$ GM. The fraction of molecules excited and of photons absorbed are displayed in Fig. 5 as a function of pulse energies up to $E=0.4$ mJ (average power 4 mW).

It can be clearly seen from Fig. 5 that it is quite easy to approach optical saturation of the 2PA transition by using nanosecond (ns) pulses: in this example more than 10% of the molecules are excited by a 0.25 mJ pulse. (Saturation was also illustrated in one of the numerical examples discussed by Birge [29], page 138, where about 1/3 of molecules could be excited by a focused ns laser beam even with $\delta=20$ GM.) The implications for 2PA experiments when molecules can undergo ESA after 2PA will be discussed in Subsection 4.3. Measurements with an optical setup of this type should be conducted by using pulse energies not exceeding 0.05–0.1 mJ (this excitation regime is very similar to the one used in our own laboratory [119,124]). If the pulse energy is kept within this range, both $\Delta_m^{(2)}$ and $\Delta_{\text{ph}}^{(2)}$ are very similar to those reported above for the amplified fs laser case 3.1b, while the photon flux is comparable with that obtained in the high-repetition-rate fs case 3.1a. Thus, if the experiment is conducted properly, there are no *a priori* reasons why indirect measurements in the ns regime cannot be employed to provide intrinsic 2PA cross sections (see also Subsection 4.3). Because of the large number of photons per pulse in the ns case, it is usually possible to record signals S for each pulse and, with appropriate monitoring of the pulse energy, to correct for shot-to-shot fluctuations of the laser system.

Figure 5



Fraction of photons per pulse absorbed $\Delta_{\text{ph}}^{(2)}$ (left-hand axis) and of molecules excited $\Delta_m^{(2)}$ (right-hand axis) by 2PA for 5 ns, 10 Hz pulses at 700 nm (see legend for list of other parameters) as a function of pulse energy; the solid curve is from the approximate Eq. (15), the dashed curve from Eq. (14).

3.2. Direct Methods

Many of the concepts introduced above are also applicable to direct measurements. However, in this case approximation (i) usually needs to be relaxed; otherwise the quantity $\Delta_{\text{ph}}^{(2)}$ is too small to be measurable with sufficient precision in commonly used detection schemes. (It is usually hard to measure a small change in a large signal; increases in sensitivity in this type of measurements can be achieved, though, by modulation of the input intensity and lock-in detection of the signal [69].) If approximation (ii) is still valid (so that $N_g \approx N_0$) and we again consider a pulse with a square profile in time, Eq. (1) can be easily solved by dividing both sides of the equation by ϕ^2 , integrating over space, and using the initial condition for the flux $\phi(0)$ at $z=0$:

$$\begin{aligned}\frac{d\phi}{\phi^2} &= -\delta N_0 dz, \\ \int \frac{d\phi}{\phi^2} &= -\int \delta N_0 dz, \\ -\frac{1}{\phi} + \frac{1}{\phi(0)} &= -\delta N_0 z.\end{aligned}\tag{26}$$

Thus, the photon flux is given by the following equation at every position z in the sample over which the diameter of the beam is constant (for clarity, the argument, z , of the flux is shown explicitly):

$$\phi(z) = \frac{\phi(0)}{1 + \delta N_0 z \phi(0)}.\tag{27}$$

In principle, a single measurement of the pulse energy before and after a sample could lead to an estimate of the 2PA cross section of a material by using Eq. (27). In practice, however, this measurement would not be very precise, because the uncertainty in δ would typically be much larger than the uncertainty in each pulse energy measurement [125] [δ is proportional to the difference between two quantities with similar values, $\phi(0)^{-1}$ and $\phi(z)^{-1}$; see Eq. (26)]. The experiments are instead conducted by repeating the measurement for various photon flux values (either by changing the pulse energy as in NLT measurements, or the beam size at the sample, as in Z-scans). Equation (27) or equations derived from it can then be used to determine 2PA cross sections, as described in the following subsections.

3.2a. Collimated Beam, Rectangular Profile in Space and Time

When the beam is collimated over the length of the sample and has a rectangular profile in space and time, the transmittance of a sample (of length L) and the fraction of photons absorbed are, respectively,

$$T = \frac{\phi(L)}{\phi(0)} = \frac{1}{1 + \delta N_0 L \phi(0)},\tag{28}$$

$$\Delta_{\text{ph}}^{(2)} = 1 - T = \frac{\delta N_0 L \phi(0)}{1 + \delta N_0 L \phi(0)}. \quad (29)$$

It can be easily seen that for $\delta N_0 L \phi \ll 1$, the fraction of photons absorbed given in Eq. (29) reduces to Eq. (19); also, for a nominal value of the flux, the number of photons absorbed is smaller as expressed in Eq. (29) than in Eq. (19), because the latter portion of the sample experiences a lower flux, as the beam is being attenuated by the front sections of the sample. The transmittance in Eq. (28) is equivalent to the typical expression used to fit data in NLT experiments:

$$1/T = 1 + \beta IL, \quad (30)$$

where $\beta = \delta N_0 / E_{\text{ph}}$ [126], and I is related to ϕ by Eq. (3) [6,26,127]. NLT experiments are usually conducted at larger concentrations than those used in indirect measurements. In this way, $\Delta_{\text{ph}}^{(2)}$ can be increased without affecting $\Delta_m^{(2)}$, which is independent of concentration. For example, in a situation similar to the case detailed in Subsection 3.1c but with a concentration two orders of magnitude larger, $N_0 = 6.0 \times 10^{18}$ molecules/cm³ (1.0×10^{-2} M), a beam attenuation of 10% can be achieved for $\delta N_0 L \phi = 0.11$ and a corresponding pulse energy of $E = 0.21$ mJ ($I = 5.3 \times 10^8$ W/cm² with $\beta = 0.21$ cm/GW). The corresponding fraction of excited molecules is $\Delta_m^{(2)} \approx 8.2\%$ (see Fig. 5), which is quite large. This implies that in NLT measurements with ns pulses the energy range should be chosen in such a way that the lowest transmittance be above 90% (or even higher for molecules expected to have very large cross sections), if the data analysis utilizes Eqs. (28)–(30) (or similar ones for other beam shapes) [128]. This small dynamic range could limit the accuracy of the measurement, especially if the laser exhibits large pulse energy instability. A similar argument applies to the case of excitation with amplified fs pulses, which also leads to high $\Delta_m^{(2)}$, as shown in Subsection 3.1b. Unfortunately, the experimental conditions described in many reports on NLT experiments led to relatively large beam attenuations and $\Delta_m^{(2)}$ values. Only if the time evolution of the state populations during the excitation pulse is explicitly accounted for in the analysis of the data is it safe to expand the dynamic range of the experiment to where approximation (ii) is not satisfied.

3.2b. Collimated Beam, Gaussian Profile in Space, Rectangular Profile in Time

If the flux (or intensity) of the beam is not constant across its section, but has a Gaussian profile [129],

$$\phi(0, r) = \phi(0, 0) e^{-2r^2/w_0^2}, \quad (31)$$

w_0 being defined by the points at which the flux is reduced to $1/e^2$ of the maximum value, then the decrease in photon flux due to 2PA is consequently not uniform across the beam, because the number of photons absorbed is largest where the flux is most intense, that is, near the optical axis, and becomes progressively smaller away from the optical axis. It follows that the profile of the beam does not remain Gaussian as it propagates through the sample. Equation (27) is not valid for the overall flux of the beam, but it can still be used to describe the local changes in the flux for each point in the beam cross section. The pulse energy after a path length L (if $L \ll z_0$) in the 2PA material for pulses with a rectangular time profile with width τ can be obtained as follows, integrating Eq. (27) over the beam cross section and for an initial flux given by Eq. (31):

$$\begin{aligned}
E(L) &= \tau E_{\text{ph}} \int_0^\infty \phi(L, r) 2\pi r dr \\
&= \tau E_{\text{ph}} \int_0^\infty \frac{\phi(0, r)}{1 + \delta N_0 L \phi(0, r)} 2\pi r dr \\
&= \tau E_{\text{ph}} \int_0^\infty \frac{\phi(0, 0) e^{-2r^2/w_0^2}}{1 + \delta N_0 L \phi(0, 0) e^{-2r^2/w_0^2}} 2\pi r dr \\
&= \tau E_{\text{ph}} \frac{\pi w_0^2}{2 \delta N_0 L} \ln(1 + \delta N_0 L \phi(0, 0)).
\end{aligned} \tag{32}$$

The transmission of the material (defined in this case as the ratio between the energy of the pulse before, $E(0)$ [130], and after, $E(L)$, the sample) is [6,26]

$$T = \frac{E(L)}{E(0)} = \frac{\tau E_{\text{ph}} \frac{\pi w_0^2}{2 \delta N_0 L} \ln(1 + \delta N_0 L \phi(0, 0))}{\tau E_{\text{ph}} \frac{\pi w_0^2}{2} \phi(0, 0)} = \frac{\ln(1 + \delta N_0 L \phi(0, 0))}{\delta N_0 L \phi(0, 0)}. \tag{33}$$

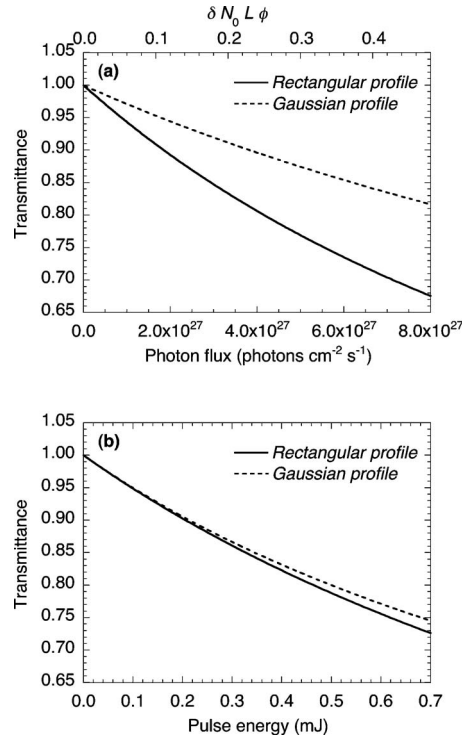
Equation (33) is applicable only to situations where $\Delta_m^{(2)} \ll 1$ (this quantity should now be calculated by integration over the cross section of the beam), because all the steps assumed that the density of molecules available for excitation is N_0 . If $\Delta_m^{(2)}$ is large, the flux dependence of N_g should be included in the analysis, which is not routinely done in practice.

The functional dependence of T on photon flux is different in the case of beams of rectangular [Eq. (28)] and Gaussian spatial profiles [Eq. (33)], as illustrated in Fig. 6(a). For example, a larger peak flux is needed in the Gaussian beam case to achieve the same attenuation as in the rectangular profile case, if the two beams have the same spatial width, w_0 (defined as described above). However, for a given photon flux, the pulse energies of the two pulses are also different. If we consider the situation where the two beams have the same pulse energy and the $1/e^2$ radius of the Gaussian beam is equal to the radius of the rectangular profile beam, the peak photon flux of the Gaussian beam is twice the flux of the rectangular beam, but the attenuation is only slightly smaller in the Gaussian case [Fig. 6(b)].

3.2c. Focused Beam, Rectangular Profile in Space

Until now, we have described the attenuation of a beam by 2PA when its size does not change over the length of the sample. However, when the beam is focused in the sample, the intensity of the pulse changes with z not only because photons are removed from the beam by 2PA, but also because the beam size changes. The response of the material in this case depends on the position of the sample with respect to the focal plane of the beam. Equation (27) is not directly applicable to the whole sample, but it can be used to describe the behavior of a thin layer of material along which the beam area is approximately constant. The light transmitted by this layer is the input for the next layer, and the analysis is repeated for each subsequent thin layer. The transmission curve obtained in this way and by including the effect of ground state depletion [described by Eq. (7)] for an f/10 optical configuration and a pulse with a rectangular time profile

Figure 6

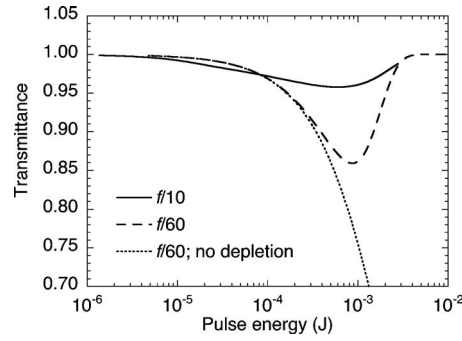


Dependence of the transmittance of a 2PA material when excited by a beam with rectangular [from Eq. (28)] or Gaussian spatial profiles [from Eq. (33)]. (a) Comparison of beams with the same peak photon flux (see also Sutherland [26], p. 504). (b) Comparison of beams with the same pulse energy. Other parameters are $N_0 = 6.0 \times 10^{18} \text{ cm}^{-3}$, $\delta = 1000 \text{ GM}$, $L = 1.0 \text{ cm}$, $\tau = 5 \text{ ns}$ (rectangular temporal profile in all cases), $w_0 = 50 \mu\text{m}$ (for the Gaussian case this is the $1/e^2$ radius), $\lambda = 700 \text{ nm}$ (the scale on the top horizontal axis in (a) is in units of $\delta N_0 L \phi(0, 0)$, and is independent of any specific choice of parameters; this corresponds to the parameter q_0 that will be introduced in Subsection 3.2d).

($\tau = 5 \text{ ns}$) is displayed in Fig. 7 and compared with an approximately collimated beam case (f/60). With increasing pulse energy, the transmittance first decreases from 1 to a minimum value, which depends on the optical configuration, the path length, and the number density, then increases again because of ground state depletion (as in previous examples, we are still assuming that $\tau_{\text{fl}} > \tau$). Ground state depletion is easier to attain and the excitation volume is smaller in the tighter focusing situation. As a consequence, the minimum transmittance in the f/10 case ($T \approx 0.96$) is larger than for the f/60 case ($T \approx 0.86$) [131]. If ground state depletion could be neglected, the transmittance would continue to decrease with increasing energy (see the dotted curve in Fig. 7); this could happen if the relaxation time of the molecules is very fast or if the diffusion of molecules in and out of the excitation volume occurs on a much shorter time scale than the pulse duration.

This optical configuration (in some respects similar to the one for Z-scan experiments on thick samples) is actually not frequently used in measurements aimed at obtaining estimates of 2PA cross sections. One of its drawbacks is that the overall material response also depends on the position of the focus, which could be difficult to locate with precision inside the material. The beam refraction at

Figure 7



Transmittance of a 2PA material in two different optical configurations. Solid curve, $f/10$ (focused beam, $L=0.5 \text{ cm} \gg z_0$); dashed and dotted curves, $f/60$ (approximately collimated beam, $L=1 \text{ cm} < z_0$). The effect of ground state depletion is included in an approximate way [using Eq. (7)] in the first two cases, but not in the last (dotted curve). In all cases $\lambda=700 \text{ nm}$, $\delta=1000 \text{ GM}$, $N_0=6.0 \times 10^{18} \text{ cm}^{-3}$, $\tau=5 \text{ ns}$; the focal plane is located at $z=L/2$.

the interface between air and the nonlinear material needs also to be considered. In addition, for tightly focused beams it could be difficult to ascertain whether the transmitted beam is completely collected by the detector, especially in cases where the material exhibits nonlinear refraction in addition to nonlinear absorption effects, as the former could lead to self-focusing or defocusing of the beam and thus to a change in beam size [132]. On the other hand, this configuration could be encountered in devices designed to achieve nonlinear pulse suppression; thus the beam characteristic and focusing conditions are critical parameters, in addition to the 2PA cross section of a material, in determining the dynamic range of operation and suppression factor for the device.

3.2d. Focused Beam, Gaussian Profile in Space and Time: Open-Aperture Z-Scan

The most common experimental configuration involving a focused beam is called the “open-aperture Z-scan” measurement. In its original description, this experiment involved the use of a focused beam with a Gaussian spatial profile (Eq. (31), $1/e^2$ radius at the waist w_0 , as in case 3.2b above) and a sample whose thickness is small with respect to the Rayleigh range of the beam ($L \ll z_0$, so that the beam size is approximately constant along the sample) [30]. At a fixed input pulse energy, the sample is translated along the beam propagation direction, z , and the transmitted energy is measured for every position of the sample. At each position z , the beam size at the entrance face of the sample, w_z , is different ($w_z = w_0(1 + (z/z_0)^2)^{1/2}$ [111, 112]), and thus the incident photon flux, ϕ_z [133], varies from point to point in the scan. The term “open-aperture” refers to the fact that the transmitted beam is not limited by any aperture (including the detector sensitive area) after the sample, as opposed to the “closed-aperture” case [30], where only the fraction of the beam passing through a small aperture is measured. The discussion of closed-aperture experiments is outside the scope of this review.

If the pulse has a rectangular shape in time (over the pulse duration τ), then Eq. (33) can be used to describe the transmittance of the sample at any given position

z , replacing $\phi(0, 0)$ with ϕ_z [31], which now depends on z because of the change in the beam area at that sample position [134].

For a pulse with a temporal Gaussian profile, instead, Eq. (33) needs to be appropriately modified to account for changes in the instantaneous photon flux during the pulse. We need first to introduce the parameters and equations that describe a beam with Gaussian spatial and temporal profile. The photon flux at a generic point in space and time on the front face of the sample can be written as [112]

$$\phi_z(r; t) = \phi_0(r=0; t=0) \frac{w_0^2}{w_z^2} e^{-2r^2/w_z^2} e^{-t^2/\tilde{\tau}^2} = \phi_z(r=0; t=0) e^{-2r^2/w_z^2} e^{-t^2/\tilde{\tau}^2}, \quad (34)$$

where r is again the radial distance from the optical axis, t is a generic time coordinate, and $\phi_z(r=0; t=0)$ represents the peak photon flux on the optical axis for position z of the sample and for time $t=0$, and w_z is the beam size for position z , as described above. $\tilde{\tau}$ is the pulse duration of the Gaussian pulse, defined here as the interval between the maximum of the pulse and the time when the intensity is reduced to $1/e$ of the maximum. The relationship between peak flux and pulse energy is not given by Eq. (17) in this case, but by [135]

$$\phi_0(r=0; t=0) = \frac{2}{\pi \sqrt{\pi} w_0^2 \tilde{\tau}} \frac{E}{E_{\text{ph}}}. \quad (35)$$

Similar to what was done previously for Eq. (32), the pulse energy at the exit face the sample of length L ($L \ll z_0$) is obtained by integrating Eq. (27) over the beam area and pulse duration for each position of the sample along z [26,30]:

$$\begin{aligned} E_z(L) &= E_{\text{ph}} \int_{-\infty}^{+\infty} dt \int_0^{\infty} 2\pi r dr \frac{\phi_z(r; t)}{1 + \delta N_0 L \phi_z(r; t)} \\ &= E_{\text{ph}} \int_{-\infty}^{+\infty} dt \int_0^{\infty} 2\pi r dr \frac{[\phi_z(r=0; t=0) e^{-t^2/\tilde{\tau}^2}] e^{-2r^2/w_z^2}}{1 + \delta N_0 L [\phi_z(r=0; t=0) e^{-t^2/\tilde{\tau}^2}] e^{-2r^2/w_z^2}} \\ &= E_{\text{ph}} \frac{\pi w_z^2}{2 \delta N_0 L} \int_{-\infty}^{+\infty} dt \ln(1 + \delta N_0 L [\phi_z(r=0; t=0) e^{-t^2/\tilde{\tau}^2}]) \\ &= E_{\text{ph}} \frac{\pi w_z^2}{2 \delta N_0 L} \int_{-\infty}^{+\infty} dt \ln(1 + q_z e^{-t^2/\tilde{\tau}^2}). \end{aligned} \quad (36)$$

In the last step, the parameter q_z was introduced [26,30]:

$$q_z \equiv \delta N_0 L \phi_z(r=0; t=0) = \frac{\delta N_0 L \phi_0(r=0; t=0)}{(1 + (z/z_0)^2)} = \frac{q_0}{(1 + (z/z_0)^2)}, \quad (37)$$

where

$$q_0 \equiv \delta N_0 L \phi_0(r=0; t=0). \quad (38)$$

Now the transmittance of the material can be obtained as the ratio of $E_z(L)$ [Eq. (36)] and the pulse energy before the sample [similar to Eq. (35) for a generic z] [136]:

$$T_z = \frac{E_z(L)}{E} = \frac{E_{\text{ph}} \frac{\pi w_z^2}{2 \delta N_0 L} \int_{-\infty}^{+\infty} \ln(1 + q_z e^{-t^2/\tilde{\tau}^2}) dt}{E_{\text{ph}} \frac{\pi \sqrt{\pi w_z^2 \tilde{\tau}}}{2} \phi_z(r=0; t=0)} = \frac{\int_{-\infty}^{+\infty} \ln(1 + q_z e^{-t^2/\tilde{\tau}^2}) dt}{\sqrt{\pi \tilde{\tau} q_z}}. \quad (39)$$

For a generic value of q_z the integral in Eq. (39) needs to be evaluated numerically, but in the case of $0 \leq q_z \leq 1$ it is possible to expand the logarithm function in a power series and perform the integral on each of the series terms:

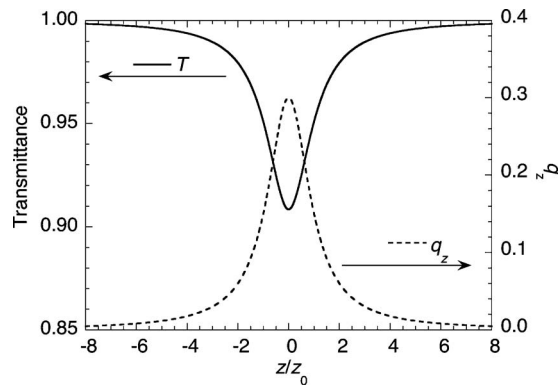
$$\begin{aligned} T_z &= \frac{\int_{-\infty}^{+\infty} dt \sum_1^{\infty} \frac{1}{m} (q_z e^{-t^2/\tilde{\tau}^2})^m (-1)^{m+1}}{\sqrt{\pi \tilde{\tau} q_z}} = \frac{\sum_1^{\infty} \frac{1}{m} (q_z)^m (-1)^{m+1} \int_{-\infty}^{+\infty} e^{-m t^2/\tilde{\tau}^2} dt}{\sqrt{\pi \tilde{\tau} q_z}} \\ &= \sum_1^{\infty} \frac{(q_z)^{m-1} (-1)^{m+1}}{m \sqrt{m}} \end{aligned} \quad (40)$$

or, equivalently,

$$T_z = \sum_0^{\infty} \frac{(-q_z)^m}{(m)^{3/2}} \quad (\text{valid for } 0 \leq q_z \leq 1). \quad (41)$$

According to Eqs. (39) and (41), the transmittance of the sample approaches the value of one [137] far away from the focal plane. As the sample is moved toward the focus, the transmittance decreases, reaches a minimum at $z=0$, where the flux is largest, and then increases again for $z > 0$ (the transmittance trace is symmetrical with respect to the focal plane $z/z_0=0$), as illustrated in Fig. 8. The value of the minimum transmittance depends on q_0 , and it is larger than the transmittance for the case in Fig. 6(a) at the same q_0 , because in the former case

Figure 8



Z-scan transmittance trace for a material exhibiting 2PA (solid curve) as a function of normalized sample position, z/z_0 , for $q_0=0.3$. The corresponding values of q_z [from Eq. (37)] as a function of z are also displayed. The transmittance was calculated from Eq. (41), which is equivalent to Eq. (39) for all the values of q_z in this example.

the flux has a Gaussian shape in time and the leading and trailing edges of the pulse contribute less to the beam attenuation than the central portion of the pulse.

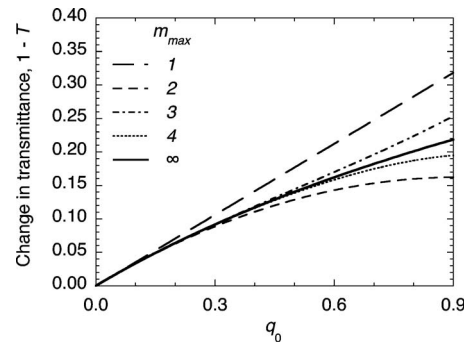
Equation (39) and similar ones obtained for different temporal pulse shapes are derived under the assumption that the only variable in the experiment is the photon flux; that is, all the terms defining q_0 in Eq. (38) are constant in space and time during the excitation. As mentioned in previous sections, this implies that approximation (ii) [$\Delta_m^{(2)} \ll 1$, Eq. (23)] still holds and experimental parameters should be adjusted to work in this regime.

The depth of the transmission valley in a Z-scan trace at $z=0$ (or equivalently the largest change in transmittance) is not directly proportional to the photon flux, except for $q_0 \ll 1$ (Fig. 9). The number of terms in the series in Eq. (41) that make a significant contribution to T_z also depends on the magnitude of q_0 . A few cases as shown in Fig. 9, where the results from the infinite series of Eq. (41) ($m=0, 1, \dots, \infty$) are compared with truncated series ($m=0, 1, \dots, m_{\max}$). It can be seen that starting at $q_0=0.3-0.4$ the $m=3$ term needs to be included to provide an accurate description of the transmittance. Higher-order terms are needed for even larger q_0 . Approximate expressions of this type are often used to fit experimental Z-scan traces. It should be stressed again that Eq. (41) is applicable *only* for $0 \leq q_0 \leq 1$. Indeed, for $q_0 > 1$, the infinite series in Eq. (41) does not converge; thus, in this regime, the truncated series for any value of m_{\max} are also not appropriate, because they do not represent an approximation for Eq. (39), even if they do assume finite values. As a consequence, for $q_0 > 1$ (and, correspondingly, transmittance changes $1 - T \gtrsim 0.25$; see Fig. 9), the data analysis of experimental Z-scan traces to obtain 2PA cross section values needs to be based on Eq. (39).

Focused beams with different spatial and temporal profiles have also been considered in open-aperture Z-scan experiments, including top-hat beams [138], elliptical Gaussian beams [139], Gaussian–Bessel beams [140], and beams of arbitrary shapes [141]. The analysis has been extended to thick samples ($L \gtrsim z_0$), for which the beam size is not constant along the sample [31,142]. These extensions of the Z-scan technique have not been widely applied in 2PA cross section measurements to date.

The accuracy of 2PA cross sections determined by using Eq. (39) or (41) to fit

Figure 9



Change in transmittance, $1 - T$, observed in a Z-scan experiment at $z=0$ as a function of q_0 (solid curve). The effect of truncation of the series in Eq. (41), that is, the inclusion of only terms with $m \leq m_{\max}$, is shown for a few values of m_{\max} .

data from a Z-scan experiment depends on how close the actual beam profile and pulse shape are to the ideal Gaussian function assumed in the derivation of the equations. The effects of deviations from the ideal profiles have been analyzed in more details for closed-aperture experiments, but they have also been observed in open-aperture ones [31,140,143]. In the case of deviations from the Gaussian profile in the time domain, the data can be accurately described by substituting the experimental pulse profile in Eq. (39) for $\exp(-t^2/\tau^2)$ and calculating the integral numerically. In the case of the spatial profile, large deviations from a Gaussian shape would likely lead to unsatisfactory fits of the data and could be easily recognized. However, the effect of small deviations may be harder to notice in the Z-scan traces and could be erroneously assigned to random fluctuations in the measurement or to the presence of other nonlinear processes. Indeed, deviations from the ideal beam profile can lead to systematic errors that are difficult to quantify and correct for. For example, a slightly larger photon flux near the peak (the tail) of the intensity distribution with respect to the Gaussian case for a given beam waist would result in an overestimate (underestimate) of the beam attenuation and thus of the 2PA cross section [31]. Chapple and Wilson investigated the effect of beam shape on the beam attenuation due to 2PA for a wide range of beam profiles that are only approximately Gaussian and that are not cylindrically symmetrical, by modeling the beam propagation in the nonlinear material by a 2D Fourier transform technique [143]. As shown in Fig. 10(a), they found that the change in transmittance at $z=0$ is always larger for a non-Gaussian beam than for a Gaussian beam with the same waist and pulse energy. For example, a beam with the cross section at $z=0$ given by Fig. 10(b) would lead to the Z-scan trace represented by the solid curve in Fig. 10(c), which clearly exhibits a deeper transmission dip than a Gaussian beam with the same waist [143]. Using Eq. (41) for the fitting would thus not lead to a good agreement with experimental data for the overall trace, and the 2PA cross section obtained from the fitting could be significantly different from the intrinsic 2PA cross section of the material. The error introduced by the ellipticity of the beam could also be difficult to quantify.

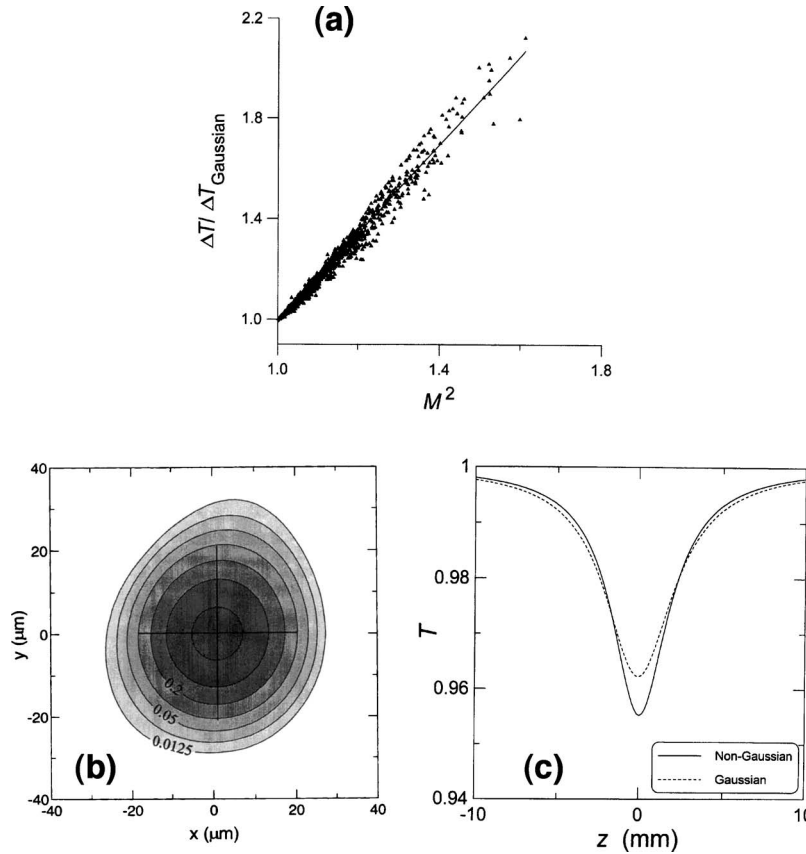
An accurate characterization of the beam profile should be performed for every experimental setup, some measure of the deviation from the Gaussian behavior reported, and this deviation should then be considered in the estimate of the uncertainty in the measurement. When the deviation from the Gaussian profile is significant, the data should be more appropriately analyzed by modeling numerically the beam propagation for the beam profile observed experimentally, for example by using the approach that in [143] yielded the results in Fig. 10, or by extending to 2PA beam propagation techniques that have already been applied in other situations [140,141,144–146]. As an alternative, problems associated with irregular beam shapes could be circumvented if the measurements were conducted in a relative (instead of absolute) way, that is, if the trace from a material of interest were compared with that of a sample of known 2PA properties under the same experimental conditions.

4. Pulse Width Effects and Other Temporal Considerations

4.1. Significance of the $\langle \phi^2 \rangle$ Term

We have seen in Subsection 3.1 that the density of photons absorbed and of the molecules excited per unit time by 2PA is proportional to the square of the pho-

Figure 10



(a) Change in transmittance, $\Delta T = 1 - T$, at $z=0$ in a Z-scan trace for beams with non-Gaussian spatial profiles; the parameter M^2 is a measure of the deviation of the actual profile from the ideal Gaussian shape ($M^2=1$). $\Delta T_{\text{Gaussian}}$ is the corresponding change in transmittance for a Gaussian beam with the same waist and pulse energy. Each triangle corresponds to a different beam profile. The slope of the best-fit straight line is 1.77. (b) Beam cross section at $z=0$ for one of the beam profiles included in plot (a) and with $M^2=1.08$. (c) Z-scan traces for the beam with the profile in (b) (solid curve) and for a Gaussian beam with the same beam waist and pulse energy (dashed curve). Reproduced with permission from Chapple and Wilson [143]. Copyright 1996 World Scientific Publishing Company.

ton flux, ϕ^2 [Eqs. (5) and (6)]. In general, the photon flux depends on time, $\phi(t)$, not just on space, but we have not always explicitly indicated this dependence in the equations until now, because most of the simple cases we discussed assumed that pulses had a rectangular temporal profile (except for the Z-scan case of Subsection 3.2d). The temporal pulse shape and the fact that the excitation rate scales with the second power of the flux have significant consequences on the way 2PA experiments are conducted.

In direct measurements, the beam attenuation as a function of peak photon flux or of the position of the sample depends on the temporal pulse profile (we discussed in particular the case of a Gaussian beam in Subsection 3.2d). Thus, the measurement of 2PA cross sections and spectra requires the prior knowledge of the pulse shape. We have briefly discussed at the end of Subsection 3.2d how de-

viations of the actual beam shape from the ideal (or its change over the course of the measurement and with wavelength) can lead to systematic errors.

We now discuss in more detail how the pulse shape dependence influences 2PA measurements by indirect methods. In indirect measurements for low excitation regimes [that is, if Eqs. (22) and (23) are satisfied], the observable of choice is typically proportional to the number of molecules excited per unit volume and time, $n_m^{(2)}$ [Eq. (6)]. In principle, for a relatively long excitation pulse it is possible to monitor both the instantaneous flux, $\phi(t)$, and the evolution in time of the 2PA-induced signal, and thus $n_m^{(2)}(t)$ [29]. However, the time evolution of the latter also depends on other material factors, such as the fluorescence lifetime in the case of fluorescence-based methods [29,122], or the heat diffusion characteristics in thermal lensing experiments [75], and the interpretation of the results could be complicated. It is instead more common and straightforward, especially for short pulses, to measure

1. The pulse energy E , which is proportional to the average of the flux during the pulse, $\langle \phi(t) \rangle$ [147];
2. The 2PA-induced signal S integrated over time (even for single pulse measurements), which is proportional to the average of the square of the flux, $\langle \phi^2(t) \rangle$. For a 2PIF measurement, after including the time dependence in Eq. (13) and integrating over one period of the laser [148], we obtain

$$\int_T^{T+1/f} S(t) dt = \int_T^{T+1/f} \frac{1}{2} \eta G \delta N_0 \phi^2(t) dt = \frac{1}{2} \eta G \delta N_0 f^{-1} \langle \phi^2(t) \rangle \quad (42)$$

or, equivalently,

$$\langle S(t) \rangle = \frac{1}{2} \eta G \delta N_0 \langle \phi^2(t) \rangle. \quad (43)$$

Introducing the second-order temporal coherence function, $g^{(2)}$ [17,149–151], defined here as

$$g^{(2)} = \frac{\langle \phi^2(t) \rangle}{\langle \phi(t) \rangle^2}, \quad (44)$$

Eq. (43) can be rewritten as

$$\langle S(t) \rangle = \frac{1}{2} \eta G \delta N_0 g^{(2)} \langle \phi(t) \rangle^2. \quad (45)$$

In general, $\langle \phi^2(t) \rangle \neq \langle \phi(t) \rangle^2$ ($g^{(2)} \neq 1$) for a pulse of generic shape [152]. Consequently a measurement of the quantities described in points 1 and 2 above is *not* sufficient to determine the 2PA cross section, even if η , N_0 , and G can be independently obtained (some considerations about G will be presented in Subsection 4.4). Instead, $\langle \phi^2(t) \rangle$ or $g^{(2)}$ also need to be independently measured in order to relate the measured 2PA-induced signals to absolute 2PA cross sections or to obtain fully corrected 2PA spectra. For example, Krasinski *et al.* showed that the value of the 2PIF signal, that is $\langle S(t) \rangle$, was larger for multimode operation of the laser than for single-mode operation for any given average pulse power, for two different compounds [153]. In all cases $\langle S(t) \rangle$ scaled approximately with the square of $\langle \phi(t) \rangle$. In addition, Johnson and Lytle have shown that 2PA spectra col-

lected by using single-mode and multimode lasers appear to be different in shape if the fluorescence signals are scaled simply with respect to $\langle \phi(t) \rangle^2$, and the difference has been ascribed to changes in the value of $g^{(2)}$ when the wavelength of the laser is tuned [151].

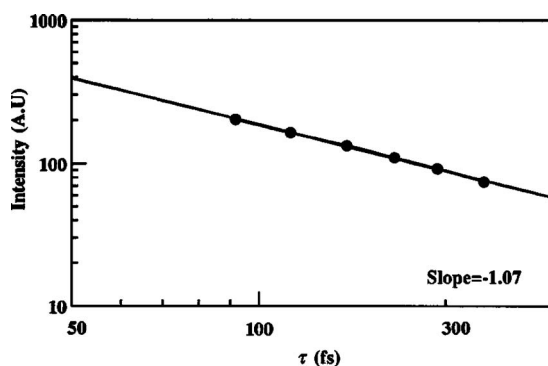
Owing to the difficulty in measuring the quantities $\langle \phi^2(t) \rangle$ or $g^{(2)}$ with accuracy on a routine basis, 2PA cross sections are often derived from relative measurements. Absolute and relative measurements will be discussed further in Subsection 4.4. Conversely, Eq. (45) shows that 2PA could be used as a technique to measure the second-order coherence function and to obtain information on the pulse shape and duration [154–157].

4.2. Pulse Width Effects

As mentioned above, $g^{(2)}$ depends on the distribution of the photon flux during the pulse. In general, $g^{(2)}$ is given by the product of $(\tau)^{-1}$ and a numerical factor that depends on the specific pulse shape. $g^{(2)}$ values can be of the order of 10^5 for high-repetition-rate fs lasers and 10^7 for low-repetition-rate ns lasers.

In a pure 2PA process, in which two photons are absorbed simultaneously (that is, when the intermediate state for the transition is a virtual state, with a lifetime much shorter than the pulse duration and the lifetime of real excited states of the molecule, see the beginning of Section 2), the 2PA transition probability and the 2PA cross section do *not* depend on the pulse duration. If δ is constant, from Eq. (45) and the fact that $g^{(2)}$ is inversely proportional to τ , the magnitude of a 2PA-induced signal is expected to scale as τ^{-1} . Xu and Webb showed in their seminal paper in 1996 that this is indeed the case for molecule Indo-1 when excited with pulses of duration between 90 and about 300 fs (Fig. 11) [20]. They also showed that the intensity of the 2PA-induced fluorescence signal from the same molecule and for pulse widths from 0.5 to 1.2 ps (at constant average power) scales linearly with the intensity of the second harmonic of the excitation beam (generated in a powdered sample of KDP, a material with second-order nonlinearities); as the

Figure 11

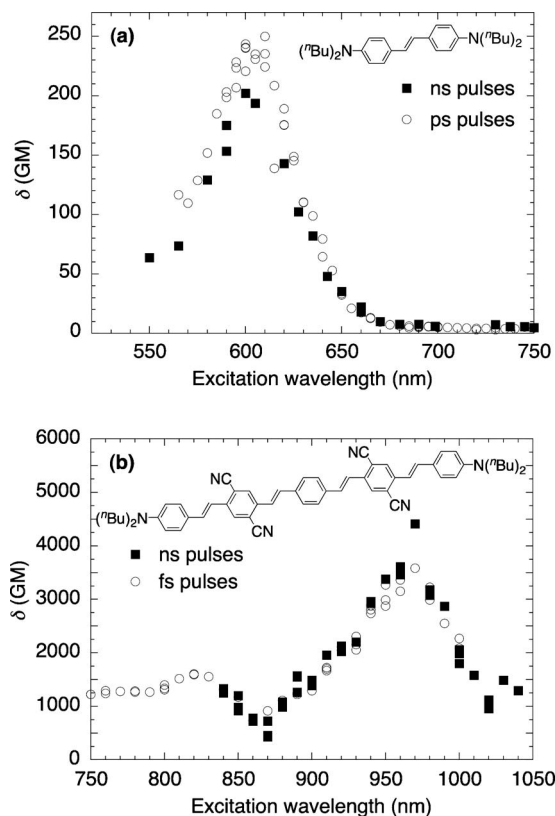


Dependence of the time-averaged 2PIF signal on the excitation pulse width ($\lambda = 770$ nm, 10^{-4} M solution of chromophore Indo-1 in water). The line in the log-log plot is the best fit of the experimental data (dots) and has slope ≈ -1 . This dependence of $\langle S(t) \rangle$ [Eq. (45)] on τ^{-1} through $g^{(2)}$ indicates that δ is constant over this pulse duration range. Reproduced with permission from Xu and Webb [20]. Copyright 1996 Optical Society of America.

second-harmonic generation process is proportional to $\langle \phi^2(t) \rangle$, the experimental findings indicate that the same is true for the 2PA-induced fluorescence process. If δ were pulse-width dependent, a deviation from the expected behavior of the 2PA-induced fluorescence signal (signal proportional to τ^{-1}) would have been observed in these experiments.

Figure 12 displays additional experimental data from our previous work to support the statement that δ does not depend on pulse duration (at least up to the ns time scale in the cases discussed here). Figure 12(a) shows the 2PA spectrum of a chromophore (see inset for molecular structure) obtained by the 2PIF relative method and using pulse durations in two very different time regimes: ns and ps [124]. It can be clearly seen that the shapes of the spectra and the magnitude of the cross sections obtained with ns and ps pulses are in very good agreement, the differences being smaller than, or on the order of, the typical uncertainties associated with this type of measurement ($\approx 15\%$ when the same reference material is used). The spectra in Fig. 12(b) show good agreement between the results obtained by ns and fs 2PIF relative measurements for a different compound [158]. We have observed a similar behavior for a wide range of chromophores [158–160]. Overall, this body of information indicates not only that δ is pulse-width independent, but also that indirect methods for 2PA measurements are not sensitive

Figure 12



2PA spectra of two compounds (molecular structures included in figures) obtained by relative 2PIF measurements using excitation sources with different pulse durations: (a) ns and ps; (b) ns and fs. Adapted from (a) Rumi *et al.* [124] and (b) Chung *et al.* [158].

to pulse duration, if the experimental conditions are chosen appropriately to ensure that the induced signal, S , depends on the square of the pulse energy, approximations (i) and (ii) are valid [Eqs. (22) and (23)], and sources of spurious signals are eliminated. (Subsection 4.3 will discuss further why ESA does not affect the measurement under these conditions.)

4.3. Excited State Absorption

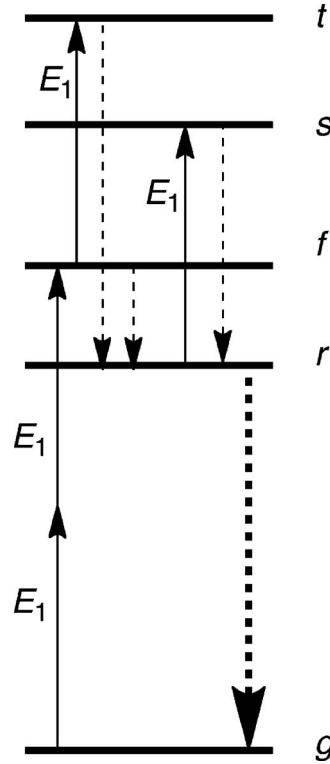
Despite what has been mentioned above, differences in 2PA cross sections measured using pulses with different pulse durations or with different methods have been reported. It is discussed here how some of these differences can originate from the fact that other excitation and de-excitation processes may occur in the material after the initial 2PA event, within the pulse duration and before the molecule returns to the ground state. Some experimental methods or detection schemes may not be able to isolate the 2PA contribution from that of other processes and thus only provide a *cumulative signal*, resulting in measured 2PA cross sections that appear to be pulse-width or intensity dependent, as discussed by many authors [23,26,91]. It has become common to refer to these quantities as *effective* 2PA cross sections.

Let us consider a material that can be excited by 2PA from the ground state, g , to one of the excited states, for example f (see Fig. 13). As discussed above (Section 2), the molecule generally relaxes from f to the lowest excited state, r , in particular to the lowest vibrational level of that state by internal conversion and vibrational relaxation on a short time scale (ps or less). If the molecule can be excited by 2PA directly into r , fast vibrational relaxation to the lowest vibrational level of r will still occur. The molecule can fluoresce from r with a certain yield, η , or relax back to the ground state via nonradiative processes (time scale $\approx 10^{-11} - 10^{-8}$ s). However, if the fluorescence lifetime is comparable with or longer than the pulse duration ($\tau_{fl} > \tau$) or if the photon flux is very high, the population of the excited state r can be large enough during the pulse that other processes become competitive with radiative and nonradiative relaxations. For example, the molecule could absorb a third photon from the same pulse and be excited from state r to a higher-lying state, s (ESA) [23,91,106,161–166]. In addition, for pulse durations of the order of or shorter than the relaxation time between f and r , ESA can occur directly from state f , leading to some population in the higher-lying state t . In the presence of ESA, a new term should be added to the propagation equation [Eq. (1)]:

$$\frac{d\phi}{dz} = -\delta N_g \phi^2 - \sigma_{\text{ex}} N_{\text{ex}} \phi, \quad (46)$$

where σ_{ex} is the one-photon absorption cross section for the transition between excited states r and s (or f and t), and N_{ex} is density of molecules in the excited state at a given time. If more than one ESA process is active, a term $\sigma_{\text{ex}} N_{\text{ex}} \phi$ for each should be included in Eq. (46) [167]. It should be noted that the beam attenuation due to ESA depends effectively on the third power of ϕ , because N_{ex} depends on ϕ^2 [Eq. (12)], and thus it represents a fifth-order contribution to the optical response in the material [164]. The modified propagation equation [Eq. (46)] and appropriate rate equations for the population of all the states involved in addition to g need to be solved self-consistently and taking into account the spatial profile of the beam, the pulse shape in time, the focusing conditions of the beam, etc. This task is generally mathematically complicated and is typically addressed by using numerical methods.

Figure 13



Modification of the energy level diagram of Fig. 1 (degenerate case) to include ESA pathways. After the simultaneous absorption of two photons of energy E_1 (solid arrows) and relaxation by internal conversion from state f to r (short dashed arrow), the material can absorb additional photons at the same energy, building up population in excited state s . For very short pulses, direct absorption from the state f , before relaxation, is also possible, leading to population of state t . From any of the excited states the system then relaxes to r by internal conversion (other dashed arrows) and then to the ground state by radiative or nonradiative de-excitation processes (bold dashed arrow).

It can be easily seen, however, that the attenuation of a beam as described by Eq. (46) could be significantly larger than in the case of a pure two-photon process [Eq. (1)]. If approximations (i) and (ii) of Subsection 3.1 are valid ($\Delta_{\text{ph}}^{(2)} \ll 1$, $\Delta_m^{(2)} \ll 1$), at any given time during the pulse, the population of the excited states would be small with respect to that of the ground state ($N_{\text{ex}} \ll N_g$). However, because ESA is a one-photon absorption process, the number of photons absorbed by ESA could be comparable with or even larger than the number of photons absorbed by 2PA [as given, for example, by Eq. (18)]. In a very approximate way, this can be seen through the following argument. From Eq. (46), the relative changes in the photon flux due to 2PA and ESA can be written, respectively, as

$$\left(\frac{d\phi}{\phi} \right)_{2\text{PA}} = -\delta N_g \phi dz,$$

$$\left(\frac{d\phi}{\phi}\right)_{\text{ESA}} = -\sigma_{\text{ex}}N_{\text{ex}}dz. \quad (47)$$

If we now consider the same conditions as for the numerical example of Subsection 3.1c (ns excitation, collimated beam; see Fig. 5) for $\Delta_m^{(2)}=0.010$ (corresponding to $\phi=6.3 \times 10^{26}$ photons $\text{cm}^{-2} \text{s}^{-1}$), and we assume $\sigma_{\text{ex}}=1.0 \times 10^{-17} \text{ cm}^2/\text{molecule}$, we obtain for Eq. (47)

$$-(d\phi/\phi)_{2\text{PA}} = 3.8 \times 10^{-4} \text{ cm}^{-1} dz,$$

$$-(d\phi/\phi)_{\text{ESA}} = 6.0 \times 10^{-3} \text{ cm}^{-1} dz.$$

In this case, the number of photons absorbed by ESA is an order of magnitude larger than the number absorbed by 2PA, even if the fraction of molecules excited is still low (and $\Delta_{\text{ph}}^{(2)}=3.8 \times 10^{-4}$ over 1 cm, so no significant beam attenuation due to 2PA is expected).

Using Eq. (12) to estimate N_{ex} in Eq. (47), the relative effect of 2PA and ESA can be expressed as

$$\frac{\left(\frac{d\phi}{\phi}\right)_{\text{ESA}}}{\left(\frac{d\phi}{\phi}\right)_{2\text{PA}}} \approx \frac{\sigma_{\text{ex}}\left(\frac{1}{2}\delta\phi^2\tau N_0\right)}{\delta N_0\phi} = \frac{1}{2}\sigma_{\text{ex}}\phi\tau. \quad (48)$$

A more detailed analysis would need to consider that N_{ex} is time dependent during the pulse and that, at a given time, only the molecules excited by the portion of the pulse that has already passed through a given element of the sample can undergo ESA by absorbing a photon from the remaining portion of the pulse. However, the analysis provided by Eq. (48) should be sufficient to compare the effects within an order of magnitude. Thus, ESA may well be relevant for materials and experimental conditions for which $(\phi\tau)^{-1}$ is comparable with or smaller than the excited state cross section σ_{ex} at the wavelength of interest [168].

ESA can affect 2PA measurements when $(\phi\tau)^{-1} \lesssim \sigma_{\text{ex}}$.

We can now discuss in more detail when and how ESA can influence the different types of 2PA measurements.

4.3a. ESA and Indirect Measurements: 2PIF Methods

After ESA, the molecule is in the excited state s (or t), from where it can relax back to state r and then to the ground state through one of the normal relaxation pathways (Fig. 13). The lifetime of state s is typically short (due to the high density of vibronic states, internal conversion is usually very efficient for high-lying excited states). Thus, a molecule that underwent ESA will eventually lead to fluorescence emission of a photon (with efficiency η), and this will be detected

together with the photons emitted by the molecules not involved in ESA [169]. The experimentally measured signal $\langle S(t) \rangle$ (as defined in Subsection 4.1) is not influenced or modified by ESA and is still proportional to $\langle \phi^2(t) \rangle$, N_0 , and η [Eq. (43)]. Consequently, the 2PA cross section obtained from the signal $\langle S(t) \rangle$ under these conditions does not depend on the pulse duration or the photon flux. It should be mentioned, though, that it is critical that 2PIF experiments are conducted in a regime where $\Delta_{\text{ph}}^{(2)} \ll 1$ [Eq. (22)] for an additional reason relative to what was discussed earlier in Subsection 3.1, when the material exhibits ESA. It was seen in the numerical example introduced for the discussion of Eqs. (47) and (48) that the relative change in photon flux due to ESA can be comparable with, or even larger than, that due to 2PA [170]. Thus, unless $\Delta_{\text{ph}}^{(2)} \ll 1$, the photons absorbed by ESA could reduce the pulse energy to the point where Eqs. (12) and (43), and similar would no longer be applicable. This would lead to a smaller fluorescence signal detected during the experiment and thus to smaller cross sections than under ideal conditions. A measurement of the beam attenuation over the range of pulse energies used for the 2PIF experiment can be employed to monitor this possibility.

In conclusion, even if it is comparatively easy to induce ESA by using ns pulsed excitation relative to high-repetition-rate fs pulsed excitation (because N_{ex} is typically larger for long, high-energy excitation pulses, see examples in Subsections 3.1a and 3.1c), the measured 2PA cross sections should be the same in the two cases if the experimental conditions are chosen within the range allowed by approximations (i) and (ii) [Eqs. (22) and (23)]. The pulse-width independence of δ values obtained from 2PIF measurements was clearly illustrated by the examples in Fig. 12. We will see below in Subsection 4.3c that the compound in Fig. 12(a) is known to exhibit 2PA-induced ESA and have a large excited state cross section, and yet the δ values from ns and ps 2PIF experiments are in very good agreement. We can thus say that 2PIF methods are *selective* for measuring only the 2PA contribution in a material system that can also undergo ESA, *irrespective of the pulse duration*, when the experimental conditions are judiciously chosen (such that they satisfy Eqs. (22) and (23) and that the dependence of $\langle S(t) \rangle$ on $\langle \phi^2(t) \rangle$ is verified). Similar arguments can be applied to indirect measurements based on the detection of phosphorescence emission.

Only in cases where, after ESA into s or t , new de-excitation processes with a final state different from r become active (for example, if the molecule can dissociate, ionize, or undergo some photochemical transformation when in state s [161]), would a deviation from the $\langle \phi^2(t) \rangle$ dependence of $\langle S(t) \rangle$ be observed, and consequently would δ appear to depend on the photon flux. Other effects can also lead to deviations from the ideal $\langle \phi^2(t) \rangle$ dependence of $\langle S(t) \rangle$, including ground state depletion and stimulated emission at high photon flux, and nonnegligible 1PA absorption at λ for low flux [101,161,171,172]. These effects can manifest themselves in different excitation regimes for various molecules, and it is thus imperative that the $\langle \phi^2(t) \rangle$ dependence of $\langle S(t) \rangle$ be tested in all experimental setups and for all compounds under investigation. Any deviation from the ideal power law $\langle S(t) \rangle \propto \langle \phi^2(t) \rangle$ leads to an *effective* intensity and/or pulse-width dependent 2PA cross section.

4.3b. ESA and Indirect Measurements: Thermal Methods

In thermal lensing, calorimetry, or other photothermal detection schemes, the measured signal is proportional to $N_m^{(2)}(\tau)$ of Eq. (12) if 2PA is the only active absorption mechanism. However, if the material exhibits ESA (or other absorp-

tion mechanisms, such as 1PA), the energy of the additional absorbed photons is also going to be dissipated as heat, effectively increasing the thermal or acoustic signal from the material at a given photon flux. The detected signal, thus, depends on the total number of photons absorbed, and the results from these measurements can appear to be pulse-width or intensity dependent, in a way similar to direct method results, which are discussed below. The presence of other absorption mechanisms in thermal detection schemes can be inferred from deviations from the expected $\langle S(t) \rangle \propto \langle \phi^2(t) \rangle$ behavior.

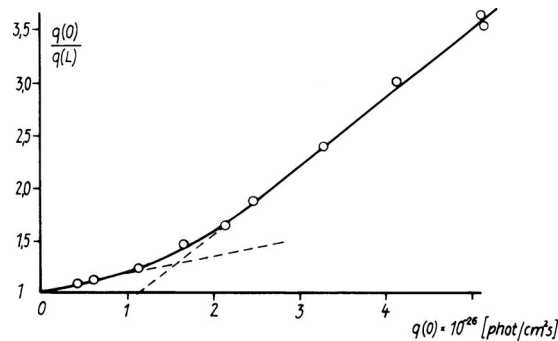
4.3c. ESA and Direct Measurements: NLT and Z-scan Methods

In contrast with the findings for 2PIF methods, which are not sensitive to ESA, nonlinear transmission and Z-scan experiments (as well as thermal indirect measurements, as discussed above) can be significantly affected by ESA, especially if long excitation pulses are used.

As described in Subsection 3.2, the behavior of a 2PA material can be obtained by solving the propagation equation [Eq. (1)] to obtain Eq. (27). For a collimated beam with rectangular profile in time and space, the transmittance of a sample is expressed by Eq. (28) or (30). However, if ESA contributes to the attenuation of the beam, the correct propagation equation is Eq. (46), and deviations from the $1/T$ versus ϕ (or I) straight line of Eq. (30) should be expected. This can be easily observed in NLT experiments using ns and, sometimes, even ps or fs pulses.

One of the first examples of this behavior was reported for *trans*-stilbene by Kleinschmidt *et al.* in 1974 using 20 ns, 693 nm pulses [162]. It can be seen from Fig. 14 that only the first few data points fall on a line with a y intercept of 1, which

Figure 14



Dependence of the inverse of the transmittance, $1/T$, on laser photon flux incident on a *trans*-stilbene sample. In the original work, $q(0)$ was the symbol used for the incident flux and $q(L)$ that for the transmitted flux after a sample of length L . In our formalism, these correspond to $\phi(0)$ and $\phi(L)$, respectively. Thus the ordinate is the inverse of the sample transmittance (using the nomenclature of the original paper: $q(0)/q(L) = 1/T$). The scale on the abscissa spans from 0 to 5×10^{26} photons $\text{cm}^{-2} \text{s}^{-1}$. Sample, *trans*-stilbene in chloroform; $\lambda = 693$ nm, $\tau = 20$ ns, $L = 20$ cm. The open circles are experimental data points, the solid curve a theoretical prediction (see text), and the dashed lines the limiting behaviors for low and high flux. Reproduced from Kleinschmidt *et al.* [162]. Copyright 1974, with permission from Elsevier.

is the line that would be expected from Eq. (30). For $\phi > 1.5 \times 10^{26}$ photons $\text{cm}^{-2} \text{s}^{-1}$, the data points curve upward and then follow another straight line, with a steeper slope and an intercept below 1. By solving the rate equations for the ground and excited states and a propagation equation inclusive of 2PA and ESA terms [173], Kleinschmidt *et al.* obtained the trend represented by the solid curve in the figure, which agrees closely with the experimental data if $\sigma_{\text{ex}} \approx 3 \times 10^{-17} \text{ cm}^2$.

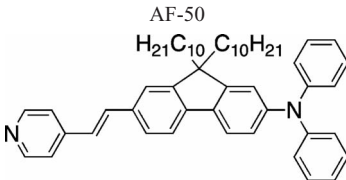
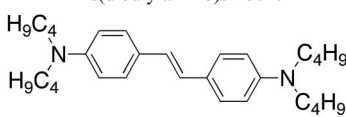
As seen from Eq. (48), the relative contribution of ESA to the total beam attenuation is largest when N_{ex} is largest, that is, for long pulses or high photon flux. ESA can thus play a role in NLT experiments with ns pulses or with high-energy fs pulses.

If the range of T values spanned in the experiment were small, if the flux were varied over a limited range, or if the signal-to-noise ratio were small, it could be hard to distinguish the upward curvature in a plot of $1/T$ as a function of ϕ , and the data might still seem to follow the trend of Eq. (30), for a beam of flat profile. Similarly, only small deviations from the shape of the ideal curve of Eq. (33) could be observed in the case of a Gaussian beam. This situation is even more complicated when the beam profile is irregular or if the excitation conditions are outside the range allowed by Eq. (23) [approximation (ii)]. However, if Eq. (30) or (33) is used for fitting the data from ns-NLT measurements, the δ values obtained can be one to three orders of magnitude larger than those measured by 2PIF methods or by direct methods with ps or fs pulses, depending on the parameters in Eq. (48). This type of behavior has been reported by many investigators [21,23,37,91,138,174]. Among other compounds, two molecules have been investigated under a wide range of experimental conditions, and it is worth mentioning some of the results to illustrate further the influence of ESA in the measurement of 2PA cross sections. The first molecule is *N,N*-diphenyl-7-[2-(4-pyridinyl)ethenyl]-9,9-di-*n*-decylfluoren-2-amine, and it is generally referred to in the literature with the abbreviation AF-50; the second molecule is the one previously shown in Fig. 12(a). Some of the 2PA cross sections reported for these compounds are collected in Table 1, which includes information on the pulse duration, the excitation wavelength, and the experimental method used for each measurement.

For both molecules, the results from NLT experiments with ns pulses are clearly much larger than the cross sections from all other types of measurement. Thus, the results obtained by ns-NLT measurement have to be regarded as *effective* cross sections, δ_{eff} [23,37,91,138,174,177]. These are not intrinsic material properties, as δ is, but depend on the experimental conditions used. In particular, δ_{eff} is *pulse-width and intensity dependent*. Other effects beyond ESA can influence direct measurements, for example, stimulated emission and nonlinear scattering processes. As these effects result in additional photons, they could lead to an apparent increase in the transmitted intensity measured by the detector, unless the beam is spectrally filtered, and thus to an underestimation of the 2PA cross section [91].

Even if ns-NLT is most affected by ESA among the direct techniques, the results from ps- or fs-NLT and Z-scan measurements can also be influenced by ESA [163–165,178,179]. In Z-scan measurements, the effect of ESA can be determined by repeating the experiment over a range of photon fluxes. If the equations of Subsection 3.2d (or similar ones for different beam or pulse shapes) are used when ESA is present, the values of 2PA cross sections that give the best fit to the experimental data for each flux at the focus depend on the flux itself. Ex-

Table 1. 2PA Cross Section of AF-50 and Bis(dibutylamino)stilbene Obtained by Various Experimental Methods for Excitation Wavelength λ and Pulse Duration τ

| Compound | δ (GM) ^a | λ (nm) | τ | Method | Ref. |
|---|---|----------------|--------|-------------|----------|
|  | 25 | 790 | 430 fs | NLT | [21] |
| | 30 | 796 | 160 fs | Z-scan, NLT | [175] |
| | 170 | ~790 | 120 fs | DFWM | [37] |
| | 1.0×10^4 – 1.9×10^4 (depending on solvent) | 800 | 8 ns | NLT | [176] |
| | 1.2×10^4 | 800 | 8 ns | NLT | [177] |
| | 1.9×10^4 | 800 | 8 ns | NLT | [175] |
| | $\sim 3 \times 10^{3b}$ | 694 | 4.3 ns | NLT | [21] |
|  | 210 | 600 | 5 ns | 2PIF | [23,159] |
| | 230 | 600 | 3 ps | 2PIF | [124] |
| | 310 | 600 | 4 ps | NLT | [23] |
| | 9.3×10^3 (in toluene), 1.8×10^4 (in acetone) | 600 | 5 ns | NLT | [174] |
| | 200 ^c | 640 | 30 ps | 2PIF | [116] |
| | | | | | |

^aReported with two significant digits.

^bValue estimated from Fig. 5 of [21], ns nonlinear absorption data set, at 0.1 GW/cm².

^cThis measurement is for a molecule closely related to the one at left, with *N*-carbazolyl instead of dibutylamino donor substituents.

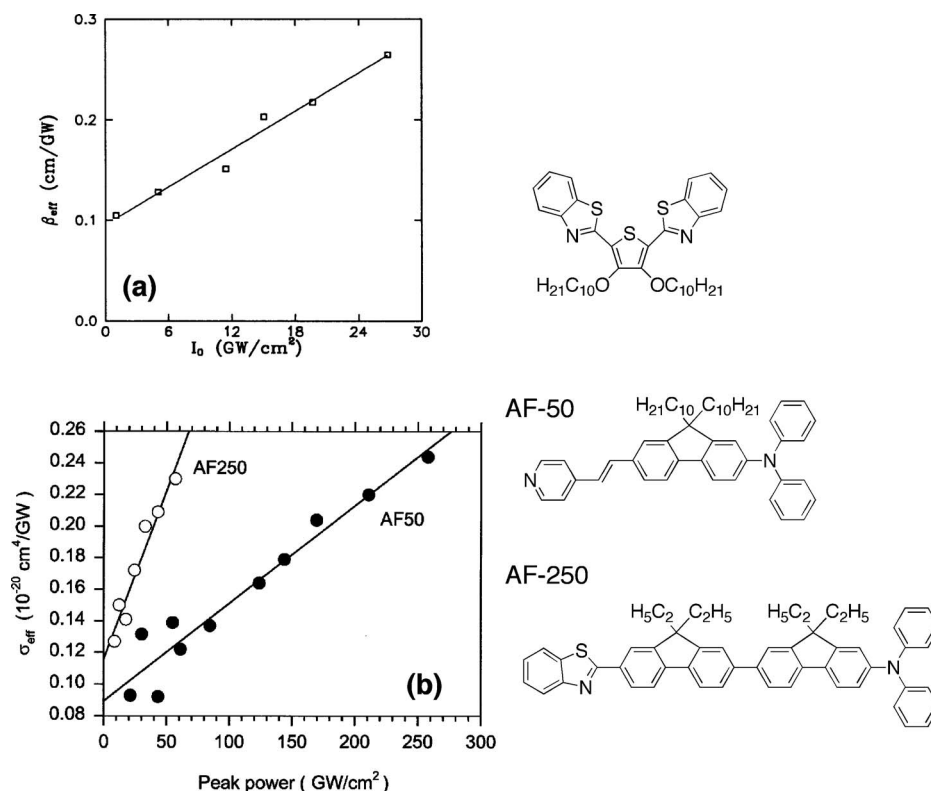
amples of this behavior for Z-scan experiments with ps and fs pulses are given in Fig. 15 for three molecules [164,165]. In all cases displayed in the figure, δ_{eff} (or the corresponding 2PA coefficient β_{eff}) is found to increase approximately linearly with flux, at least in the range investigated:

$$\delta_{\text{eff}}(\phi_0) \approx \delta + u\sigma_{\text{ex}}\phi_0, \quad (49)$$

the intrinsic cross section, δ , being the intercept with the $\phi_0=0$ axis and the slope being proportional to the excited state cross section (u is a constant). It should be pointed out that in these situations the application of the pure 2PA equations for data fitting is not actually correct, because they were obtained neglecting the second term on the right-hand side of Eq. (46). As $\delta_{\text{eff}} \geq \delta$ and the effect of ESA is more evident for sample positions near $z=0$, where the transmittance is minimum, the pure 2PA equations could lead to a good fit of the experimental points near the trough of the trace, but they could overestimate the attenuation in the wings of the Z-scan trace. However, if the slope of the δ_{eff} versus ϕ_0 line is not too large, the quality of fittings is still acceptable, and δ_{eff} versus ϕ_0 plots give the experimenter a simple, if approximate, tool to separate the 2PA from the ESA contributions, without resorting to numerical integration of the differential equations, or to find experimental conditions under which the ESA is negligible.

It is instructive to calculate the parameter $\Delta_m^{(2)}$ for the compounds and conditions of Fig. 15. Let us first consider the case of Fig. 15(a). Using the value of β_{eff} in the limit of small intensity ($\beta_{\text{eff}}=0.1$ GW/cm²) [164] and the conversion equation

Figure 15



Dependence of the 2PA coefficient or cross section on incident flux from Z-scan measurements. (a) Results for 2,5-bis(benzothiazolyl)-3,4-didecyloxythiophene at $\lambda = 532$ nm, using 32 ps pulses. In our formalism of Subsection 3.2d, the abscissa corresponds to $\phi_0(r=0; t=0) \times E_{\text{ph}}$, the ordinate to $\delta_{\text{eff}} N_0 / E_{\text{ph}}$. Reproduced from Said *et al.* [164], Copyright 1994, with permission from Elsevier. (b) Results for compounds AF-50 and AF-250 at $\lambda = 796$ nm, using 150 fs pulses. In our formalism, the abscissa corresponds to $\phi_0(r=0; t=0) \times E_{\text{ph}}$, the ordinate to $\delta_{\text{eff}} / E_{\text{ph}}$. Reproduced from Swiatkiewicz *et al.* [165], Copyright 1998, with permission from Elsevier. The molecular structures are displayed to the right of the corresponding plots. The solid lines are the best linear fits to the experimental data [Eq. (49)].

in the caption of the figure, we obtain $\delta \approx 3.1 \times 10^2$ GM. For $I = 20$ GW/cm² (corresponding to a flux at 532 nm of $\phi = 5.4 \times 10^{28}$ photons cm⁻² s⁻¹), we obtain $\Delta_m^{(2)} \approx 0.14$ from Eq. (15) and $\sigma_{\text{ex}} \phi \tau \approx 11$ (Eq. (48), using the value $\sigma_{\text{ex}} = 6.2 \times 10^{-18}$ cm² reported in the original paper [164]). As discussed previously, $\Delta_m^{(2)}$ and $\sigma_{\text{ex}} \phi \tau$ of this magnitude are consistent with the experimental observation that the ESA is not negligible for this compound, because of a buildup of population in the excited state during each pulse. In the case of Fig. 15(b), the intercepts of the fitting lines correspond to a 2PA cross section of about 22 GM for AF-50 and 30 GM for AF-250. The excited state cross sections estimated by Swiatkiewicz *et al.* are $\sigma_{\text{ex}} = 1.0 \times 10^{-17}$ and 2.7×10^{-17} cm² for AF-50 and AF-250, respectively [165]. Considering now $I = 200$ GW/cm² (corresponding to a flux at 796 nm of $\phi = 8.0 \times 10^{29}$ photons cm⁻² s⁻¹), we obtain $\Delta_m^{(2)} \approx 1.1 \times 10^{-2}$ and $\sigma_{\text{ex}} \phi \tau \approx 1.2$ for AF-50 and $\Delta_m^{(2)} \approx 1.4 \times 10^{-2}$ and $\sigma_{\text{ex}} \phi \tau \approx 3.2$ for AF-250. These estimates indicate that for these compounds, even if a small fraction of molecules is excited ($\Delta_m^{(2)} \ll 1$, so that

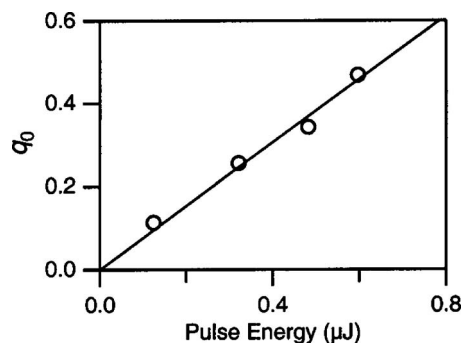
approximation (ii) still holds) and fs pulses are used for the excitation, the effect of ESA is not negligible, at least on the high-intensity side of the plots in Fig. 15(b), again consistent with the experimental finding that δ_{eff} depends on the photon flux. On the other hand, Fleitz *et al.* did not observe an intensity dependence of δ_{eff} when the same AF-50 chromophore was studied by using the NLT method with 430 fs pulses (at 790 nm), but at a lower overall photon flux (up to about 8×10^{28} photons $\text{cm}^{-2} \text{s}^{-1}$) [21]. This discussion supports the use of Eqs. (15) and (48) to estimate whether ESA may be making a contribution under a set of experimental conditions.

When ESA is not effective [for example, if $\phi\tau\sigma_{\text{ex}} \ll 1$, see Eq. (48)], the 2PA cross section measured at each incident flux $\phi_0(r=0; t=0)$ is the same. Equivalently, if the parameter q_0 [Eq. (38)] increases linearly with the photon flux or pulse energy, the beam attenuation for the material and experimental conditions is only due to 2PA, as q_0 is also proportional to the intrinsic value of δ . One such case is displayed in Fig. 16 for 4-*N,N*-dimethylamino-4'-nitrostilbene [33].

4.3d. Conclusions Regarding ESA Effect on 2PA Measurements

To summarize, fluorescence-based indirect measurements of 2PA spectra and cross sections are selective between the 2PA excitation process and the subsequent ESA process. As such, if experimental conditions are chosen judiciously, the results do *not* depend on pulse duration or pulse energy and yield intrinsic δ values. Indirect methods that rely on the measurement of phosphorescence, other de-excitation mechanisms occurring from the lowest triplet state, or that probe the population of the first excited state should also be unaffected by ESA. However, other indirect methods, namely, those based on the detection of photothermal effects, are generally not selective for 2PA or ESA excitation and yield a response proportional to the total energy absorbed, not of the energy absorbed only by 2PA. For wave mixing techniques, the pulse width or intensity dependence of the material response depends on the details of the method and the experimental configuration chosen, and it will not be discussed here. In the case of

Figure 16



Parameter q_0 [defined in Eq. (38)] as a function of pulse energy, E , as obtained from fitting of Z-scan traces for 4-*N,N*-dimethylamino-4'-nitrostilbene in chloroform ($\lambda=639$ nm, $\tau=130$ fs). The direct proportionality of q_0 with E indicates that δ is constant and that ESA does not contribute to the beam attenuation. Reproduced with permission from Kamada *et al.* [33]. Copyright 2003 Optical Society of America.

direct methods, the measured signals derive from the cumulative effect of 2PA and ESA, and the results could depend on pulse energy, pulse duration, or both. For many material systems, this effect is particularly evident when measurements are performed with ns (or longer) pulses. However, ESA can manifest itself also in NLT and Z-scan experiments when ps or fs pulses are used, and additional control experiments need to be carried out to quantify the ESA contribution or demonstrate its absence. Performing Z-scans over a range of incident pulse energies and testing the linear dependence between q_0 and $\phi_0(r=0; t=0)$ is the direct measurement equivalent of ascertaining that $\langle S(t) \rangle$ is directly proportional to $\langle \phi^2(t) \rangle$ or E^2 in the case of 2PIF measurements. As a final reminder, the excitation conditions should always be tested to ensure that $\Delta_m^{(2)} \ll 1$; otherwise the ground state population cannot be assumed to be constant, and all the equations summarized in the above section (and in most of the current literature) are not applicable.

4.4. Absolute and Relative Measurements

In the context of this contribution, an absolute measurement of a 2PA cross section can be defined as a measurement in which δ is obtained as function of a series of parameters (x, y, \dots) that are characteristic of the material under investigation and the optical setup used and that can all be independently measured: $\delta = f(x, y, \dots)$. In a relative measurement, the 2PA cross section of a material is determined by comparing the material response to that of a reference substance of known 2PA cross section (primed symbols) under the same experimental conditions: $\delta = f(x, y, \dots, x', y', \dots, \delta')$ [122]. The feasibility of relative measurements is usually predicated on the availability of absolute measurements on other materials to be used as references, unless the dependence on δ' is left explicit in the results.

In general, direct measurements such as Z-scan and NLT are considered to be easier to implement as absolute techniques. However, absolute δ measurements via Z-scan or NLT rely on a series of assumptions and approximations that could be difficult to attain experimentally in some cases. For example, any fitting equation that can be used is specific for given pulse shapes in space and time. Deviations from these shapes can lead to systematic errors (see Subsection 3.2d). The temporal profile can be even more critical than the spatial one to assess when ultrafast pulses are used, because the pulse shape and duration are typically determined by intensity autocorrelation techniques, which intrinsically yield symmetric shapes [180–182]. The identification of pulse profile asymmetries requires higher-order autocorrelation measurements [180,183,184] or techniques that allow for the determination of both the amplitude and the phase of the pulse, such as frequency-resolved optical gating (FROG) [185–187]. In cases where beam quality cannot be improved sufficiently to apply standard fitting equations, direct methods can still be used in a relative way, by including a reference material in the measurement.

Indirect methods are typically more difficult to perform in an absolute fashion. The main problems are the measurement of $g^{(2)}$ (or $\langle \phi^2(t) \rangle$, see Subsection 4.1), and the evaluation of the excitation volume and the detection efficiency. The large majority of 2PIF studies in the past fifteen years were based on relative measurements and used as reference materials some of the chromophores characterized by Xu and Webb [20] by an absolute method (see below).

In a relative experiment, Eq. (45) can be used to describe the 2PIF signal for the sample under test and for the reference material (and similar equations can be obtained when monitoring other indirect processes induced by 2PA). If the photon flux and the excitation volume [188] are the same for the two samples, the 2PA cross section of the sample under test can be expressed as follows:

$$\delta = \delta' \frac{\eta' N'_0 G' \langle S(t) \rangle}{\eta N_0 G \langle S'(t) \rangle}, \quad (50)$$

where the primed quantities refer to the reference and the unprimed to the sample material. As mentioned in Subsection 3.1, G is a collection efficiency factor that depends on a number of parameters for the sample (fluorescence wavelength/s, λ_{fl} ; refractive index [189] at λ and λ_{fl} , n and n_{fl} ; reabsorption of the fluorescence emission) and the optical setup (λ , dispersion of optics and detector response, cone angle imaged by the detector,...). The functional dependence of G on these parameters varies with the details of the setup [190], and the ratio G'/G is not always independent of λ .

Over the years, various approaches have been proposed and employed to obtain absolute 2PA cross sections and spectra using 2PIF detection schemes. As mentioned above, the key requirements for absolute 2PIF measurements are accurate determinations of the parameters $g^{(2)}$ and G .

One avenue to address the first requirement is the use of single-mode lasers in the measurement, as $g^{(2)}=1$ for these lasers [20,151,191,192]. However, owing to the high average powers required in order to obtain sizable 2PIF signals from a cw excitation source, scattering or one-photon induced fluorescence may lead to deviations in the intensity dependence of the signal and limit the applicability of the approach in some molecules [20]. Nonetheless, 2PA cross sections obtained in this way are among the most reliable reported and have been routinely used as reference values (see below in this section for examples from two separate studies in Figs. 18 and 19).

As an alternative to the use of single-mode lasers, Xu *et al.* utilized an interferometric method that allows for the simultaneous measurement of $g^{(2)}$ and δ (but still requires the independent measurement of G) [193]. It was shown that the 2PA cross sections obtained in this way are in good agreement with those from the single-mode laser determination. Webb and coworkers have also found that $g^{(2)}$ for the mode-locked Ti:sapphire laser used in one of their experiments was approximately constant over the wavelength range investigated, but that its value was at least 30% lower than what would be expected if the pulse had ideal Gaussian or hyperbolic-secant-square shapes [17,20].

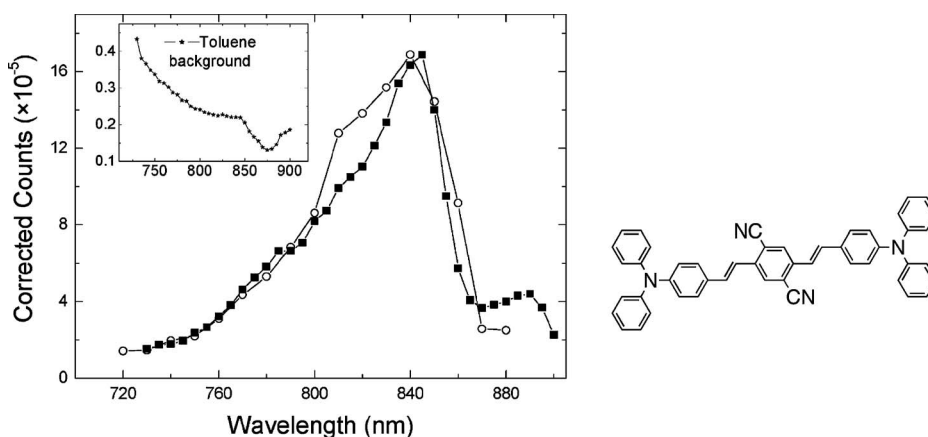
As for the second requirement, the actual measurement of the collection efficiency G can be circumvented if the 2PA-induced signal (fluorescence, phosphorescence, etc.) is compared with that obtained by using an excitation wavelength for which the material undergoes 1PA (in some cases [24] this wavelength needs to be exactly $\frac{1}{2} \lambda$). If the same excitation configuration and collection geometry are used, G assumes the same value in the 1PA and 2PA cases. The 1PA-induced fluorescence signal can thus be used as an internal calibration for the 2PA cross section of the material, as the corresponding 1PA cross section or the absorbance of the sample can be easily measured in an independent experiment [20,24,25,102,103,191,194,195]. One of the difficulties in this approach is ensuring that the excitation configuration is actually the same, for example, that the

beam size is the same; otherwise the excitation volumes for the 1PA and 2PA cases would be different. Also, it may be necessary to use a lower concentration or a shorter path length for the 1PA measurement, so that the pulse energy is constant along the sample [20,191,196]. Unfortunately, it is not always possible to assess whether all of these conditions were satisfied from the experimental details included in reports of absolute 2PA cross sections in the literature, and this may partly explain the wide range of values reported for some compounds.

The calibration for the 2PIF signal in absolute measurements can also be provided by processes other than 2PA that depend on $\langle \phi^2(t) \rangle$. In these cases, an independent measurement of $g^{(2)}$ is not required. For example, Hermann and Ducuing used second-harmonic generation in quartz [194], whereas Kaatz and Shelton used hyper-Rayleigh scattering from para-nitroaniline [22].

Arnbjerg *et al.* calculated $g^{(2)}$ from the measured intensity autocorrelation trace of the pulse and determined absolute 2PA cross sections at a single wavelength (800 nm) by monitoring either a photoacoustic signal or singlet oxygen phosphorescence and comparing signals after 1PA and 2PA excitation under otherwise identical experimental conditions [24]. The absolute δ values obtained for two test compounds with the two independent detection schemes were in reasonable agreement with each other. They then obtained 2PA spectra of the same compounds by 2PIF, taking into account changes in pulse width and beam waist with excitation wavelength and calibrating the cross section scale by using the absolute value at 800 nm described above. Figure 17 displays the results obtained by this method for one compound (structure shown on the right-hand side of the figure) [24]. In particular, the filled symbols in the graph represents the relative 2PA cross section of the compound as obtained from the induced fluorescence signal; the peak cross section, at 845 nm,

Figure 17



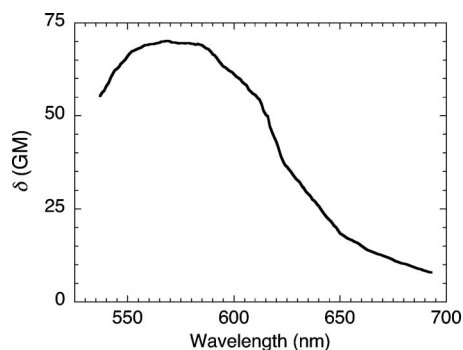
Comparison of the 2PA spectrum for the compound shown at the right in toluene as obtained by Arnbjerg *et al.* [24] (filled squares) using an absolute method (see text) and as obtained by Pond *et al.* [160] (open circles) using a relative 2PIF measurement (excitation with fs pulses; reference material, fluorescein, based on [20]). The ordinate axis is the intensity of the signal for the measurement as conducted in [24], and the other spectrum is normalized to the same intensity at the maximum. The inset is the background signal assigned to toluene for the measurement in [24]. Graph reproduced with permission from Arnbjerg *et al.* [24]. Copyright 2006 American Chemical Society.

was measured to be $(2.8 \pm 0.4) \times 10^3$ GM, when using the photoacoustic result at 800 nm as a scaling factor. The results showed a very good agreement in peak position and band shape with the spectrum of the same compound measured previously in our laboratory by using 2PIF detection in a relative measurement, which is also displayed in Fig. 17 [160]. However, some differences in the magnitude of the cross sections were observed (in our most recent measurements on this compound, we found $\delta = (1.9 \pm 0.3) \times 10^3$ GM and $(1.6 \pm 0.2) \times 10^3$ GM at 840 nm for 2PIF measurements with fs and ns pulses, respectively [160]). As an additional comparison, it should be mentioned that the compound in Fig. 17 was also investigated by Cho and coworkers, who reported a spectrum (obtained by a relative 2PIF methods, with ns pulses and fluorescein as reference) with a peak at 840 nm and corresponding $\delta = 1.4 \times 10^3$ GM, but with a overall shape different from that of the two measurements in Fig. 17 [197]. This example illustrates that repeatability issues still exist in the field when comparing results obtained by different techniques or in different laboratories.

It should be mentioned that, in the absence of a complete calibration for the magnitude of the 2PA cross section, a 2PA spectrum can be considered to be fully corrected if it is obtained after measuring $g^{(2)}$ and G or at least measuring how both these quantities depend on λ . Fully corrected 2PA spectra without a calibration for the cross section have been reported, using second-harmonic generation as a monitor for $\langle \phi^2(t) \rangle$ or single-mode lasers for a few compounds, including naphthalene [151,198], some naphthalene derivatives [199], phenylalanine, tyrosinamide and tryptophan [200], and Coumarin 480 [192,201].

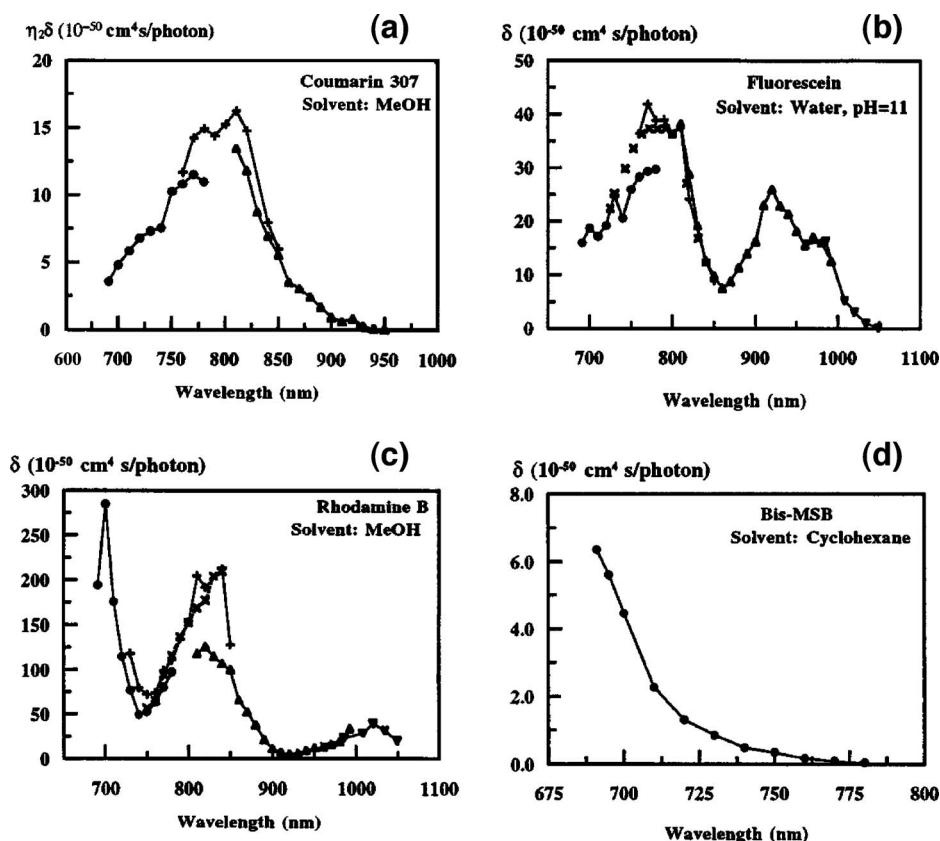
Despite the variety of approaches, absolute 2PIF measurements are very demanding experimentally, and they are rarely employed for routine studies of new materials. Absolute methods have been applied to date only to a limited number of chromophores, especially in the case of spectra covering wide excitation wavelength ranges and not just single wavelengths. A few notable examples are presented here. The 2PA spectrum of *p*-bis-*o*-methylstyryl)benzene has been reported by Lytle and collaborators [191,192] in the range 537–693 nm, obtained by using a single-mode laser as the excitation source (Fig. 18). Figure 19 displays 2PA spectra obtained by absolute methods for *p*-bis(*o*-methylstyryl)benzene and

Figure 18



2PA spectrum obtained by an absolute fluorescence-based method for *p*-bis(*o*-methylstyryl)benzene in cyclohexane. The shape of the spectrum is based on the tabulated values reported by Kennedy and Lytle [191]; the 2PA cross section is scaled to match the value at 585 nm, $\delta = 69$ GM, reported by Fisher *et al.* [192].

Figure 19

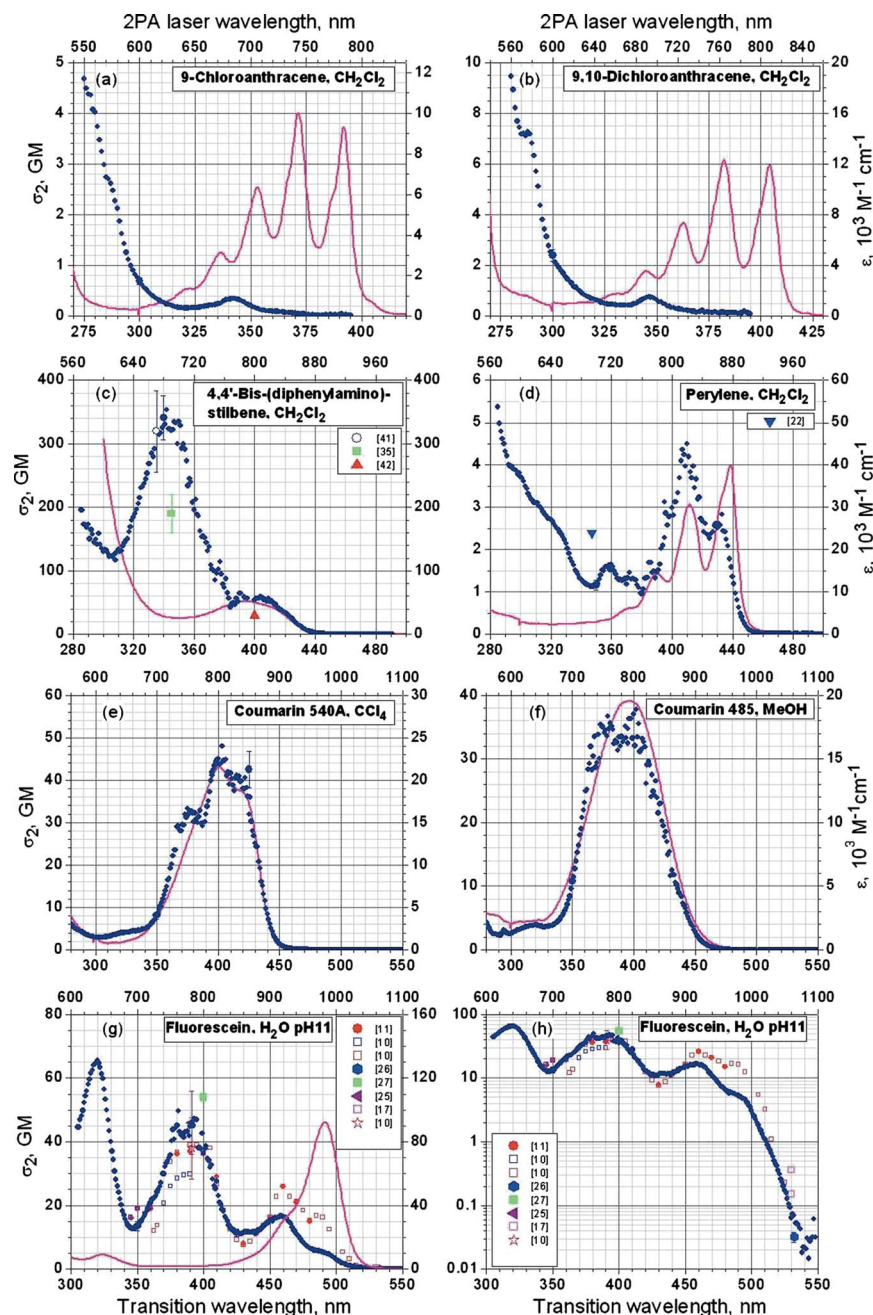


2PA spectra of selected compounds obtained by absolute fluorescence-based methods: (a) Coumarin 307, (b) fluorescein, (c) Rhodamine B, and (d) *p*-bis(*o*-methylstyryl)benzene (the solvent is indicated in the legend) obtained by Xu and Webb [20]. In the case of Coumarin 307, the ordinate displays the quantity $\eta\delta$. Different symbols refer to different mirror sets used to tune the laser. Reproduced with permission from Xu and Webb [20]. Copyright 1996 Optical Society of America.

three other compounds by Xu and Webb [20]. The uncertainty reported for the cross sections for these materials was between 25% and 33% [20]. All the materials for the data in Figs. 18 and 19 are commercially available, have relatively large peak cross sections, and have been widely used in recent years as reference standards in 2PA spectroscopy. For two of these compounds, Coumarin 307 and Rhodamine B, the imaginary component of the third-order polarizability, $\text{Im}(\gamma)$, which is proportional to the 2PA cross section, has also been reported over a wide range of wavelengths, as measured by the Z-scan technique [202].

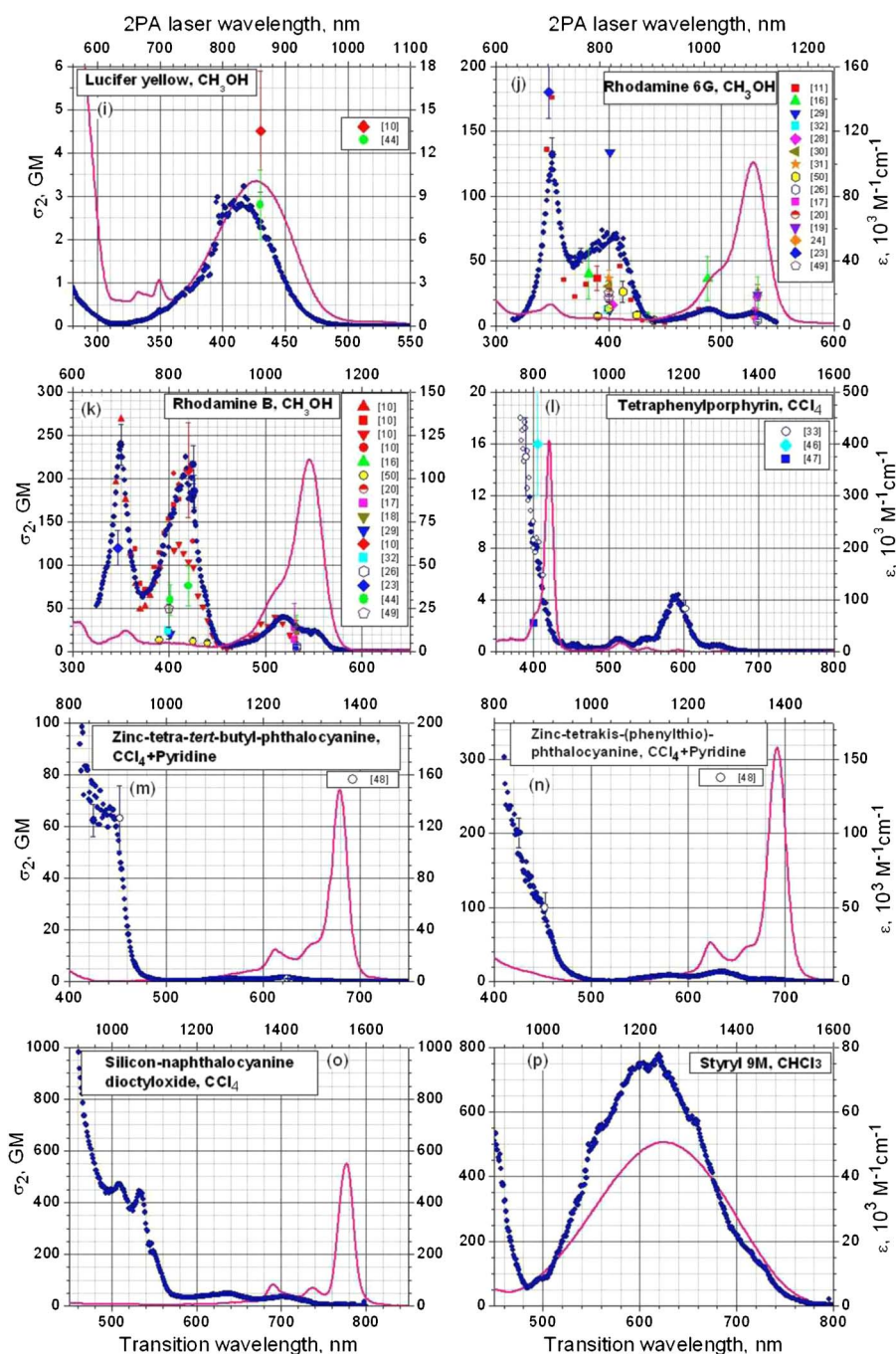
More recently, Rebane and coworkers reported absolute 2PA cross sections obtained by a fluorescence-based method for a larger selection of compounds and spanning a wider spectral range (from 550 to 1600 nm) than previously available [25]. The measurement relied on the characterization of the pulse duration with an autocorrelator and the beam size with a CCD camera, and on using one-photon and two-photon excitation under the same conditions to calibrate the collection efficiency of the setup. The spectra are reproduced in Figs. 20 and 21. The uncertainty in the measurement is reported to be $\pm 15\%$. In this case, again, all the compounds are

Figure 20



2PA spectra (blue circles) of seven different compounds obtained by an absolute fluorescence-based method, as reported by Makarov *et al.* [25]. The compound name and solvent are indicated in the title of each plot. The pink solid curves represent the linear absorption spectrum of each compound. For some compounds results from other sources in the literature are also included (symbols of various shapes and colors; the numbers in square brackets in the legends refer to references cited by Makarov *et al.*). Reproduced with permission from Makarov *et al.* [25]. Copyright 2008 Optical Society of America. Continues in Fig. 21.

Figure 21



Continued from Fig. 20: 2PA spectra (blue circles) of eight different compounds obtained by an absolute fluorescence-based method, as reported by Makarov *et al.* [25]; colors and symbols are the same as in Fig. 20. Reproduced with permission from Makarov *et al.* [25]. Copyright 2008 Optical Society of America.

commercially available, so that they are easily accessible to other research groups. The authors of this study also provided a relatively detailed comparison of these new 2PA cross section data with results previously reported in the literature [25]. Aside

from the specific details of the measurement, the significance of this work is specifically in the large number of compounds and wide wavelength range investigated using a *single* setup in a single laboratory. Because of the overlap of the 2PA bands of various compounds in the series, δ values for more than one chromophore have been reported for various wavelengths. This redundancy can be very useful in testing other setups or configurations, because one known material can be used as a control sample, while another can be picked as reference. It is expected that the results in Figs. 20 and 21 will be used extensively in coming years in relative measurements of 2PA spectra and cross sections of new materials.

With time, more accurate determinations of the 2PA cross sections of these compounds may become available, but relative measurements based on the currently available ones could be easily scaled without the need to repeat the experiments.

Despite recent advances, it is clear that the field of two-photon spectroscopy and, consequently, that of applications based on the 2PA process, could benefit from improvements in the precision and repeatability of absolute and relative 2PA cross section measurements.

5. Advantages and Disadvantages of Various Methods

5.1. Direct Methods

The main advantage of direct measurements is the relative simplicity of the optical setup and the fact that they can be applied to both fluorescent and nonfluorescent materials, as well as to liquid and solid samples. However, as discussed in Subsection 4.3c, these methods are not selective for 2PA and measure the cumulative absorption and scattering or other losses from all processes taking place in the sample. The effect of ESA can be particularly large in the case of NLT measurements with ns or longer pulses, but for some materials it may not be negligible even with ps or fs pulses, as illustrated in the examples of Fig. 15. As a consequence, extreme care must be used in selecting the excitation conditions and in testing the setup. These techniques can provide absolute 2PA cross sections only if the spatial and temporal profiles of the beam are known with good accuracy. Unless ground state depletion is explicitly included in the equations used to process the data, experiments should be conducted in a regime where $\Delta_m^{(2)}$ is small and for small beam attenuations, even if this limits the dynamic range of the method. As a reminder, in this contribution we have always assumed that $\Delta_m^{(2)} \ll 1$ [approximation (ii), Eq. (23)] in our derivations. As a consequence, the use of the equations listed in Subsections 3.2a–3.2d (which are the most commonly encountered in the literature on 2PA materials) is justified only if approximation (ii) is satisfied. This condition is also necessary, but often not sufficient, to limit the influence of ESA during the measurements, which can be crudely estimated from Eq. (48).

5.2. Indirect Methods

Indirect measurements based on the detection of fluorescence, phosphorescence or that otherwise probe the population of the first excited state are truly selective for detecting 2PA if the measured signal is proportional to $\langle \phi^2(t) \rangle$ and the excitation conditions satisfy approximations (i) and (ii) of Subsection 3.1: $\Delta_{ph}^{(2)} \ll 1$ [Eq. (22)] and $\Delta_m^{(2)} \ll 1$ [Eq. (23)].

This important characteristic of fluorescence-based indirect measurement justifies and explains its widespread use in 2PA spectroscopy. If performed in the regime mentioned above, the 2PIF method is generally *independent of pulse duration*. Relatively low concentrations (typically $<10^{-4}$ M) can be used, reducing possible effects due to aggregation of chromophores or self-quenching of the fluorescence. The dynamic range of these methods can be large, and background noise due to scattering can be reduced significantly if the detected signal is spectrally resolved.

The principal drawback of the 2PIF method is that, obviously, it cannot be used for nonfluorescing or weakly fluorescing materials. Phosphorescence detection may be feasible for some of the nonfluorescent materials. 2PIF is also difficult to implement in compounds that exhibit wavelength-dependent emission (in either band shape or efficiency) or dual emission, as well as in solid-state samples. Phosphorescence-based methods are also selective for 2PA in the regime of approximations (i) and (ii) and are pulse-width independent.

Indirect measurements based on thermal lensing or photoacoustic effects can be used for fluorescent and nonfluorescent materials. In the case of fluorescent materials, an independent measurement of the quantum yield is still necessary. If the quantum yield is small, a 2PA cross section obtained from a thermal-based measurement is less sensitive to small change in quantum yield or to the uncertainty in quantum yield value than from a 2PIF measurement [78]. For both absolute and relative measurement, knowledge of the thermal properties of the medium is required. This is usually not a problem for solution measurements, as a wide range of solvents has been well characterized in the literature, but this information could be difficult to obtain or measure independently in solid samples. Unlike the 2PIF method, thermal lensing and photoacoustic measurements are *not selective* for the 2PA process, limiting their applicability to chromophores without competitive 1PA processes from the ground or the excited state. For this reason, it should always be confirmed that the 2PA cross sections obtained with these methods are pulse-width and intensity independent.

Multiphoton ionization spectroscopy has been used mainly to obtain high-resolution information on the position of excited states of molecules. However, limited efforts have been devoted to recording 2PA (and higher-order absorption) spectra that are fully corrected or to measuring 2PA cross sections.

As is the case for direct methods, all indirect measurements critically depend on the spatial and temporal profile of the excitation beam.

5.3. Wave Mixing Methods

In general, wave mixing techniques provide a promising approach for nonfluorescent materials, but usually require complex setups and careful control of the overlap in space and time of two or more ultrafast pulses. In most cases, both the real and the imaginary parts of the hyperpolarizabilities can be measured, and the use of a single setup in more than one measurement can be advantageous if nonlinear optical properties other than 2PA cross sections are of interest.

CARS has been utilized mainly for the measurement of cross sections at specific excitation wavelengths, and it requires two narrowband laser sources, one of which has to be tunable. Measurements of 2PA spectra would require tunability of both sources. The method is calibrated by using absolute Raman cross sec-

tions of solvents and, as a consequence, secondary standards may be necessary if the solvent of choice has not been well characterized in the literature. However, the use of solvents as standards has advantages, as these are easily available and of constant quality across laboratories. Additionally, their CARS signals should not be affected by small traces of impurity, as could be the case for materials used as standards in 2PIF.

DFWM is a very powerful technique for the measurement of optical nonlinearities of materials, allowing not only the measurement of real and imaginary components of the hyperpolarizability, but also the measurement of various tensor elements of the hyperpolarizability by appropriately selecting the polarization direction of the beams. These potentials are not fully exploited in the 2PA case, and the complexity of the optical setup, especially if spectrally resolved information is of interest, may be discouraging.

2PA measurements based on the optical Kerr effect can be very sensitive, as the intensity of a signal near extinction between two crossed polarizers is measured. Also, the method does not require calibration and thus provides absolute cross sections. However, because of the dependence of the measured signal on the difference between two $\chi^{(3)}$ components, $\chi^{(3)}_{XXXX}$ and $\chi^{(3)}_{YYYY}$, information on the 2PA cross section can be obtained only for materials for which those two components are not independent, for example, for one-dimensional molecules [203]. Also, in the implementation by Nunzi and coworkers, $E_1 \neq E_2$ (E_2 is from the white light generated by beam E_1 in a liquid medium) [100,203], and the experiment thus provides only nondegenerate 2PA cross sections and spectra.

6. Conclusions and Outlook

The range of 2PA materials that will be investigated is expected to continue to increase in the near future, both for fundamental studies of the spectroscopy of materials and for the use of 2PA materials as active components in practical applications. The widening in the scope of the field should be accompanied by an improvement in the characterization techniques available to researchers. Specifically, a renewed emphasis should be given to reducing the experimental uncertainty in 2PA measurements and in increasing the agreement of results from various techniques and laboratories. The development of new generations of lasers, detectors, and electronic instrumentation may help in achieving the former goal. A significant effort from the global nonlinear optics community is likely to be needed to achieve the second. In particular, even greater care than what has been applied to date needs to be taken in the selection of the optical configurations and excitation conditions to be used for each sample, and papers and other reports to the scientific community should always include a detailed description of the conditions used and of the control experiments conducted to exclude spurious effects. The concepts overviewed in this contribution and the guidelines regarding parameters $\Delta_m^{(2)}$ and $\Delta_{ph}^{(2)}$ should provide a step toward the development of more standardized procedures for the measurement of 2PA spectra.

7. List of Symbols Used

- β two-photon absorption coefficient ($\delta N_0 \lambda / hc$)
- γ third-order polarizability
- δ two-photon absorption cross section

| | |
|----------------------------|--|
| δ_{eff} | effective two-photon absorption cross section |
| $\Delta_{\text{ph}}^{(2)}$ | fraction of molecules excited per pulse |
| $\Delta_{\text{ph}}^{(2)}$ | fraction of photons absorbed per pulse |
| η | fluorescence quantum yield |
| λ | wavelength of the excitation beam (in vacuum) |
| λ_{fl} | wavelength of fluorescence emission |
| σ | one-photon absorption cross section for the ground state |
| σ_{ex} | excited state one-photon absorption cross section (for example, for transition $r \rightarrow s$ or $f \rightarrow t$) |
| τ | pulse width (generic) |
| $\tilde{\tau}$ | pulse width of a pulse with Gaussian pulse shape (half-width at $1/e$) |
| τ_{fl} | excited state lifetime |
| τ_{v} | lifetime of virtual state in simultaneous two-photon absorption |
| $\chi^{(3)}$ | third-order susceptibility |
| ϕ | photon flux (number of photons per unit area and unit time) |
| ω | angular frequency of excitation beam |
| a | area of the light beam at the focal plane |
| c | speed of light |
| E | energy per pulse |
| $E_{1,2}$ | photon energy for each photon involved in two-photon absorption (in the degenerate case $E_1 = E_2$) |
| $E_{\text{ph}}(\lambda)$ | energy of a single photon of wavelength λ and angular frequency ω ($E_{\text{ph}}(\lambda) = \hbar\omega = hc/\lambda$) |
| f | repetition rate |
| $f/\#$ | ratio of focal length to diameter of the lens |
| $g^{(2)}$ | second-order temporal coherence function |
| G | collection efficiency factor |
| h | Planck's constant |
| I | intensity of the light beam (power/area) |
| L | path length in the sample |
| $M_{\alpha\beta}$ | transition dipole moment between states α and β |
| n | refractive index of the sample at the excitation wavelength λ |
| n_{fl} | refractive index of the sample at the fluorescence wavelength λ_{fl} |
| $n_m^{(2)}$ | number of molecules excited via 2PA, per unit volume and unit time |
| $n_{\text{ph}}^{(2)}$ | number of photons absorbed via 2PA, per unit volume and unit time |
| N_0 | total number of molecules per unit volume |
| N_{ex} | number of molecules in excited state (r or f) per unit volume |
| N_g | number of molecules in the ground state g per unit volume |
| $N_g(t)$ | number of molecules in the ground state at time t per unit volume |
| $N_m^{(2)}(t)$ | number of molecules excited per unit volume from time 0 to time t |
| $N_{\text{ph}}^{(2)}(t)$ | number of photons absorbed per pulse from time 0 to time t |
| N_{ph} | number of photons per pulse |
| q_0 | $\delta N_0 L \phi$ (dimensionless parameter often used in Z-scan analysis) |
| $S(t)$ | intensity of detected signal (e.g., fluorescence) per unit volume of 2PA material due to a single excitation pulse |
| t | generic time |
| V | excitation volume |
| w_0 | beam radius at the focal plane |
| z | beam propagation direction |
| z_0 | Rayleigh range, $\pi w_0^2 n / \lambda$ |

8. List of Abbreviations Used

| | |
|------|---------------------------------------|
| 1PA | one-photon absorption |
| 2PA | two-photon-absorption |
| 2PIF | two-photon-induced fluorescence |
| CARS | coherent anti-Stokes Raman scattering |
| DFWM | degenerate four-wave mixing |
| MPI | multiphoton ionization |
| NLT | nonlinear transmission |

Acknowledgments

This work was supported in part by the STC program of the National Science Foundation under agreement DMR-0120967 and by the Center for Organic Photonics and Electronics, Georgia Institute of Technology. The authors thank Prof. Seth R. Marder, Prof. Eric W. Van Stryland, and Prof. David J. Hagan for helpful discussions.

References and Notes

1. J. H. Strickler and W. W. Webb, "Two-photon excitation in laser scanning fluorescence microscopy," *Proc. SPIE* **1398**, 107–118 (1990).
2. D. A. Parthenopoulos and P. M. Rentzepis, "Three-dimensional optical storage memory," *Science* **245**, 843–845 (1989).
3. J. H. Strickler and W. W. Webb, "Three-dimensional optical data storage in refractive media by two-photon point excitation," *Opt. Lett.* **16**, 1780–1782 (1991).
4. W. Denk, J. H. Strickler, and W. W. Webb, "Two-photon laser scanning fluorescence microscopy," *Science* **248**, 73–76 (1990).
5. P. Sperber and A. Penzkofer, " S_0 – S_n two-photon absorption dynamics of rhodamine dyes," *Opt. Quantum Electron.* **18**, 381–401 (1986).
6. L. W. Tutt and T. F. Boggess, "A review of optical limiting mechanisms and devices using organics, fullerenes, semiconductors and other materials," *Prog. Quantum Electron.* **17**, 299–338 (1993).
7. D. M. Friedrich and W. M. McClain, "Two-photon molecular electronic spectroscopy," *Annu. Rev. Phys. Chem.* **31**, 559–577 (1980).
8. P. R. Callis, "Two-photon-induced fluorescence," *Annu. Rev. Phys. Chem.* **48**, 271–297 (1997).
9. B. Strehmel and V. Strehmel, "Two-photon physical, organic and polymer chemistry: theory, techniques, chromophore design, and applications," in *Advances in Photochemistry*, D. C. Neckers, W. S. Jenks, and T. Wolff, eds. (Wiley, 2007), Vol. 29, pp. 111–354.
10. M. Rumi, S. Barlow, J. Wang, J. W. Perry, and S. R. Marder, "Two-photon absorbing materials and two-photon-induced chemistry," *Adv. Polym. Sci.* **213**, 1–95 (2008).
11. G. S. He, L.-S. Tan, Q. Zheng, and P. N. Prasad, "Multiphoton absorbing materials: molecular designs, characterizations, and applications," *Chem. Rev.* **108**, 1245–1330 (2008).
12. M. Pawlicki, H. A. Collins, R. G. Denning, and H. L. Anderson, "Two-photon absorption and the design of two-photon dyes," *Angew. Chem. Int. Ed.* **48**, 3244–3266 (2009).

13. H. M. Kim and B. R. Cho, "Two-photon materials with large two-photon cross sections. Structure-property relationship," *Chem. Commun. (Cambridge)* 153–164 (2009).
14. H.-B. Sun and S. Kawata, "Two-photon photopolymerization and 3D lithographic microfabrication," *Adv. Polym. Sci.* **170**, 169–273 (2004).
15. S. M. Kuebler and M. Rumi, "Nonlinear optics—applications: three-dimensional microfabrication," in *Encyclopedia of Modern Optics*, B. D. Guenther, D. G. Steel, and L. Bayvel, eds. (Elsevier, 2004), Vol. 3, pp. 189–206.
16. C. N. LaFratta, J. T. Fourkas, T. Baldacchini, and R. A. Farrer, "Multiphoton fabrication," *Angew. Chem. Int. Ed.* **46**, 6238–6258 (2007).
17. C. Xu and W. W. Webb, "Multiphoton excitation of molecular fluorophores and nonlinear laser microscopy," in *Nonlinear and Two-Photon-Induced Fluorescence*, Vol. 5 of *Topics in Fluorescence Spectroscopy*, J. Lakowicz, ed. (Plenum, 1997), pp. 471–540.
18. P. T. C. So, C. Y. Dong, B. R. Masters, and K. M. Berland, "Two-photon excitation fluorescence microscopy," *Annu. Rev. Biomed. Eng.* **2**, 399–429 (2000).
19. R. M. Hochstrasser, H.-N. Sung, and J. E. Wessel, "High resolution two-photon excitation spectra," *J. Chem. Phys.* **58**, 4694–4695 (1973).
20. C. Xu and W. W. Webb, "Measurement of two-photon excitation cross sections of molecular fluorophores with data from 690 to 1050 nm," *J. Opt. Soc. Am. B* **13**, 481–491 (1996).
21. P. A. Fleitz, M. C. Brant, R. L. Sutherland, F. P. Strohkendl, R. J. Larsen, and L. R. Dalton, "Nonlinear measurements on AF-50," *Proc. SPIE* **3472**, 91–97 (1998).
22. P. Kaatz and D. P. Shelton, "Two-photon fluorescence cross-section measurements calibrated with hyper-Rayleigh scattering," *J. Opt. Soc. Am. B* **16**, 998–1006 (1999).
23. J. W. Perry, S. Barlow, J. E. Ehrlich, A. A. Heikal, Z.-Y. Hu, I.-Y. S. Lee, K. Mansour, S. R. Marder, H. Röckel, M. Rumi, S. Thayumanavan, and X. L. Wu, "Two-photon and higher-order absorptions and optical limiting properties of bis-donor substituted conjugated organic chromophores," *Nonlinear Opt.* **21**, 225–243 (1999).
24. J. Arnbjerg, M. Johnsen, P. K. Frederiksen, S. E. Braslavsky, and P. R. Ogilby, "Two-photon photosensitized production of singlet oxygen: optical and photoacoustic characterization of absolute two-photon absorption cross sections for standard sensitizers in different solvents," *J. Phys. Chem. A* **110**, 7375–7385 (2006).
25. N. S. Makarov, M. Drobizhev, and A. Rebane, "Two-photon absorption standards in the 550–1600 nm excitation wavelength range," *Opt. Express* **16**, 4029–4047 (2008).
26. R. L. Sutherland, *Handbook of Nonlinear Optics* (Marcel Dekker, 1996).
27. P. N. Prasad and D. J. Williams, *Introduction to Nonlinear Optical Effects in Molecules and Polymers* (Wiley, 1991).
28. S. Kershaw, "Two-photon absorption," in *Characterization Techniques and Tabulations for Organic Nonlinear Optical Materials*, M. G. Kuzyk and C. W. Dirk, eds. (Marcel Dekker, 1998), pp. 515–654.
29. R. R. Birge, "One-photon and two-photon excitation spectroscopy," in *Ultrasensitive Laser Spectroscopy*, D. S. Kliger, ed. (Academic, 1983), pp. 109–174.
30. M. Sheik-Bahae, A. A. Said, T.-H. Wei, D. J. Hagan, and E. W. Van Stry-

- land, "Sensitive measurement of optical nonlinearities using a single beam," *IEEE J. Quantum Electron.* **26**, 760–769 (1990).
31. P. B. Chapple, J. Staromlynska, J. A. Hermann, T. J. McKay, and R. G. McDuff, "Single-beam Z-scan: measurement techniques and analysis," *J. Nonlinear Opt. Phys. Mater.* **6**, 251–293 (1997).
 32. E. W. Van Stryland and M. Sheik-Bahae, "Z-scan," in *Characterization Techniques and Tabulations for Organic Nonlinear Optical Materials*, M. G. Kuzyk and C. W. Dirk, eds. (Marcel Dekker, 1998), pp. 655–692.
 33. K. Kamada, K. Matsunaga, A. Yoshino, and K. Ohta, "Two-photon-absorption-induced accumulated thermal effect on femtosecond Z-scan experiments studied with time-resolved thermal-lens spectrometry and its simulation," *J. Opt. Soc. Am. B* **20**, 529–537 (2003).
 34. H. J. Eichler, P. Günther, and D. W. Pohl, *Laser-Induced Gratings* (Springer-Verlag, 1986).
 35. S. M. Kuebler, "Studies of the third-order nonlinear optical properties of some materials by degenerate four-wave mixing," D. Phil. thesis (Univ. of Oxford, 1997).
 36. R. A. Norwood, "Four wave mixing," in *Characterization Techniques and Tabulations for Organic Nonlinear Optical Materials*, M. G. Kuzyk and C. W. Dirk, eds. (Marcel Dekker, 1998), pp. 693–765.
 37. K. A. Drenser, R. J. Larsen, F. P. Strohkendl, and L. R. Dalton, "Femtosecond, frequency-agile, phase-sensitive-detected, multi-wave-mixing nonlinear optical spectroscopy applied to π -electron photonic materials," *J. Phys. Chem. A* **103**, 2290–2301 (1999).
 38. S.-Y. Tseng, W. Cao, Y.-H. Peng, J. M. Hales, S.-H. Chi, J. W. Perry, S. R. Marder, C. H. Lee, W. N. Herman, and J. Goldhar, "Measurement of complex $\chi^{(3)}$ using degenerate four-wave mixing with an imaged 2-D phase grating," *Opt. Express* **14**, 8737–8744 (2006).
 39. M. Göppert-Mayer, "Über Elementarakte mit zwei Quantensprüngen," *Ann. Phys. (Leipzig)* **9**, 273–294 (1931).
 40. W. L. Peticolas, "Multiphoton spectroscopy," *Annu. Rev. Phys. Chem.* **18**, 233–260 (1967).
 41. W. M. McClain, "Two-photon molecular spectroscopy," *Acc. Chem. Res.* **7**, 129–135 (1974).
 42. If ΔE represents the uncertainty in the energy of the system after the interaction of the molecule with the first photon, it follows from the uncertainty principle that $\Delta E \tau_v \geq \hbar$ [17,40]. For example, if $E_1 = E_2 = 1.55$ eV (photon wavelength = 800 nm), $\Delta E \sim E_1$, and then $\tau_v \geq 4.3 \times 10^{-16}$ s.
 43. W. M. McClain and R. A. Harris, "Two-photon molecular spectroscopy in liquids and gases," in *Excited States*, E. C. Lim, ed. (Academic, 1977), Vol. 3, pp. 1–56.
 44. P. R. Monson and W. M. McClain, "Polarization dependence of the two-photon absorption of tumbling molecules with application to liquid 1-chloronaphthalene and benzene," *J. Chem. Phys.* **53**, 29–37 (1970).
 45. W. M. McClain, "Excited state symmetry assignment through polarized two-photon absorption studies of fluids," *J. Chem. Phys.* **55**, 2789–2796 (1971).
 46. O. S. Mortensen and E. N. Svendsen, "Initial and final molecular states as "virtual states" in two-photon processes," *J. Chem. Phys.* **74**, 3185–3189 (1981).
 47. B. Dick and G. Hohlneicher, "Importance of initial and final states as inter-

- mediate states in two-photon spectroscopy of polar molecules,” *J. Chem. Phys.* **76**, 5755–5760 (1982).
48. R. R. Birge and B. M. Pierce, “A theoretical analysis of the two-photon properties of linear polyenes and the visual chromophores,” *J. Chem. Phys.* **70**, 165–178 (1979).
 49. B. Honig, J. Jortner, and A. Szöke, “Theoretical studies of two-photon absorption processes. I. Molecular benzene,” *J. Chem. Phys.* **46**, 2714–2727 (1967).
 50. Vibronic coupling can give rise to finite 2PA transition probabilities even for symmetry-forbidden transitions [see [49] and M. W. Dowley, K. B. Eisenthal, and W. L. Peticolas, “Two-photon laser excitation of polycyclic aromatic molecules,” *J. Chem. Phys.* **47**, 1609–1619 (1967)].
 51. W. Denk, D. W. Piston, and W. W. Webb, “Two-photon molecular excitation in laser-scanning microscopy,” in *Handbook of Biological Confocal Microscopy*, J. B. Pawley, ed. (Plenum Press, 1995), pp. 445–458.
 52. E. S. Wu, J. H. Strickler, W. R. Harrell, and W. W. Webb, “Two-photon lithography for microelectronic application,” *Proc. SPIE* **1674**, 776–782 (1992).
 53. S. Maruo, O. Nakamura, and S. Kawata, “Three-dimensional microfabrication with two-photon-absorbed photopolymerization,” *Opt. Lett.* **22**, 132–134 (1997).
 54. G. Witzgall, R. Vrijen, E. Yablonovitch, V. Doan, and B. J. Schwartz, “Single-shot two-photon exposure of commercial photoresist for the production of three-dimensional structures,” *Opt. Lett.* **23**, 1745–1747 (1998).
 55. B. H. Cumpston, S. P. Ananthavel, S. Barlow, D. L. Dyer, J. E. Ehrlich, L. L. Erskine, A. A. Heikal, S. M. Kuebler, I.-Y. S. Lee, D. McCord-Maughon, J. Qin, H. Röckel, M. Rumi, X.-L. Wu, S. R. Marder, and J. W. Perry, “Two-photon polymerization initiators for three-dimensional optical data storage and microfabrication,” *Nature* **398**, 51–54 (1999).
 56. A. S. Dvornikov and P. M. Rentzepis, “Novel organic ROM materials for optical 3D memory devices,” *Opt. Commun.* **136**, 1–6 (1997).
 57. S. Hell and E. H. K. Stelzer, “Fundamental improvement of resolution with a 4Pi-confocal fluorescence microscope using two-photon excitation,” *Opt. Commun.* **93**, 277–282 (1992).
 58. S. W. Hell, S. Lindek, and E. H. K. Stelzer, “Enhancing the axial resolution in far-field light microscopy: two-photon 4Pi confocal fluorescence microscopy,” *J. Mod. Opt.* **41**, 675–681 (1994).
 59. P. E. Hänninen, S. W. Hell, J. Salo, E. Soini, and C. Cremer, “Two-photon excitation 4Pi confocal microscope: enhanced axial resolution microscope for biological research,” *Appl. Phys. Lett.* **66**, 1698–1700 (1995).
 60. S. M. Kirkpatrick, J. W. Baur, C. M. Clark, L. R. Denny, D. W. Tomlin, B. R. Reinhardt, R. Kannan, and M. O. Stone, “Holographic recording using two-photon-induced photopolymerization,” *Appl. Phys. A* **69**, 461–464 (1999).
 61. T. J. Bunning, S. M. Kirkpatrick, L. V. Natarajan, V. P. Tondiglia, and D. W. Tomlin, “Electronically switchable gratings formed using ultrafast holographic two-photon-induced photopolymerization,” *Chem. Mater.* **12**, 2842–2844 (2000).
 62. H. Guo, H. Jiang, L. Luo, C. Wu, H. Guo, X. Wang, H. Yang, Q. Gong, F. Wu, T. Wang, and M. Shi, “Two-photon polymerization of gratings by interference of a femtosecond laser pulse,” *Chem. Phys. Lett.* **374**, 381–384 (2003).
 63. R. A. Negres, J. M. Hales, A. Kobayakov, D. J. Hagan, and E. W. Van Stry-

- land, "Two-photon spectroscopy and analysis with a white-light continuum probe," *Opt. Lett.* **27**, 270–272 (2002).
64. R. A. Negres, J. M. Hales, A. Kobayakov, D. J. Hagan, and E. W. Van Stryland, "Experiment and analysis of two-photon absorption spectroscopy using a white-light continuum probe," *IEEE J. Quantum Electron.* **38**, 1205–1216 (2002).
 65. The 2PA cross section δ is proportional to the square modulus of the two-photon tensor mentioned earlier in the section (see, for example, [29,40,41]).
 66. The symbols σ_2 and $\sigma^{(2)}$ are also commonly used in the literature to represent the 2PA cross section.
 67. Typical units for δ are $\text{m}^4 \text{s}/(\text{molecule photon})$ in the SI system and $\text{cm}^4 \text{s}/(\text{molecule photon})$ in the cgs system, or $\text{m}^4 \text{s}$ and $\text{cm}^4 \text{s}$, respectively, if omitting dimensionless parameters. The derived unit GM (Göppert-Mayer) is also frequently used and is defined as follows: $1 \text{ GM} \equiv 1 \times 10^{-50} \text{ cm}^4 \text{s}/(\text{molecule photon}) = 1 \times 10^{-58} \text{ m}^4 \text{s}/(\text{molecule photon})$.
 68. Typical SI units for δ^* are $\text{cm}^4/(\text{molecule W})$ or $\text{cm}^4/(\text{molecule GW})$. Sometimes "molecule" is omitted (because it is dimensionless), and the units are simply reported as cm^4/W or cm^4/GW .
 69. P. Tian and W. S. Warren, "Ultrafast measurement of two-photon absorption by loss modulation," *Opt. Lett.* **27**, 1634–1636 (2002).
 70. D. M. Hercules, "Theory of luminescence processes," in *Fluorescence and Phosphorescence Analysis. Principles and Applications*, D. M. Hercules, ed. (Interscience, 1966), pp. 1–40.
 71. J. R. Lakowicz, *Principles of Fluorescence Spectroscopy*, 2nd ed. (Kluwer Academic/Plenum, 1999).
 72. P. Esherick, P. Zinsli, and M. A. El-Sayed, "The low energy two-photon spectrum of pyrazine using the phosphorescence photoexcitation method," *Chem. Phys.* **10**, 415–432 (1975).
 73. L. Singer, Z. Baram, A. Ron, and S. Kimel, "The two-photon phosphorescence excitation spectrum of triphenylene," *Chem. Phys. Lett.* **47**, 372–376 (1977).
 74. P. K. Frederiksen, M. Jørgensen, and P. R. Ogilby, "Two-photon photosensitized production of singlet oxygen," *J. Am. Chem. Soc.* **123**, 1215–1221 (2001).
 75. A. J. Twarowski and D. S. Kliger, "Multiphoton absorption spectra using thermal blooming. I. Theory," *Chem. Phys.* **20**, 253–258 (1977).
 76. D. S. Kliger, "Thermal lensing: a new spectroscopic tool," *Acc. Chem. Res.* **13**, 129–134 (1980).
 77. H. L. Fang, T. L. Gustafson, and R. L. Swofford, "Two-photon absorption photothermal spectroscopy using a synchronously pumped picosecond dye laser. Thermal lensing spectra of naphthalene and diphenylbutadiene," *J. Chem. Phys.* **78**, 1663–1669 (1983).
 78. J. K. Rice and R. W. Anderson, "Two-photon, thermal lensing spectroscopy of monosubstituted benzenes in the ${}^1B_{2u}({}^1L_b) \leftarrow {}^1A_{1g}({}^1A)$ and ${}^1B_{1u}({}^1L_a) \leftarrow {}^1A_{1g}({}^1A)$ transition regions," *J. Phys. Chem.* **90**, 6793–6800 (1986).
 79. M. Bass, E. W. Van Stryland, and A. F. Stewart, "Laser calorimetric measurement of two-photon absorption," *Appl. Phys. Lett.* **34**, 142–144 (1979).
 80. A. M. Bonch-Bruevich, T. K. Razumova, and I. O. Starobogatov, "Single- and two-photon spectroscopy of liquid media using the pulsed acousto-optical effect," *Opt. Spectrosc.* **42**, 45–48 (1977).

81. A. C. Tam and C. K. N. Patel, "Two-photon absorption spectra and cross-section measurements in liquids," *Nature* **280**, 304–306 (1979).
82. E. W. Van Stryland and M. A. Woodall, "Photoacoustic measurement of nonlinear absorption in solids," in *Laser Induced Damage in Optical Materials, 1980*, National Bureau of Standards Special Publication 620 (National Bureau of Standards, 1981), pp. 50–57.
83. J. A. Wilder and G. L. Findley, "Construction of a two-photon photoacoustic spectrometer," *Rev. Sci. Instrum.* **58**, 968–974 (1987).
84. J. P. Gordon, R. C. C. Leite, R. S. Moore, S. P. S. Porto, and J. R. Whinnery, "Long-transient effects in lasers with inserted liquid samples," *J. Appl. Phys.* **36**, 3–8 (1965).
85. J. R. Whinnery, "Laser measurement of optical absorption in liquids," *Acc. Chem. Res.* **7**, 225–231 (1974).
86. P. G. Seybold, M. Gouterman, and J. Callis, "Calorimetric, photometric, and lifetime determinations of fluorescence yields of fluorescein dyes," *Photochem. Photobiol.* **9**, 229–242 (1969).
87. M. Mardelli and J. Olmsted III, "Calorimetric determination of the 9,10-diphenyl-anthracene fluorescence quantum yield," *J. Photochem.* **7**, 277–285 (1977).
88. J. H. Brannon and D. Madge, "Absolute quantum yield determination by thermal blooming. Fluorescein," *J. Phys. Chem.* **82**, 705–709 (1978).
89. S. E. Braslavsky and G. E. Heibel, "Time-resolved photothermal and photoacoustic methods applied to photoinduced processes in solution," *Chem. Rev.* **92**, 1381–1410 (1992).
90. P. M. Johnson, "Molecular multiphoton ionization spectroscopy," *Acc. Chem. Res.* **13**, 20–26 (1980).
91. D. A. Oulianov, I. V. Tomov, A. S. Dvornikov, and P. M. Rentzepis, "Observations on the measurement of the two-photon absorption cross-section," *Opt. Commun.* **191**, 235–243 (2001).
92. See, for example, P. N. Butcher and D. Cotter, *The Elements of Nonlinear Optics* (Cambridge Univ. Press, 1990).
93. B. Dick, R. M. Hochstrasser, and H. P. Trommsdorff, "Resonant molecular optics," in *Nonlinear Optical Properties of Organic Molecules and Crystals*, D. S. Chemla and J. Zyss, eds. (Academic, 1987), Vol. 2, pp. 159–212.
94. R. J. M. Anderson, G. R. Holtom, and W. M. McClain, "Absolute two-photon absorptivity of *trans*-stilbene near the two-photon absorption maximum via three wave mixing," *J. Chem. Phys.* **66**, 3832–3833 (1977).
95. R. J. M. Anderson, G. R. Holtom, and W. M. McClain, "Two-photon absorptivities of the all *trans* α, ω -diphenylpolyenes from stilbene to diphenyloctatetraene via three wave mixing," *J. Chem. Phys.* **70**, 4310–4315 (1979).
96. H. P. Trommsdorff, R. M. Hochstrasser, and G. R. Meredith, "Raman and two-photon resonances in the three wave mixing in organic crystals: benzene, naphthalene and biphenyl," *J. Lumin.* **18/19**, 687–692 (1979).
97. M. Zhao, Y. Cui, M. Samoc, P. N. Prasad, M. R. Unroe, and B. A. Reinhardt, "Influence of two-photon absorption on third-order nonlinear optical processes as studied by degenerate four-wave mixing: the study of soluble didecyloxy substituted polyphenyls," *J. Chem. Phys.* **95**, 3991–4001 (1991).
98. R. L. Sutherland, E. Rea, L. V. Natarajan, T. Pottenger, and P. A. Fleitz, "Two-photon absorption and second hyperpolarizability measurements in diphenylbutadiene by degenerate four-wave mixing," *J. Chem. Phys.* **98**, 2593–2603 (1993).
99. M. E. Orczyk, M. Samoc, J. Swiatkiewicz, N. Manickam, M. Tomoaia-

- Cotisel, and P. N. Prasad, “Optical heterodyning of the phase-tuned femto-second optical Kerr gate signal for the determination of complex third-order susceptibilities,” *Appl. Phys. Lett.* **60**, 2837–2839 (1992).
100. N. Pfeffer, F. Charra, and J. M. Nunzi, “Phase and frequency resolution of picosecond optical Kerr nonlinearities,” *Opt. Lett.* **16**, 1987–1989 (1991).
 101. D. J. Bradley, M. H. R. Hutchinson, and H. Koetser, “Interactions of picosecond laser pulses with organic molecules. II. Two-photon absorption cross-sections,” *Proc. R. Soc. London Ser. A* **329**, 105–119 (1972).
 102. S. Li and C. Y. She, “Two-photon absorption cross-section measurements in common laser dyes at 1.06 μm ,” *Opt. Acta* **29**, 281–287 (1982).
 103. I. M. Catalano and A. Cingolani, “Absolute two-photon fluorescence with low-power cw lasers,” *Appl. Phys. Lett.* **38**, 745–747 (1981).
 104. For example, in some cases [101–103], the cross section is defined to “count” directly the number of molecules excited, instead of the photons absorbed, leading to the relationship

$$n_m^{(2)} = \tilde{\delta} N_g \phi^2. \quad (\text{I})$$

In this case, the propagation equation (1) becomes

$$\frac{d\phi}{dz} = -2\tilde{\delta} N_g \phi^2. \quad (\text{II})$$

Obviously, the right-hand sides of the two versions of the propagation equation [Eqs. (1) and (II)] and of the equation describing the excitation rate due to 2PA [Eqs. (6) and (I)] differ only by a constant factor and become equivalent if

$$\delta = 2\tilde{\delta}. \quad (\text{III})$$

105. More precisely, any absorption process that would take place at this stage, via 1PA, 2PA or other nonlinear processes, would reflect properties of the excited state r , not of the ground state g , and thus describe a very different sample, from a spectroscopic point of view. All processes, though, contribute to the attenuation of the propagating beam and Eq. (1) would have to be appropriately modified. This situation will also be discussed in Subsection 3.2. ESA following 2PA will also be considered in Subsection 4.3.
106. S. M. Kirkpatrick, C. Clark, and R. L. Sutherland, “Single state absorption spectra of novel nonlinear optical materials,” in *Thin Films for Optical Waveguide Devices and Materials for Optical Limiting*, K. Nashimoto, R. Pachter, B. W. Wessels, A. K.-Y. Jen, K. Lewis, R. Sutherland, and J. W. Perry, eds., Vol. 597 of Materials Research Society Symposium Proceedings (Materials Research Society, 2000), pp. 333–338.
107. It is generally assumed that the fluorescence quantum yield is the same after 1PA and 2PA excitation, as for most molecules the system relaxes, after absorption, to the lowest excited state, r , by internal conversion, irrespective of the photon energy and the manner of excitation, as discussed above. However, there are exceptions to this general rule, as some molecules are known that exhibit a wavelength dependent quantum yield or emission spectrum, and fluorescence emission from upper excited states.
108. $\Delta_m^{(2)}$ is equivalent to the “saturation parameter” α discussed by Xu and Webb [17], pp. 518–520.
109. It should be kept in mind that Eq. (14) was obtained under a series of as-

- sumptions (for example regarding the change in photon flux through the sample). Thus, strictly speaking, Eq. (14) is also an approximate description of the fraction of molecules excited.
110. The total number of photons absorbed per pulse depends on the excitation volume. For a collimated beam, as the case considered in this section, the volume scales with the sample path length L . However, for a focused beam, only a path length of the order of twice the Rayleigh range of the beam, $z_0 = \pi w_0^2 n / \lambda$ (if this is shorter than L), may have to be considered [29], at least as a first approximation, because of the decrease in photon flux away from the focal plane. See also examples in Subsection 3.1b. We have used here for the Rayleigh range z_0 the definition typically introduced for Gaussian beams, for which it corresponds to the distance along z between the waist and the point at which the beam radius is $\sqrt{2}w_0$ [111]. The term *confocal parameter* is also sometimes used when referring to the quantity z_0 (see, for example, [112], p. 117) or $2z_0$ [see, for example, H. Kogelnik and T. Li, "Laser beams and resonators," Appl. Opt. **5**, 1550–1567 (1966)].
 111. A. E. Siegman, *An Introduction to Lasers and Masers* (McGraw-Hill, 1971).
 112. A. Yariv, *Quantum Electronics*, 2nd ed. (Wiley, 1975).
 113. J. N. Demas and G. A. Crosby, "The measurement of photoluminescence quantum yields. A review," J. Phys. Chem. **75**, 991–1024 (1971).
 114. The 1PA equivalent of parameter $\Delta_{\text{ph}}^{(2)}$ is $\sigma N_0 L$, the fraction of light absorbed in the limit of thin sample or weak absorption.
 115. In the case of the 2PIF method, an additional limitation on the concentration is imposed by reabsorption of the emitted photons within the material (inner filter effect). This effect is observed to different extents depending on how the fluorescence signal is collected (for example, under back-scattering conditions or at 90° with respect to the incident beam).
 116. J. Segal, Z. Kotler, M. Sigalov, A. Ben-Asuly, and V. Khodorkovsky, "Two-photon absorption properties of (*N*-carbazolyl)-stilbenes," Proc. SPIE **3796**, 153–159 (1999).
 117. D. Beljonne, W. Wenseleers, E. Zojer, Z. Shuai, H. Vogel, S. J. K. Pond, J. W. Perry, S. R. Marder, and J.-L. Brédas, "Role of dimensionality on the two-photon absorption response of conjugated molecules: the case of octupolar compounds," Adv. Funct. Mater. **12**, 631–641 (2002).
 118. B. Strehmel, A. M. Sarker, and H. Detert, "The influence of σ and π acceptors on two-photon absorption and solvatochromism of dipolar and quadrupolar unsaturated organic compounds," ChemPhysChem **4**, 249–259 (2003).
 119. G. P. Bartholomew, M. Rumi, S. J. K. Pond, J. W. Perry, S. Tretiak, and G. C. Bazan, "Two-photon absorption in three-dimensional chromophores based on [2.2]-paracyclophane," J. Am. Chem. Soc. **126**, 11529–11542 (2004).
 120. S. K. Lee, W. J. Yang, J. J. Choi, C. H. Kim, S.-J. Jeon, and B. R. Cho, "2,6-Bis[4-(*p*-dihexylaminostyryl)-styryl]anthracene derivatives with large two-photon cross sections," Org. Lett. **7**, 323–326 (2005).
 121. When a photon counting approach is used, signal discrimination procedures can be used to reject noise.
 122. R. L. Swofford and W. M. McClain, "The effect of spatial and temporal laser beam characteristics on two-photon absorption," Chem. Phys. Lett. **34**, 455–460 (1975).
 123. We will introduce beams with a Gaussian spatial profile in Subsection 3.2.

To explain the results in Fig. 4, it is sufficient to mention that the beam size depends on z as follows: $w_0(1+(z/z_0)^2)^{1/2}$. The total number of excited molecules is obtained by integrating $N_m^{(2)}(\tau)$ over the excitation volume. The result for a generic path length L and for a sample with the focal plane at $L/2$ (and with photon flux ϕ_0 at $z=0$) is

$$\begin{aligned}\int_V N_m^{(2)}(\tau) dV &= \frac{1}{2} \delta \tau N_0 \int_{-L/2}^{L/2} dz \int_0^\infty 2\pi r dr \phi^2 = \frac{1}{2} \delta \tau N_0 \frac{\pi w_0^2 z_0 \phi_0^2}{2} \arctan \frac{L}{2z_0} \\ &= \frac{\delta N_0 N_{ph}^2}{2\tau} \left(\frac{2n}{\lambda} \arctan \frac{L}{2z_0} \right).\end{aligned}$$

The asymptotic value for $L \gg z_0$ is in this case $\delta N_0 N_{ph}^2 \pi n / (2\tau \lambda)$.

124. M. Rumi, J. E. Ehrlich, A. A. Heikal, J. W. Perry, S. Barlow, Z. Hu, D. McCord-Maughon, T. C. Parker, H. Röckel, S. Thayumanavan, S. R. Marder, D. Beljonne, and J.-L. Brédas, “Structure-property relationships for two-photon absorbing chromophores: bis-donor diphenylpolyene and bis(styryl)benzene derivatives,” *J. Am. Chem. Soc.* **122**, 9500–9510 (2000).
125. For example, if the flux is reduced by 5% by 2PA [$\phi(z)/\phi(0)=0.95$] and each time the photon flux is measured with an uncertainty of 2% (the two measurements before and after the beam are independent), from error propagation, the relative uncertainty in δ would be over 50%.
126. It should be kept in mind that this common definition of β implicitly assumes that approximation (ii) is valid, as this parameter is proportional to N_0 . β , usually called the “2PA coefficient,” is a macroscopic equivalent of the molecular parameter δ . In cases for which (ii) is not valid, β is not a constant of the material, but depends on ϕ through N_g , the concentration of molecules in the ground state ($N_g \leq N_0$).
127. V. I. Bredikhin, M. D. Galanin, and V. N. Genkin, “Two-photon absorption and spectroscopy,” *Sov. Phys. Usp.* **16**, 299–321 (1974).
128. In Subsection 4.3 we will discuss how ESA can also limit the applicability of Eq. (29) in NLT measurements, especially for ns pulse durations. At the moment, we are considering instead the case of materials for which 2PA is the only absorption process that can take place at the excitation wavelength λ .
129. In this context, the first argument for the function ϕ is the coordinate along the propagation direction, z , the origin being the front face of the material; the second argument refers to the radial distance, r , from the axis z . Thus, in this notation $\phi(0, 0)$ corresponds to the peak on-axis flux at the entrance of the material.
130. The initial pulse energy is now $E(0) = \tau E_{ph} \int_0^\infty \phi(0, 0) e^{-2r^2/w_0^2} 2\pi r dr = \tau E_{ph} \phi(0, 0) \pi w_0^2 / 2$.
131. When the results for the f/60 case in Fig. 7 are compared with those in Fig. 6 for the same pulse energy, it can be seen that the transmittance is larger in the former situation, even when ground state depletion is neglected. This is due to the effect of focusing: even if $L < z_0$ in the f/60 case, the beam size increases slightly away from the focal plane within the sample; instead, the beam was assumed to be perfectly collimated in Fig. 6.
132. This change in beam size is indeed exploited in closed-aperture Z-scan experiments [30] to measure the nonlinear refractive index of a material (which is related to the real part of the susceptibility $\chi^{(3)}$).

133. To differentiate between the examples discussed above, where z represented the position within the sample along the propagation direction, and the current example, where z is the position of the front face of the sample with respect to the focal plane, the z dependence of ϕ is now expressed with a subscript.
134. This is true not only for a Gaussian beam, but also for a beam with a generic beam profile, as long as the z dependence of the flux is known.
135. For this type of beam the relationship between pulse energy and peak flux is

$$E = E_{\text{ph}} \int_0^\infty \phi_0(r=0) e^{-2r^2/w_0^2} 2\pi r dr \int_{-\infty}^\infty e^{-t^2/\tau^2} dt = E_{\text{ph}} \phi_0(r=0) \frac{\pi \sqrt{\pi} w_0^2 \tau}{2}.$$

136. The value of the transmittance at a generic point within the sample can be obtained by substituting z' , the distance of the point from the front face, for L .
137. It should be remembered that we are assuming that 1PA absorption is negligible.
138. W. Zhao, J. H. Kim, and P. Palffy-Muhoray, “Z-scan measurement on liquid crystals using top-hat beams,” *Proc. SPIE* **2229**, 131–147 (1994).
139. S. M. Mian and J. P. Wicksted, “Measurement of optical nonlinearities using an elliptic Gaussian beam,” *J. Appl. Phys.* **77**, 5434–5436 (1995).
140. S. Hughes and J. M. Burzler, “Theory of Z-scan measurements using Gaussian–Bessel beams,” *Phys. Rev. A* **56**, R1103–R1106 (1997).
141. P. Chen, D. A. Oulianov, I. V. Tomov, and P. M. Rentzepis, “Two-dimensional Z scan for arbitrary beam shape and sample thickness,” *J. Appl. Phys.* **85**, 7043–7050 (1999).
142. J. A. Hermann, “Nonlinear optical absorption in thick media,” *J. Opt. Soc. Am. B* **14**, 814–823 (1997).
143. P. B. Chapple and P. J. Wilson, “Z-scan with near-Gaussian laser beams,” *J. Nonlinear Opt. Phys. Mater.* **5**, 419–436 (1996).
144. J. A. Hermann, “Beam propagation and optical power limiting with nonlinear media,” *J. Opt. Soc. Am. B* **1**, 729–736 (1984).
145. S. Hughes, J. M. Burzler, G. Spruce, and B. S. Wherrett, “Fast Fourier transform techniques for efficient simulation of Z-scan measurements,” *J. Opt. Soc. Am. B* **12**, 1888–1893 (1995).
146. J. M. Burzler, S. Hughes, and B. S. Wherrett, “Split-step Fourier methods applied to model nonlinear refractive effects in optically thick media,” *Appl. Phys. B* **62**, 389–397 (1996).
147. In this context, we define the time average of a function Y as follows:

$$\langle Y(t) \rangle = f \int_T^{T+1/f} Y(t) dt,$$

where T is a generic time and $Y(t)$ is a periodic function with period $1/f$.

148. This assumes that $\tau_{\text{n}} \ll 1/f$, so that effectively all molecules that have been excited during the pulse duration τ have decayed back to the ground state. For other indirect methods $1/f$ needs to be large with respect to the time constant of the process to be monitored (thermal time constant, phosphorescence lifetime, ...). If this requirement is not satisfied, the sample conditions are different every time a new pulse arrives, and ground state depletion may become relevant after a large number of pulses. In the case of single pulse measurements, the integration time for the signal needs to be long with respect to the time con-

stant of the process monitored, if results for different materials are to be compared under the same excitation conditions.

149. H. P. Weber, "Two-photon-absorption laws for coherent and incoherent radiation," *IEEE J. Quantum Electron.* **QE-7**, 189–195 (1971).
150. R. Loudon, *The Quantum Theory of Light*, 3rd ed. (Oxford Univ. Press, 2000).
151. M. C. Johnson and F. E. Lytle, "Studies of the single-mode and multimode cw dye lasers as sources for obtaining power-squared corrected two-photon spectra," *J. Appl. Phys.* **51**, 2445–2449 (1980).
152. For ideal monochromatic light with constant intensity and in the absence of noise, $g^{(2)} = 1$. For a square pulse of duration τ , $g^{(2)} = (\tau f)^{-1}$. For a Gaussian pulse with $1/e$ width τ , $g^{(2)} = (\tau f (2\pi)^{1/2})^{-1}$.
153. J. Krasinski, S. Chudzyński, W. Majewski, and M. Głodź, "Experimental dependence of two-photon absorption efficiency on statistical properties of laser light," *Opt. Commun.* **12**, 304–306 (1974).
154. J. A. Giordmaine, P. M. Rentzepis, S. L. Shapiro, and K. W. Wecht, "Two-photon excitation of fluorescence by picosecond light pulses," *Appl. Phys. Lett.* **11**, 216–218 (1967).
155. H. P. Weber and R. Dändliker, "Intensity interferometry by two-photon excitation of fluorescence," *IEEE J. Quantum Electron.* **QE-4**, 1009–1013 (1968).
156. R. J. Harrach, "Determination of ultrashort pulse widths by two-photon fluorescence patterns," *Appl. Phys. Lett.* **14**, 148–151 (1969).
157. H. E. Rowe and T. Li, "Theory of two-photon measurement of laser output," *IEEE J. Quantum Electron.* **QE-6**, 49–67 (1970).
158. S.-J. Chung, M. Rumi, V. Alain, S. Barlow, J. W. Perry, and S. R. Marder, "Strong, low-energy two-photon absorption in extended amine-terminated cyano-substituted phenylenevinylene oligomers," *J. Am. Chem. Soc.* **127**, 10844–10845 (2005).
159. M. Albota, D. Beljonne, J.-L. Brédas, J. E. Ehrlich, J.-Y. Fu, A. A. Heikal, S. T. Hess, T. Kogej, M. D. Levin, S. R. Marder, D. McCord-Maughon, J. W. Perry, H. Röckel, M. Rumi, G. Subramaniam, W. W. Webb, X.-L. Wu, and C. Xu, "Design of organic molecules with large two-photon absorption cross sections," *Science* **281**, 1653–1656 (1998).
160. S. J. K. Pond, M. Rumi, M. D. Levin, T. C. Parker, D. Beljonne, M. W. Day, J.-L. Brédas, S. R. Marder, and J. W. Perry, "One- and two-photon spectroscopy of donor-acceptor-donor distyrylbenzene derivatives: effect of cyano substitution and distortion from planarity," *J. Phys. Chem. A* **106**, 11470–11480 (2002).
161. D. J. Bradley, M. H. R. Hutchinson, H. Koetser, T. Morrow, G. H. C. New, and M. S. Petty, "Interactions of picosecond laser pulses with organic molecules. I. Two-photon fluorescence quenching and singlet states excitation in Rhodamine dyes," *Proc. R. Soc. London Ser. A* **328**, 97–121 (1972).
162. J. Kleinschmidt, S. Rentsch, W. Tottleben, and B. Wilhelmi, "Measurement of strong nonlinear absorption in stilbene-chloroform solutions, explained by the superposition of the two-photon absorption and one-photon absorption from the excited state," *Chem. Phys. Lett.* **24**, 133–135 (1974).
163. K. McEwan and R. Hollins, "Two-photon-induced excited-state absorption in liquid crystal media," *Proc. SPIE* **2229**, 122–130 (1994).
164. A. A. Said, C. Wamsley, D. J. Hagan, E. W. Van Stryland, B. A. Reinhardt, P. Roderer, and A. G. Dillard, "Third- and fifth-order optical nonlinearities in organic materials," *Chem. Phys. Lett.* **228**, 646–650 (1994).

165. J. Swiatkiewicz, P. N. Prasad, and B. A. Reinhardt, "Probing two-photon excitation dynamics using ultrafast laser pulses," *Opt. Commun.* **157**, 135–138 (1998).
166. R. L. Sutherland, M. C. Brant, J. Heinrichs, J. E. Rogers, J. E. Slagle, D. G. McLean, and P. A. Fleitz, "Excited-state characterization and effective three-photon absorption model of two-photon-induced excited-state absorption in organic push-pull charge-transfer chromophores," *J. Opt. Soc. Am. B* **22**, 1939–1948 (2005).
167. An expression similar to Eq. (46) could be written in the case of a molecule undergoing intersystem crossing from r to the lowest level in the triplet manifold and then being excited to a higher-lying triplet state. In this case, σ_{ex} would represent a triplet–triplet ESA cross section.
168. The quantity $\phi\tau$ corresponds to the photon fluence, or the number of photons per unit area of the beam, N_{ph}/a [N_{ph} from Eq. (17) for the case of a pulse with constant profile in space and time].
169. Even if ESA occurs from the triplet state, as described in note [167], the fluorescence quantum yield and intersystem crossing rates would be unchanged if N_{ex} is small, and thus $\langle S \rangle$ would still not be affected by ESA and would not depend on pulse duration.
170. This numerical example referred to excitation with ns pulses. However, similar conditions for ESA can be reached by using fs pulses from an amplified laser, for example, with ϕ values only slightly larger than those considered in case 3.1.b.
171. M. D. Galanin, B. P. Kirsanov, and Z. A. Chizhikova, "Luminescence quenching of complex molecules in a strong laser field," *JETP Lett.* **9**, 304–306 (1969).
172. J. P. Hermann and J. Ducuing, "Dispersion of the two-photon cross section in rhodamine dyes," *Opt. Commun.* **6**, 101–105 (1972).
173. Unfortunately, there are some typographical errors in the solution of the system of equation reported by Kleinschmidt *et al.* [162].
174. J. E. Ehrlich, X. L. Wu, I.-Y. S. Lee, Z.-Y. Hu, H. Röckel, S. R. Marder, and J. W. Perry, "Two-photon absorption and broadband optical limiting with bis-donor stilbenes," *Opt. Lett.* **22**, 1843–1845 (1997).
175. O.-K. Kim, K.-S. Lee, H. Y. Woo, K.-S. Kim, G. S. He, J. Swiatkiewicz, and P. N. Prasad, "New class of two-photon-absorbing chromophores based on dithienothiophene," *Chem. Mater.* **12**, 284–286 (2000).
176. G. S. He, L. Yuan, N. Cheng, J. D. Bhawalkar, P. N. Prasad, L. Brott, S. J. Clarson, and B. A. Reinhardt, "Nonlinear optical properties of a new chromophore," *J. Opt. Soc. Am. B* **14**, 1079–1087 (1997).
177. B. A. Reinhardt, L. L. Brott, S. J. Clarson, A. G. Dillard, J. C. Bhatt, R. Kannan, L. Yuan, G. S. He, and P. N. Prasad, "Highly active two-photon dyes: design, sythesis, and characterization toward application," *Chem. Mater.* **10**, 1863–1874 (1998).
178. P. A. Fleitz, R. L. Sutherland, and T. J. Bunning, "Z-scan measurements on molten diphenylbutadiene in the isotropic liquid state," in *Materials for Optical Limiting*, R. Crane, K. Lewis, E. Van Stryland, and M. Khoshnevisan, eds., Vol. 374 of Materials Research Society Symposium Proceedings (Materials Research Society, 1995), pp. 211–216.
179. P. A. Fleitz and R. L. Sutherland, "Investigating the nonlinear optical properties of molten organic materials," *Proc. SPIE* **3146**, 24–30 (1997).
180. E. I. Blount and J. R. Klauder, "Recovery of laser intensity from correlation data," *J. Appl. Phys.* **40**, 2874–2875 (1969).

181. D. J. Bradley and G. H. C. New, "Ultrashort pulse measurements," *Proc. IEEE* **62**, 313–345 (1974).
182. J.-C. M. Diels, J. J. Fontaine, I. C. McMichael, and F. Simoni, "Control and measurement of ultrashort pulse shapes (in amplitude and phase) with femtosecond accuracy," *Appl. Opt.* **24**, 1270–1282 (1985).
183. H. P. Weber and R. Dändliker, "Method for measurement the shape asymmetry of picosecond light pulses," *Phys. Lett. A* **28**, 77–78 (1968).
184. A. A. Grütter, H. P. Weber, and R. Dändliker, "Imperfectly mode-locked laser emission and its effects on nonlinear optics," *Phys. Rev.* **185**, 629–643 (1969).
185. D. J. Kane and R. Trebino, "Single-shot measurement of the intensity and phase of an arbitrary ultrashort pulse by using frequency-resolved optical gating," *Opt. Lett.* **18**, 823–825 (1993).
186. R. Trebino and D. J. Kane, "Using phase retrieval to measure the intensity and phase of ultrashort pulses: frequency-resolved optical gating," *J. Opt. Soc. Am. A* **10**, 1101–1111 (1993).
187. R. Trebino, K. W. DeLong, D. N. Fittinghoff, J. N. Sweetser, M. A. Krumbühl, B. A. Richman, and D. J. Kane, "Measuring ultrashort laser pulses in the time-frequency domain using frequency-resolved optical gating," *Rev. Sci. Instrum.* **68**, 3277–3295 (1997).
188. The case of different excitation volumes in the two samples could be handled by including appropriate correction terms in the collection efficiency factor, G . Beside the obvious case of samples with different thicknesses in a collimated beam, the excitation volume is also different if the samples do not have the same refractive index and $L \gg z_0$.
189. Due to the relatively low concentration used in 2PA measurements, it is often assumed that the refractive index of the solution is the same as that of the pure solvent.
190. For example, the refractive index dependence of G varies with the optical setup configuration on both the excitation and the emission sides. A few cases, often used in the literature, are briefly considered here. If the excitation beam is collimated and the fluorescence signal is imaged at 90° with respect to the excitation propagation direction [124], the situation is similar to that employed in many commercial spectrofluorimeters, for which the signal dependence on n_{fl} is described as n_{fl}^{-2} [113]. If the excitation beam is focused in the sample, the excitation volume in the material depends on n , and consequently G depends on both n and n_{fl} . In the focused beam configuration described by Beljonne *et al.* [117], the refractive index dependence of G was assumed to be proportional to n/n_{fl}^2 . If the dispersion of n is small, this reduces to $G \propto n_{\text{fl}}^{-1}$. If the fluorescence signal is collected in the back-scattering direction by using the same lens or objective used for the excitation, only the change in the excitation volume with n is considered, and $G \propto n$ [M. A. Albota, C. Xu, and W. W. Webb, "Two-photon fluorescence excitation cross sections of biomolecular probes from 690 to 960 nm," *Appl. Opt.* **37**, 7352–7356 (1998)].
191. S. M. Kennedy and F. E. Lytle, "*p*-Bis(*o*-methylstyryl)benzene as a power-squared sensor for two-photon absorption measurements between 537 and 694 nm," *Anal. Chem.* **58**, 2643–2647 (1986).
192. W. G. Fisher, E. A. Wachter, F. E. Lytle, M. Armas, and C. Seaton, "Source-corrected two-photon excited fluorescence measurements between 700 and 880 nm," *Appl. Spectrosc.* **52**, 536–545 (1998).
193. C. Xu, J. Guild, W. W. Webb, and W. Denk, "Determination of absolute

- two-photon excitation cross sections by *in situ* second-order autocorrelation,” *Opt. Lett.* **20**, 2372–2374 (1995).
194. J. P. Hermann and J. Ducuing, “Absolute measurement of two-photon cross sections,” *Phys. Rev. A* **5**, 2557–2568 (1972).
 195. A. Karotki, M. Drobizhev, M. Kruk, C. Spangler, E. Nickel, N. Mamar-dashvili, and A. Rebane, “Enhancement of two-photon absorption in tetrapyrrolic compounds,” *J. Opt. Soc. Am. B* **20**, 321–332 (2003).
 196. If necessary, the attenuation of the beam can be accounted for in the equations to be used to process the data. In some experimental configurations for fluorescence signal collection, reabsorption may also have to be corrected for.
 197. J. Yoo, S. K. Yang, M.-Y. Jeong, H. C. Ahn, S.-J. Jeon, and B. R. Cho, “Bis-1,4-(*p*-diarylaminostyryl)-2,5-dicyanobenzene derivatives with large two-photon absorption cross-sections,” *Org. Lett.* **5**, 645–648 (2003).
 198. R. D. Jones and P. R. Callis, “A power-squared sensor for two-photon spectroscopy and dispersion of second-order coherence,” *J. Appl. Phys.* **64**, 4301–4305 (1988).
 199. R. D. Jones and P. R. Callis, “Two-photon spectra of inductively perturbed naphthalenes,” *Chem. Phys. Lett.* **144**, 158–164 (1988).
 200. A. A. Rehms and P. R. Callis, “Two-photon fluorescence excitation spectra of aromatic amino acids,” *Chem. Phys. Lett.* **208**, 276–282 (1993).
 201. W. G. Fisher, E. A. Wachter, M. Armas, and C. Seaton, “Titanium:sapphire laser as an excitation source in two-photon spectroscopy,” *Appl. Spectrosc.* **51**, 218–226 (1997).
 202. M. Samoc, A. Samoc, M. G. Humphrey, M. P. Cifuentes, B. Luther-Davies, and P. A. Fleitz, “Z-scan studies of dispersion of the complex third-order nonlinearity of nonlinear absorbing chromophores,” *Mol. Cryst. Liq. Cryst.* **485**, 894–902 (2008).
 203. S. Delysse, P. Raimond, and J.-M. Nunzi, “Two-photon absorption in non-centrosymmetric dyes,” *Chem. Phys.* **219**, 341–351 (1997).



Mariacristina Rumi obtained an M.S. degree in Physics (*summa cum laude*) from the University of Milano (Milano, Italy) in 1994 and undertook graduate studies at the G. Natta Advanced School in Polymer Science at the Polytechnic of Milano (Milano, Italy), obtaining a Specialist degree in 1997 under the guidance of Prof. Giuseppe Zerbi and conducting research on the vibrational properties and computational modeling of conjugated molecules and polymers. She then worked in the group of Prof. Joseph W. Perry at the California Institute of Technology and the University of Arizona, and she is currently a Senior Research Scientist at the Georgia Institute of Technology, in the group of Prof. Seth R. Marder. She has studied the fundamental photophysical properties and practical applications of two-photon absorbing materials and has contributed to the development of structure-property relationships for two-photon absorption in conjugated molecules. Her research interests and experience include the vibrational, linear and nonlinear optical spectroscopy of organic materials. She has coauthored 21 papers in peer-reviewed journals and two book chapters.



Joseph W. Perry is Professor of Chemistry and Associate Director of the Center for Organic Photonics and Electronics at the Georgia Institute of Technology. He received a B.S. in Chemistry from the University of South Florida in 1977 and a Ph.D. in Chemical Physics in 1984 from the California Institute of Technology, where he performed research on vibrational overtone spectroscopy and intramolecular vibrational energy redistribution. He received the Herbert Newby McCoy Award for his graduate research. He performed postdoctoral research on vibrational dephasing in liquids at the National Bureau of Standards. In 1985, he joined the Jet Propulsion Laboratory as a Member of the Technical Staff. He founded the Optoelectronic Materials Group and held various positions, ultimately being promoted to Senior Research Scientist. He joined the faculty of the Department of Chemistry at the University of Arizona in 1998 and was jointly appointed in the Optical Sciences Center in 1999. He was Co-Director of the Center for Advanced Nanoscale Science and Technology and the W. M. Keck Laboratory on 3D Micro- and Nano-fabrication at the University of Arizona. In 2003, he joined the School of Chemistry and Biochemistry at the Georgia Institute of Technology. His research interests include the spectroscopy, electronic structure, photophysics and optical nonlinearities of organic molecules and polymers, organic photonic materials for all-optical signal processing, optical power limiting, multiphoton 3D microfabrication and nanofabrication, two-photon absorbing probes for imaging and sensing, optical properties and dynamics of chromophores at metal nanoparticle surfaces, surface modification of nanoparticles, and metal oxide nanoparticle/polymer dielectric nanocomposites for energy storages. He served as Director of the DARPA MORPH program from 2003 to 2010 and is currently serving as Director of the DARPA ZOE program at Georgia Tech, both programs involving development of organic materials for all-optical nonlinearities. He has received several awards, including a NASA Medal for Exceptional Scientific Achievement in 1992 and NSF's Special Creativity Award in 1997. He is a Fellow of the Optical Society of America and the American Physical Society and is a member of the American Chemical Society, Materials Research Society, American Association for the Advancement of Science, and SPIE. He served as a Topical Editor for the *Journal of the Optical Society of America B* from 2007 through 2009. He has published more than 200 scientific articles and has eight patents issued. He has co-founded several technology start-up companies: Arizona Microsystems, Focal Point Microsystems, and LumoFlex.